



# UNIVERSITY OF TWENTE.

Faculty of Engineering Technology,  
Mechanical Engineering

## Theoretical modelling of liquid fractions and flow regimes during the first-stage startup of steam transport pipelines

F.C. Perizonius

Thermal & Fluid Engineering

M.Sc. Thesis

April 2023

Report #426

---

**University Supervisor:**  
dr. C. Acar

**Company Supervisors:**  
dr. ir. M. den Burger  
ir. M. Supper

Thermal Engineering Group  
Faculty of Engineering Technology,  
Mechanical Engineering  
University of Twente  
P.O. Box 217  
7500 AE Enschede  
The Netherlands

---



This thesis project was provided by, and carried out at Rotterdam Engineering.



The author hereby wants to acknowledge his supervisors and Rotterdam Engineering for an enjoyable collaboration.

---

**University Supervisor:**  
dr. C. Acar

**Company Supervisors:**  
dr. ir. M. den Burger  
ir. M. Supper

Thermal Engineering Group  
Faculty of Engineering Technology,  
Mechanical Engineering  
University of Twente  
P.O. Box 217  
7500 AE Enschede  
The Netherlands

---

**UNIVERSITY OF TWENTE.**



# Summary

Concurrently, a substantial amount of residual heat from production and recycling processes remains unused. For example, with the incineration of waste in waste incineration plants. Enormous amounts of waste are incinerated and the exhaust gases, while containing substantial amounts of heat still, are discarded into the atmosphere. Over the past decade, this has led to an increasing demand for energy recycling technologies. Rotterdam Engineering delivers intelligent designs and engineering for the appropriate installation of long distance steam transport pipelines in order to reuse the excess heat from waste incineration plants for other industrial purposes. Although many of the issues of steam transport have been overcome, avoiding obstacles in the pathway of the pipelines remains to be a problem. Despite the fact that steam transport pipelines require to be installed above surface level, Rotterdam Engineering is interested in the underground use of steam transport pipelines. Specifically, the application of the Horizontal Directional Drilling technique.

The handling of liquid condensate is a familiar inconvenience in the world of steam transport pipeline engineering. However, underground passages for steam transport pipelines opens a new set of problems. The accumulation of liquid condensate proposes a significant threat due to the disastrous effects of water hammer phenomena. Constructing an underground passage with the Horizontal Directional Drilling technique complicates the removal of liquid condensate, and therefore, results in the accumulation of any liquid condensate.

This thesis intends to investigate the mechanisms of liquid formation through condensation within pipelines and, if possible, identify how to diminish or control it. The aim is to discover whether the risk of water hammer phenomena is significant for the application of an underground passage with the Horizontal Directional Drilling Technique, and if so, how this influences the decisions regarding the application of it.

A theoretical heat transfer model that monitors the thermophysical properties of a flowing two-phase fluid was constructed. The existing literature on the modelling

of two-phase fluid flows, and the field of two-phase Flow Pattern Maps were used to determine the liquid fractions and flow regimes during the first-stage of start-up of a steam transport pipeline with regard to an underground application. The most significant results of this research are:

- Maximum liquid fractions were observed during the first-stage of start-up at mass flows of 15 and 100 kg/m<sup>2</sup>s<sup>-1</sup> for the smallest simulated pipe diameter of 300 mm, indicating a higher risk of water hammer phenomena.
- During the simulations, the fluid appears to retain a significant amount of its heat, such that the vapour quality  $\zeta$  does not decline further than  $\zeta \approx 0.33$ .
- Flow regimes were successfully determined throughout the simulation of first-stage start-up of the steam transport pipeline. No risks of slug or plug formation were identified.

Although the heat transfer model was validated with an absolute deviation of 3%, the method used to determine the two-phase heat transfer coefficients provided suspicious outcomes in its details. This needs further investigation. In order to prevent water hammer phenomena from occurring, liquid fractions must be maintained low throughout the use of the pipeline. Increasing the diameter of the pipeline showed to maintain the lowest liquid fractions throughout first-stage start-up. However, how this carries over to subsequent stages of start-up, remains to be investigated.

# Contents

<b>Summary</b>	<b>i</b>
<b>List of acronyms</b>	<b>vi</b>
<b>List of symbols</b>	<b>viii</b>
<b>1 Introduction</b>	<b>1</b>
1.1 Goals of the assignment . . . . .	2
1.2 Research questions . . . . .	3
1.3 Thesis outline . . . . .	3
<b>2 Background</b>	<b>5</b>
2.1 Steam . . . . .	5
2.1.1 Phase change & heat . . . . .	5
2.2 Steam transport pipelines . . . . .	8
2.2.1 Condensate & drainage . . . . .	9
2.2.2 Steam traps . . . . .	10
2.2.3 Warm-up & running loads . . . . .	11
2.2.4 Load estimation & optimization . . . . .	12
2.3 Horizontal Directional Drilling . . . . .	14
2.4 Concluding remarks . . . . .	16
<b>3 Literature review</b>	<b>17</b>
3.1 Water hammer phenomena . . . . .	17
3.1.1 Condensation-induced water hammer . . . . .	18
3.2 Flow regimes . . . . .	21
3.2.1 Two-phase flow regimes . . . . .	21
3.2.2 Flow pattern maps . . . . .	23
3.3 Heat transfer in steam pipelines . . . . .	28
3.3.1 Shah's study on two-phase heat transfer . . . . .	28
3.3.2 Effect of channel size . . . . .	29
3.3.3 Two-phase heat transfer coefficient . . . . .	29

3.4	Void fraction estimation & vapour quality . . . . .	31
3.4.1	Smith's void fraction estimation method . . . . .	32
3.4.2	Vapour quality . . . . .	33
3.5	Concluding remarks . . . . .	35
<b>4</b>	<b>Methodology</b>	<b>37</b>
4.1	General approach . . . . .	37
4.1.1	Mathematical hierarchy of the model . . . . .	37
4.1.2	First time use of pipelines . . . . .	38
4.2	Framework of the model . . . . .	39
4.2.1	Constraints . . . . .	39
4.2.2	Assumptions . . . . .	40
4.3	First-stage start-up . . . . .	42
4.4	The heat transfer model . . . . .	43
4.4.1	Heat transfer equations . . . . .	43
4.4.2	Fluid-pipe heat transfer interface area . . . . .	45
4.4.3	Heating up of the pipe materials . . . . .	47
4.5	Thermophysical fluid properties . . . . .	48
4.5.1	Heat contents & vapour quality . . . . .	48
4.5.2	Void fraction . . . . .	51
4.6	Determining flow patterns with FPMs . . . . .	51
4.7	Concluding remarks . . . . .	53
<b>5</b>	<b>Results</b>	<b>54</b>
5.1	Condensation induced water hammer . . . . .	54
5.2	Heat transfer model & thermophysical properties . . . . .	54
5.2.1	Length of the fluid cylinder . . . . .	54
5.2.2	Vapour quality . . . . .	57
5.2.3	Void fraction . . . . .	60
5.2.4	Two-phase heat transfer coefficient . . . . .	63
5.3	Flow properties of the fluid . . . . .	66
5.3.1	Flow Pattern Map . . . . .	66
5.4	Concluding remarks . . . . .	68
<b>6</b>	<b>Discussion</b>	<b>70</b>
6.1	Discussing results . . . . .	70
6.2	Answering research questions . . . . .	73
6.3	Limitations . . . . .	74

---

<b>7</b>	<b>Conclusions and recommendations</b>	<b>76</b>
7.1	Conclusions . . . . .	76
7.2	Recommendations . . . . .	77
	<b>References</b>	<b>79</b>
	<b>Appendices</b>	
<b>A</b>	<b>Alternative drilling techniques</b>	<b>85</b>
<b>B</b>	<b>Adiabatic two-phase Flow Pattern Maps</b>	<b>88</b>
<b>C</b>	<b>Additional water hammer articles</b>	<b>93</b>
C.1	Flow & differential shock water hammer . . . . .	93
C.2	Slug propulsion & resistance, acceleration & deceleration . . . . .	94
<b>D</b>	<b>Code</b>	<b>96</b>
<b>E</b>	<b>Additional tables</b>	<b>100</b>

# List of acronyms

<b>SCS</b>	Steam-condensate Systems
<b>HDD</b>	Horizontal Directional Drilling
<b>CS</b>	Condensate Slug
<b>CIWH</b>	Condensate Induced Water Hammer
<b>EES</b>	Engineering Equation Solver
<b>NPP</b>	Nuclear Power Plant
<b>IPPE</b>	Leipunski Institute of Physics and Power Engineering
<b>EREC</b>	Elektrogorsk Research and Engineering Center
<b>FPM</b>	Flow Pattern Map
<b>DIN</b>	Deutsches Institut für Normung



# List of symbols

## Greek Symbols

Symbol	Description	Units
$\alpha$	Heat transfer coefficient	$\frac{\text{W}}{\text{m}^2\text{K}}$
$\alpha_{\text{Nu}}$	Nusselt heat transfer coefficient	$\frac{\text{W}}{\text{m}^2\text{K}}$
$\epsilon$	Void fraction	—
$\epsilon_s$	Void fraction by Smith's estimation	—
$\lambda$	Conductive heat transfer coefficient	$\frac{\text{W}}{\text{m}^2\text{K}}$
$\mu$	Dynamic viscosity	$\frac{\text{Ns}}{\text{m}^2}$
$\rho$	Density	$\frac{\text{kg}}{\text{m}^3}$
$\sigma$	Surface tension	$\frac{\text{N}}{\text{m}^2}$
$\zeta$	Vapour quality	—

## Roman Symbols

Symbol	Description	Units
$\Delta h$	Latent heat	$\frac{\text{kJ}}{\text{kg}}$
$A$	Flow surface area	$\text{m}^2$
$a$	Acceleration	$\frac{\text{m}}{\text{s}^2}$
$c$	Speed of sound	$\frac{\text{m}}{\text{s}}$
$c_p$	Specific heat	$\frac{\text{kJ}}{\text{kgK}}$
$D$	Diameter	m
$F$	Force	N

$f$	Friction factor	—
$Fr$	Froude number	—
$G$	Mass flow per unit area	$\frac{\text{kg}}{\text{m}^2\text{s}}$
$g$	Gravitational acceleration	$\frac{\text{m}}{\text{s}^2}$
$h$	Enthalpy	$\frac{\text{kJ}}{\text{kg}}$
$K$	Dimensionless factor "K"	—
$k$	Conduction heat transfer coefficient	$\frac{\text{W}}{\text{m}^2\text{K}}$
$L$	Length as a distance	m
$M$	Condensate load	kg
$m$	Mass	kg
$N$	Multiple of section lengths	—
$P$	Pressure	$\frac{\text{N}}{\text{m}^2}$
$p_r$	Reduced pressure	$\frac{\text{N}}{\text{m}^2}$
$P_t$	Allowable burst pressure	$\frac{\text{N}}{\text{m}^2}$
$Pr$	Prandtl number	—
$Q$	Heat	kJ
$r$	Radius	m
$Re$	Reynolds number	—
$S$	Velocity ratio	—
$s$	Smith parameter	—
$S_t$	Allowable tensile strength	$\frac{\text{N}}{\text{m}^2}$
$T$	Dimensionless pressure gradient ratio	—
$t$	Time	s
$u$	Flow velocity	$\frac{\text{m}}{\text{s}}$
$V$	Volume	$\text{m}^3$

$We$	Weber number	—
$wt$	Wall thickness	m
$X$	Dimensionless pressure gradient ratio	—
$x$	Distance travelled by fluid	m

## Subscripts

Symbol	Description	Units
$\infty$	Infinite or ambient	—
a	Air	—
c	Gaseous core	—
fg	vapour to liquid increment	—
f	Fluid, both gas & liquid phase	—
Gi	Initial state of the gas	—
G	Gas	—
IF	Impact force	—
ins	Insulation	—
i	Inner	—
k	Either gaseous or liquid phase	—
LO	Liquid only	—
L	Liquid	—
m	Mixture	—
o	Outer	—
p	Pipe, carbon steel	—
s	Steel	—
TP	Two-phase	—
w	Water	—
$i$	$i = 1, 2, 3 \dots, n$	—

# Introduction

The necessity of renewable energy and energy recycling technologies has become undeniable for the twenty-first century. Most recent climate change reports issue that further heating of the planet will result in irreversible effects. IPCC [1] reports that suitable habit space will reduce significantly, and mortality rates due to heat stress will increase with up to 300% once a global warming level of 3°C has been reached. Therefore, energy companies and investment organisations are noticing the urge for cleaner energy sources and technologies, and are investing in its developments. The surge of oil and gas prices in 2022 has increased this incentive even further. Consequently, market leading energy companies could potentially use their increased earnings to accelerate the development and implementation of renewable and energy recycling technologies.

In 2020, 2153 million tonnes of waste was produced by humans in Europe [2]. A significant amount of this waste is discarded by incineration in waste incineration plants. Waste is incinerated on a daily basis and a significant amount of residual heat is present in the exhaust gases of the process. Solutions such as waste incineration plants, or waste-to-energy plants, reuse the excess heat to generate steam, and in turn, use the steam to drive turbines that generate electricity. However, electricity is not always the preferred type of energy. Industries, such as food, medical or manufacturing, benefit from the use of dry steam in their processes. For example, the producing and shrink wrapping certain foods, cleaning or sterilizing equipment, or melting and moulding plastics [3]. However, unlike the transportation of electricity, long distance steam transport is not as well-established and faces challenges still.

A system that transports steam is called a Steam-condensate Systems (SCS). Heat is used to create steam, which is transported through heavily insulated pipelines, and condensate is returned through a separate line after the heat is extracted from the steam. Recently, the need for large-scale SCS has increased significantly due to

the contemporary energy transition. These SCSs allow the re-use and distribution of heat between industrial businesses through steam over large distances. Since the heat is mostly an exhaust output of waste incineration processes, it is generally a cheaper source of energy compared to commercial energy providers. This encourages industries to heat their processes with steam instead of other polluting materials like fossil fuels, and helps to create incentive to minimize their carbon footprints.

As the demand for SCSs increases, these systems have to be designed, engineered and installed. Rotterdam Engineering provides intelligent designs and engineering for the pipelines in which the steam is transported. These pipelines are called steam transport pipelines and are the topic of this thesis. One of the issues with steam transport pipelines is the crossing of obstacles that are in the pathway of the pipeline. Frequently, for the installation of pipelines, obstacles such as roads, rivers, canals, dikes or railways form complications. In general, for most other types of pipelines, this is resolved by an underground passage. Several methods exist to create an underground passage. A reliable and affordable method is the Horizontal Directional Drilling (HDD) technique. However, this technique has not yet been applied for SCSs. Engineers foresee many difficulties in this regard, mainly due to the accumulation of liquid condensate. During the transportation of steam through steam pipelines, part of the steam condenses as a result of heat losses. It is crucial that condensate levels are maintained sufficiently low within the steam main. Otherwise, water hammer phenomena, such as Condensate Slug (CS) collision or Condensate Induced Water Hammer (CIWH) could occur, resulting in high dynamic forces on the pipework, which could ultimately lead to yielding of the pipe.

Engineers have come up with solutions for many of the issues that arise with steam transport pipelines. However, thorough understanding of the problems is usually missing due to lack of research within the specific field. In turn, this leads to sub-optimal engineering with overly cautious design choices.

## **1.1 Goals of the assignment**

The research of this thesis projects attempts to extend the knowledge on condensate related issues in steam transport pipelines. It pursues to identify the risks and consequences of water hammer phenomena and intends to ascertain familiarity with the distinct parameters that influence it. Applying the knowledge acquired from existing theory and literature, the research seeks to disclose whether a water hammer effect occurs, and whether it will be detrimental to an actual steam main for any re-

alistic operating scenario. The ultimate aim of this research is to attempt to apply the theory to a yet unapplied scenario, which is the application of a HDD bore with a steam pipeline.

## 1.2 Research questions

The goal of this research is formulated as the main research question. A set of more specific questions is constructed to guide the writer towards the main research question. The main research question is stated as:

- How do water hammer phenomena, or other condensate related issues, influence the choice and application of a HDD boring for steam-condensate system pipelines?

The sub-research questions are specified by the following list:

1. How to demonstrate if Condensate Slugs or Condensation Induced Water Hammer occurs?
2. What are the variables, at first time use of the pipelines, that can be adjusted to mitigate condensate generation?
3. What are the repercussions of Condensate Slugs and Condensation Induced Water Hammer if one of these occurs?

## 1.3 Thesis outline

This thesis starts by establishing a baseline of knowledge that is required to fathom the performed research in chapter 2, called background. In chapter 2, some fundamental concepts of phase change and heat, that are commonly used within Mechanical Engineering, are introduced. Subsequently, the basic information on the design and use of steam transport pipelines is provided, followed by a detailed description of the HDD process. By the end of chapter 2, a solid understanding of the problem and some of the basic concepts of thermodynamics and steam pipeline engineering should be established.

In chapter 3, the literature on the relevant water hammer phenomena is investigated. Two-phase flow properties, such as the distinct flow regimes are scrutinized,

and the application of Flow Pattern Maps for condensation circumstances in the literature is reported. Then, an extensive study on the heat transfer coefficients for two-phase flows is reviewed. Finally, the concepts of void fraction estimation methods and vapour quality are explained.

Based on the acquired background and literature observations, an approach to address the gap in the field is composed. In chapter 4, the approach, consisting of a detailed heat transfer model and the application of two-phase fluid theory, is elaborated in detail. It starts by establishing the framework, comprising of the necessary constraints and assumptions of the model. Subsequently, the equations for each step of the model are elaborated.

After the simulations are executed successfully, the results are reported and analyzed in chapter 5. Figures and Tables are used to display the outcomes of the model. The nature of the observations is then discussed in chapter 6, and the writer will attempt to answer the research questions that were stated in the introduction. Finally, in chapter 7, the most important contributions and findings of the thesis are presented, including several recommendations for future work

# Background

## 2.1 Steam

The use of steam has an extensive history in all types of technologies that exploit various properties of this gaseous state of water. Most notably, steam has had a substantial contribution to the industrial revolution, where industries started using large steam engines to motorize their processes. However, this research intends to have a look at the use of steam as a heat transport medium and its properties before, during and after phase change.

### 2.1.1 Phase change & heat

Phase change of a medium is a widely recognized and accepted method for transferring heat. At least for steam, the most effective way to lose its heat is through condensation. The amount of energy transferred through phase change is called latent heat [4]. In physics, the four fundamental states of matter are solid, liquid, gas, and plasma. Although plasma is acknowledged as a fundamental state of matter, compared to the other states, the phase change to the plasma state is not well-defined [5]. To support the research of this thesis, some awareness about the phase change of water between the liquid and gaseous states is desirable. Therefore, this section aims to provide a brief recollection of condensation and evaporation (vaporization), but also to touch on melting and solidification (fusion), sublimation and deposition phase changes of water. Solid has the least energetic state of the three. In the solid state, atoms are closely located to one another and have strong bonds that are not easily broken. Liquid has a more energetic state where the particles are still attracted to each other, but can move alongside each other and exchange positions. Gas is the most energetic state of the three. In this state, the particles are freed of their bonds. The change in distance between particles, when transitioning to the gas phase, is far more significant compared to the change from solid to liquid

phase. Since the energy in phase change is used to either break or form bonds, the kinetic energy of the particles does not change. Therefore, the temperature remains constant during phase change of a material [6]. Figure 2.1 depicts the phase change processes from solid to liquid, and liquid to gaseous water at atmospheric pressure. The horizontal axis displays the heat energy required per unit mass in calories per gram. One notices from the graph that the most substantial energy increment is required to transition from water to steam before it is able to reach temperatures higher than 100 °C.

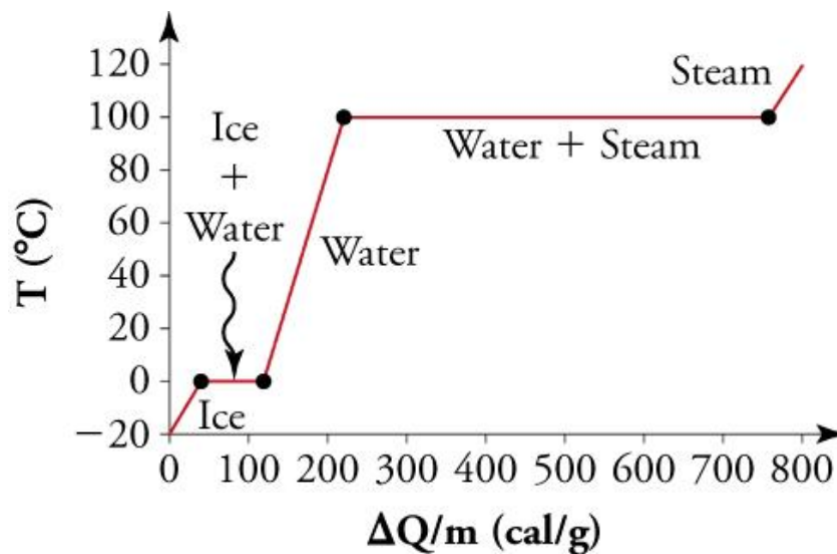


**Figure 2.1:** Phase change diagram of water at atmospheric pressure [6]

In engineering technology, the phase change of materials is widely applied in all kinds of industries, including waste heat recovery systems, preservation of food and pharmaceutical products [7]. But by far the largest segment of its applications is for the heating and cooling of households, industrial processes or energy systems. Vaporization is considerably the most prevalent type of phase change application in engineering technology, as it is extensively used in heat exchangers. This seems reasonable when one considers that vaporization is the transition to and from the most energetic state, namely gas. On a sidenote, in thermodynamics, it is established that the latent heat of vaporization is dependent on pressure and temperature, while fusion occurs at a more or less constant temperature and nearly independent of pressure. To determine the latent heat of a vaporization process at certain pressure, and codependent temperature, often times the data of steam tables is used to acquire the corresponding enthalpy values. Alternatively, a temperature-enthalpy (T-h) diagram can be used to read the enthalpy values at certain states of the material or substance. Figure 2.2, which is created in the Engineering Equation Solver (EES)

software, displays the T-h diagram for water. The specific enthalpy increments between saturated liquid and saturated vapour states are indicated at pressures 200 kPa and 3000 kPa, and they amount roughly 2200 and 1800  $\text{kJkg}^{-1}$ , respectively. To recapitulate, this represents the latent heat and is often symbolized as  $h_{fg}$  in steam tables.

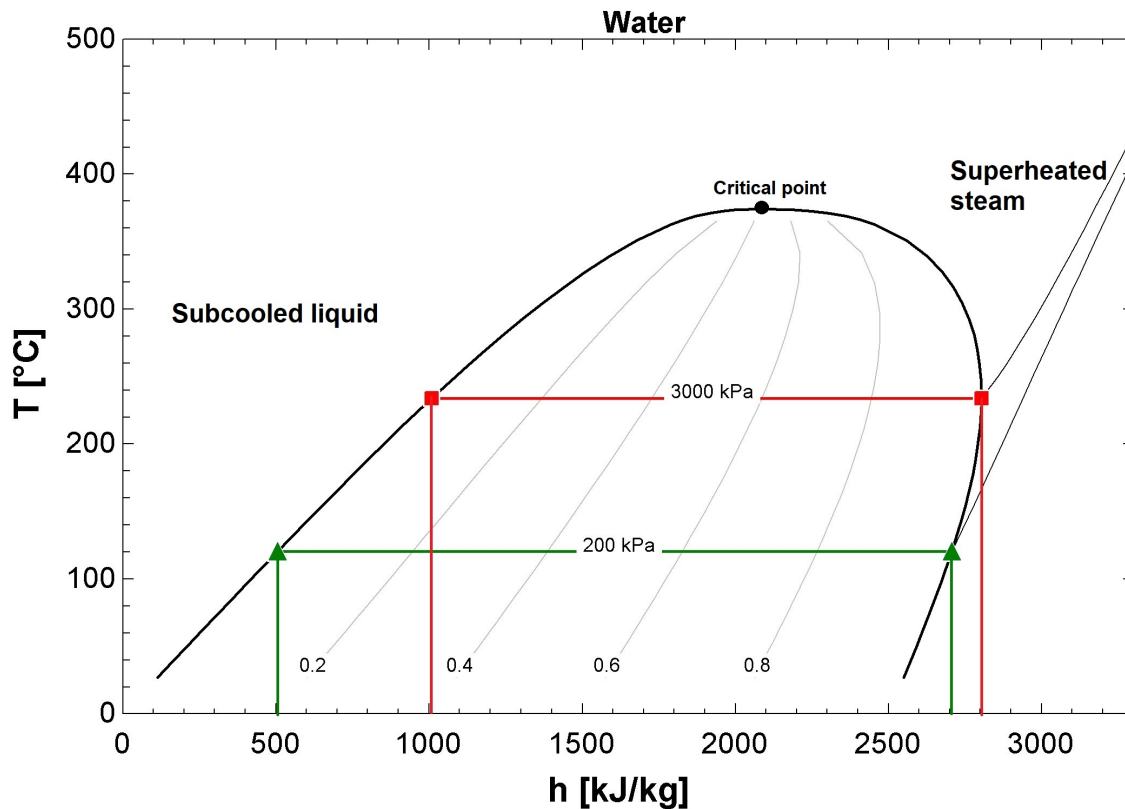


**Figure 2.2:** T-h diagram of water

Here, the writer introduces the definition of the vapour quality  $\zeta$ . As was mentioned, in Figure 2.2, the indicated points are situated at saturated liquid (left-hand side in Figure 2.2) and saturated vapour states (right-hand side in Figure 2.2), corresponding to vapour qualities of 0 and 1. For any enthalpy values in between saturated liquid and vapour states,  $0 < \zeta < 1$ . The exact vapour quality can then be determined by knowing the enthalpy of the two-phase water with Equation 2.1, where  $h_f$  and  $h_L$  are the enthalpy values of the fluid of interest and its respective saturated liquid state in  $\text{kJkg}^{-1}$ , respectively.

$$\zeta = \frac{h_f - h_L}{h_{fg}} \quad (2.1)$$

One could indicate that the phase change process of sublimation and deposition is the transition between the most and the least energetic state, and the latent heat equals that of vaporization and fusion combined. However, the application of sublimation and deposition is hardly ever achievable in engineering technology, as it almost exclusively occurs under extreme pressure and temperature conditions for most materials and substances.

## 2.2 Steam transport pipelines

In essence, the steam transportation network is anything regarding pipelines between the steam generator and heat user. This research is not so much interested in the design of pipelines, but more on the behaviour of steam within the pipelines.

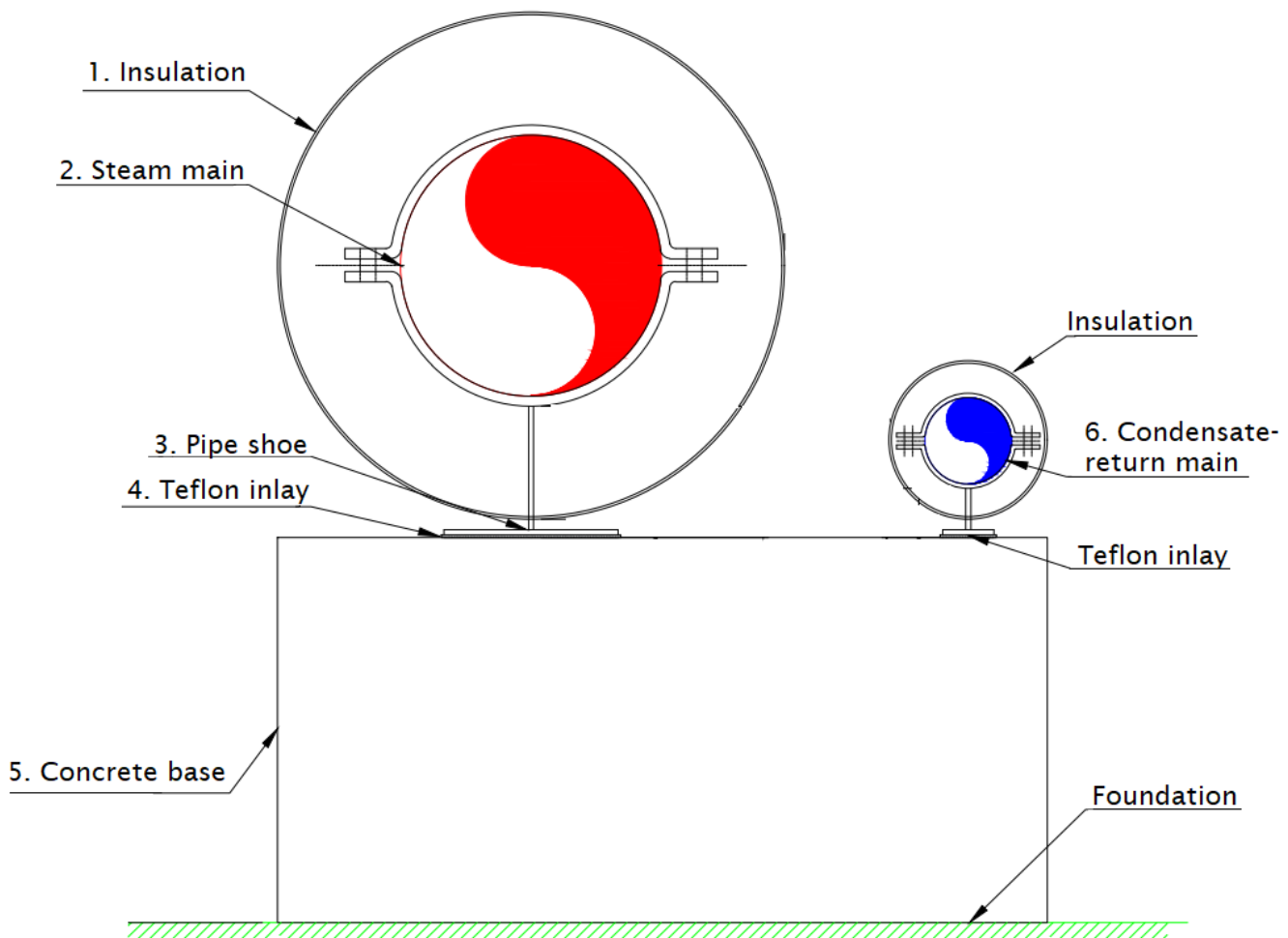


**Figure 2.3:** Cross-section of the steam & condensate pipeline [8]

However, some parameters of the steam pipeline are important in this regard. This section aims to cover some of the basics of steam transport pipelines engineering to provide a sufficient understanding of the subject.

A steam transport pipeline is generally above-ground and consists of a steam main and a separate condensate return line, as indicated in Figure 2.3. Both pipelines are generally made of carbon steel, and are insulated with mineral rock wool, indicated as number 1, to ensure minimal heat loss during the transportation of steam. To the pipelines, a so-called pipe shoe, indicated as number 3, is attached.

Essentially, the transportation network of steam is supposed to deliver steam with the right amount of heat and pressure to its heat users. Therefore, it is necessary to include pressure drops and heat losses when designing steam distribution pipelines. It is essential to choose the right dimensions for steam distribution pipelines. Oversized pipework generally leads to unnecessary costs and more heat losses. Undersized pipework usually means lower achievable pressure, and higher steam velocities, increasing the risk of erosion and water hammer.

### 2.2.1 Condensate & drainage

Although steam mains are thickly insulated, the steam will inevitably lose part of its heat to its surroundings. Therefore, a slight amount of steam will always condense. The accumulation of condensate in steam transport pipelines can cause problems such as low steam quality, which contributes to corrosion, erosion, and bad heat transfer efficiency of the system. Besides that, large amounts of condensate increase the risk of water hammer phenomena. Therefore, steam pipeline engineers have designed dewatering systems to remove inordinate amounts of condensate from the system. Figure 2.4 illustrates how these dewatering systems are used. Ac-

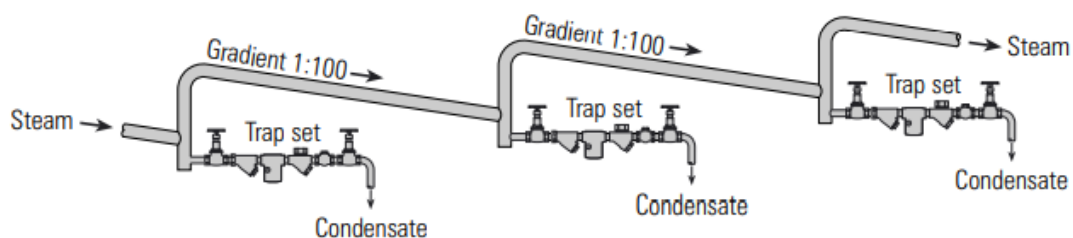


**Figure 2.4:** Steam pipe gradient to drain condensate [3]

According to the British Standard BS 806, a steam pipeline should be installed with a

minimum fall of 1 meter for every 100 m of pipe length in the direction of flow. This creates a consistent returning low-point in the pipeline, which allows for a convenient point to drain condensate [3].

### 2.2.2 Steam traps

At these specific draining points, a so-called steam trap is installed. Figure 2.5 depicts the steam trap system. Liquid condensate accumulates in the drain pocket and can manually be drained by the control valves on the drain lines. However, the drain line is only used at first stages of first time use since a large amount of condensate is expected in a relatively short time. At later stages, when virtually no liquid condensate resides within the pipeline, the drain valve should be closed at all times as it would start leaking high quality steam. Therefore, once the steam pipeline has reached this stage, the drain valves are closed, and the only way for liquid condensate to leave the system is through a steam trap, also indicated in Figure 2.5.

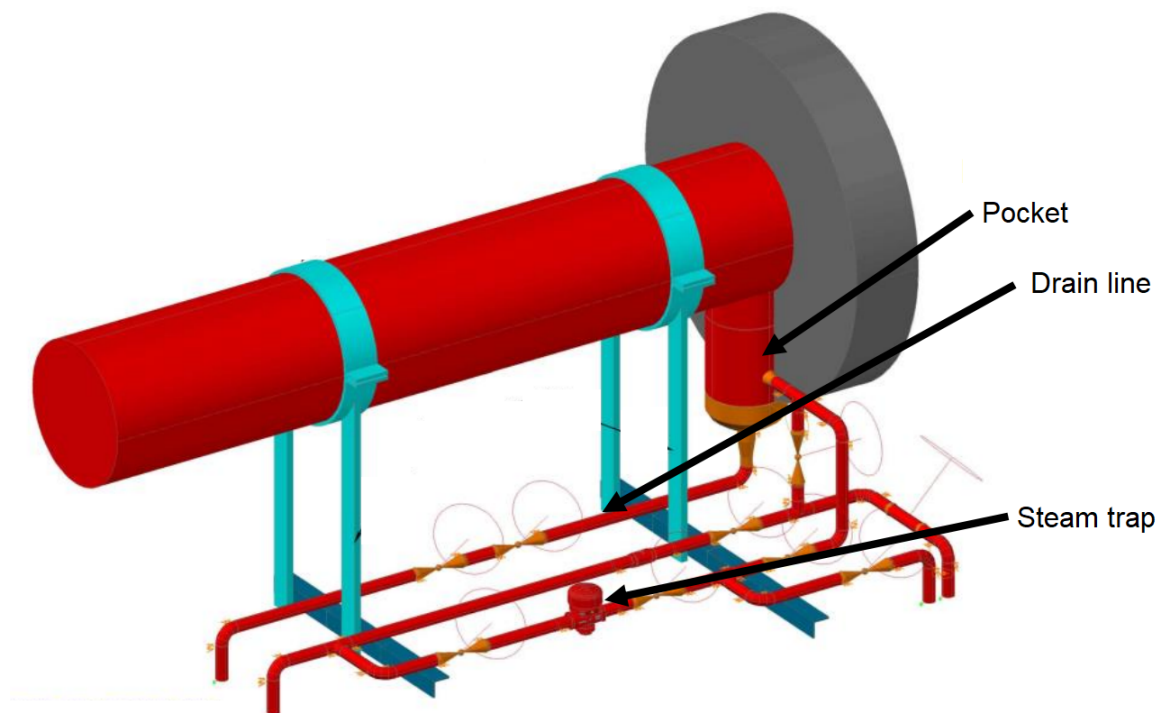


**Figure 2.5:** Typical steam trap [8]

A steam trap knows four basic variations, the thermostatic, mechanical, thermodynamic, and venturi steam trap. The thermostatic steam trap is operated by

changes in temperature of the fluid. As condensate accumulates and loses more heat, the temperature of the condensate will inevitably drop. The thermostatic steam trap will sense the reduced temperature, and let the condensate escape the system. Once the condensate is removed, steam reaches the trap, which then closes again due to the steam's temperature. A mechanical steam trap uses the density difference between the condensate and steam phases by using a spherical floater. As condensate hits the trap, the floater rises due to a smaller density than the condensate, allowing the condensate to exit the system. Once the condensate is drained, the floater will return to its initial place, blocking the steam from passing. The thermodynamic steam trap is arguably the most complex steam trap, it relies mostly on the formation of flash steam. Flash steam is steam that is re-evaporated from condensate as a result of pressure loss. This type of steam trap knows various implementations, such as the disc, impulse, or labyrinth steam traps. Lastly, the venturi steam trap, as one could understand from its name, lets condensate escape the system through a small orifice. This orifice is open at all times and uses no mechanical components. Therefore, the venturi type steam trap is extremely reliable since it contains no components that break or fail. However, since the orifice is open at all times, this type of steam trap continuously deals with losses in heat and pressure.

### 2.2.3 Warm-up & running loads

In the previous section, the use of steam traps was introduced. Naturally, these steam traps need to be designed properly. The manufacturers of steam traps state that there are different sizes of steam traps designed accordingly to the amount of expected condensate in a steam pipeline. Their understanding of condensate generation can be split up into two distinct categories [3].

- **Warm-up load**

Just after a steam pipeline is installed, it is initially cold. By running steam through the pipeline for the first time, the pipe is heated up to operating temperature. Heat, residing in the steam, is used to heat up the material of the pipe, the insulation, and the pipe shoe. Therefore, the steam loses heat and condenses into liquid water. The amount of liquid condensate that is generated, as a result of the start-up stage, is called the warm-up load. The warm-up load can either be estimated with calculation, or extracted from condensing tables provided by, among others, SpiraxSarco [3].

- **Running load**

As the pipeline reaches the steam temperature, the condensing rate drastically declines, and is, from this point onward, mainly determined by heat losses and steam

leaks. This is called the running load, and can be estimated with heat transfer calculations or obtained from condensing rate tables. Generally, the running load is calculated in kilograms of steam per hour per 50 meters of pipe distance at a certain pressure [3].

## 2.2.4 Load estimation & optimization

The common expressions for condensate load estimation, predominantly used by steam pipeline engineers, are given as Equations 2.2, 2.3 and 2.4. These equations are incorporated in many online calculators composed by companies specialized in steam engineering such as TLV and Techmatic inc. [9] [10].

$$M = M_{\text{wu}} + M_{\text{run}} \quad (2.2)$$

$$M_{\text{wu}} = \frac{(C_p + C_{\text{ins}}) * \Delta T}{\Delta h} \quad (2.3)$$

$$M_{\text{run}} = \frac{(\alpha D_o + \lambda \ln(\frac{D_o}{D_i})) \pi L \Delta T}{\Delta h} * t \quad (2.4)$$

Equation 2.2 is the governing equation for the total condensate load  $M$  in kg, consisting of a warm-up load and running load. The warm-up load, which was briefly mentioned in section 2.2.3, is predicted by Equation 2.3. The equation implies that the warm-up load in kg is determined by the heat that is required to heat up the pipe materials with a certain temperature increment, which is calculated with this temperature increment  $\Delta T$  in K times the heat capacities  $C_p$  and  $C_{\text{ins}}$  of the steel pipe and its insulation in  $\text{kJK}^{-1}$ , respectively. Dividing by the latent heat  $\Delta h$  in  $\text{kJkg}^{-1}$  gives the total warm-up load  $M_{\text{wu}}$  in kg. The running load  $M_{\text{run}}$  is mainly determined by the heat losses. The heat transfer coefficient at the outer surface of the pipe  $\alpha$ , in  $\text{Wm}^{-2}\text{K}^{-1}$ , includes convection and radiation. The conduction heat transfer coefficient  $\lambda$ , in  $\text{W/mK}^{-1}$ , represents the heat transfer across the layers of the pipe.  $D_o$ ,  $D_i$  and  $L$  are the dimensions of the pipe in m and  $t$  is the time that heat transfer occurs. Note that  $\Delta T$  is the temperature difference between the steam in the pipe and the pipe's surroundings here. Again, dividing by the latent heat, in this equation, gives the running load  $M_{\text{run}}$  in kg.

At the first time of use, the heat losses to the pipe's surroundings are insignificant compared to the rate of heat transfer to the pipe material since the steam mains are

insulated. Thus, the condensate load  $M$  is predominantly determined by Equation 2.3. Noticeably, the estimation for the warm-up load, used by steam engineers, and calculated with Equation 2.3, does not contain a time variable. In case one wants to model the warm-up load in real time, and expression for the mass of condensate per unit time is required.

During start-up, the pipe temperature ( $T_p$ ) and the insulation temperature ( $T_{ins}$ ) that increases with time. Therefore, the rate of warm-up load is presumed to be partially defined by the rate of heat transfer from the steam to the pipe, and from pipe to the insulation, and the distribution of the heat over the length and thickness of the materials. As mentioned in section 2.1.1, latent heat is the energy transferred to change the phase of a material or substance. In terms of steam condensation, this is best described as the enthalpy difference between the saturated liquid and saturated vapour states. This was mentioned before in section 2.1.1, and displayed in the T-h diagram in Figure 2.2. From the T-h diagram, it can clearly be seen that the latent heat is significantly higher at lower pressures. Essentially, this means that condensing water from the saturated vapour to the saturated liquid state, requires more energy at lower pressures. According to the warm-up load estimation in Equation 2.3, a higher enthalpy difference means a lower warm-up load. However, Figure 2.2 assumes constant pressure during the condensation process. Although the latent heat ( $\Delta h$ ) indeed depends on pressure, and co-dependently on temperature, both are inconsistent throughout the start-up of a steam pipeline. As steam enters an empty pipe, the pressure is only just slightly higher than atmospheric pressure, and the steam is cooled by the cold pipe. Over time, the pressure increases since the pipe gets filled. But at the same time, pressure lowers due to the change in volume as a result of condensation. Any change in pressure affects the condensing temperature as well. For these reasons, accurately describing or controlling the latent heat throughout the start-up process of a steam pipeline is problematic.

The example in Figure 2.2 displays an enthalpy change from saturated vapour to saturated liquid at constant pressures and temperatures. However, in section 2.2 it was mentioned that it is more beneficial for steam transport pipelines to run with superheated steam. However, the mentioned benefits are only in effect after the start-up phase. During start-up, the condensation process is used to heat up the steam main rapidly. This is desirable since this creates large amounts of condensate at the start of the process. This allows for substantial condensate removal in a short time, when the drain valves of the steam trap are still open. The heat transfer rate during condensation is significantly higher compared to the heat transfer of superheated steam. Therefore, saturated steam initially enters the steam main

and starts condensing as soon as it touches the colder walls of the steam mains. After the carbon steel of the steam main has reached operating temperature, superheated steam is used while the insulation of the steam main heats up further to operating conditions. The insulation slowly heats up, and some heat is converted into losses. This heat is taken from the steam and results in more condensate. However, the rate at which the steam condensates during operation is significantly lower.

The same equations used to calculate the warm-up load can be applied for the running load. However, since the pipe material is at saturated steam temperature, the carbon steel pipe is no longer included in the calculation. Equation 2.2 is still the governing equation, but  $M_{wu}$  equals zero since there is no temperature gradient between the pipe  $T_p$ , and the steam  $T_s$ . Therefore, the running load is mainly determined by the thermal resistance of the insulation and convectional heat losses at the outer surface of the pipeline. A significant part of the heat losses is a result of heat bridges. In essence, these are uninsulated parts of the pipeline that have a high heat transfer rate towards the surroundings of the pipeline. For example, in Figure 2.3, one could have noticed that the pipe shoe, indicated with number 3, is an uninsulated steel connection between the inner steel pipe and the pipe surroundings.

## 2.3 Horizontal Directional Drilling

One of the main issues of long distance SCS pipelines, is the obstacles that it may encounter. Obstacles such as roads, rivers, canals, dikes, or railways are common and many techniques are developed to cross these. In most cases, and especially pipelines that carry alternative fluids, obstacles are passed with drilling techniques. During this thesis, the writer has acquired knowledge on the various drilling techniques and their applications. However, since Rotterdam Engineering is interested in the application of HDD for steam transport pipelines, this technique is exclusively added to the report. In case the reader is interested, information on alternative drilling techniques for comparison can be found in Appendix A.

HDD is a drilling technique that starts drilling at ground level. As the first drill rod starts drilling into the ground, more drill rods are being linked with a screw connection, creating a drill string. The HDD process can be divided into three steps. First, a pilot bore is executed. A small bore diameter drill, navigated with the use of an above-ground tracker, is used to drill the initial channel. Secondly, the bore diameter is increased to widen the channel to the required size. Lastly, the pipeline is installed by pulling it through the channel with the drill string. This can either be one single

pipeline, or multiple pipelines bundled together.

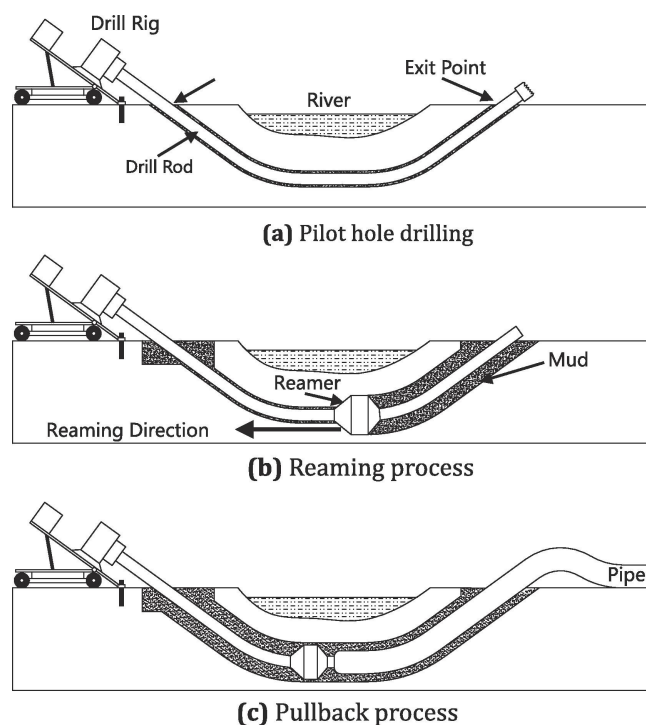


**Figure 2.6:** The HDD process [11]

The HDD technique is in particular suitable for long distance underground crossings with limited space at the drilling onset location, and when an open trench either is impossible or too expensive. On top of that, the active boring process can be steered with an above-ground navigation device, so that it is able to avoid impact with other existing pipelines or other infrastructure. Due to the fact that HDD is a trenchless technique, it is relatively environmental friendly, as it causes almost no damage to its environment. A downside to the HDD technique is the probable instability of the excavation channel. Depending on the type of soil, the empty excavation borehole, after the first or second bore, has the possibility to collapse. Potentially creating issues while dragging the pipeline through the channel [12] [11] [13].

Knowing that the steam in steam transport pipelines condenses, and this is usually solved with the use of steam traps, this creates two main issues that make the application of HDD steam transport pipelines problematic.

- **No space for dewatering system**

Since the HDD technique drills a passage, which size is more or less equivalent to the diameter of the pipeline, there is insufficient space to install the concurrently existing dewatering systems.

- **Accumulation of liquid condensate**

Due to the typical shape of the drilling process, an absolute low-point is created in the steam pipeline. This means that any liquid condensate that passes or emerges at this low-point, is expected to remain there throughout the use of the pipeline. To illustrate this, Figure 2.7 indicates this by calling it the “accumulation zone”. One can imagine that exceedingly amounts of accumulating condensate might cause issues, which will be addressed in the chapter 3.

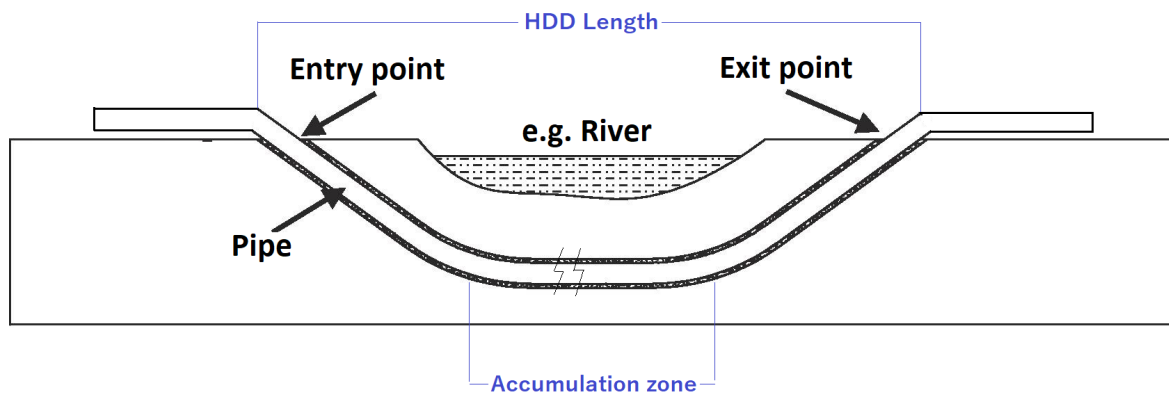


**Figure 2.7:** Illustration of an underground HDD passage and the accumulation zone

## 2.4 Concluding remarks

Now the baseline knowledge for this thesis has been established, the transition to the scientific literature can be made. To guarantee that the reader understands what this chapter encompasses, the writer wants to emphasize its most important conclusions with the following bullet points:

- The steam in steam transport pipelines undergo continuous condensation throughout its use.
- According to Equations 2.3 and 2.4, more mass condenses from vapour to liquid at a higher pressure in the pipeline due to a decrease in latent heat  $\Delta h$
- Vapour quality  $\zeta$  of a two-phase fluid is defined according to Equation 2.1.
- Any condensed liquid that passes through, or emerges in the HDD, accumulates at the lowest point of the HDD. This is called the accumulation zone and is indicated in Figure 2.7.

# Literature review

## 3.1 Water hammer phenomena

Water hammer is usually observed as loud thumping sounds in fluid pipelines, which is caused by the rapid increase or decrease of pressure in a pipeline due to changes in velocity of the fluid. It can occur in different forms, which can be divided into five different shock categories.

- Hydraulic shock
- Thermal shock
- Flow shock
- Differential shock
- Flooded shock

Hydraulic shock water hammer is the excessive acceleration of fluid due to rapid pump flow build-up, or opening valves too quickly. This is often easy to control, and therefore, it does not occur too often.

Thermal shock water hammer, also known as CIWH. This is the process when steam rapidly condenses and a volume collapses, this creates vacuum and the surrounding liquid is accelerated in its direction. This typically happens when isolated vapour bubble get surrounded by a cooler fluid [14]. The most common circumstances for CIWH to occur in steam-condensate systems, is when bubbles may end up below the condensate level. For example, when condensate is transferred from steam pipe to condensate line. Pressure is lowered in this process and flash steam may be formed and should always enter the condensate line above condensate level [15].

Flow shock water hammer is characterized by a high velocity, and high volume

of liquid condensate flowing through a pipe, that rapidly decelerates or changes direction. For example, due to a component such as an elbow, valve, or a flow meter. In SCS, the large amount of condensate usually emerges from steam flowing through a cold pipe, which was explained in section 2.2. When the condensate is insufficiently removed ahead of valves or other obstructions, flow shock may occur. Another cause is the absence of warm-up lines.

Differential shock water hammer is the water hammer as a result of condensate waves due to velocity gradient of the different phase fluids. The velocity of steam is generally ten times the velocity of the liquid, this will create waves. Once a wave is sufficiently large to seal the entire diameter of the pipe, the wave gets pushed to the same velocity as the gas. This causes severe forces on the pipes when the wave rapidly changes its direction or velocity [15].

Flooded shock, just as differential shock, creates a water hammer effect as a result of waves. However, with flooded shock water hammer, although it is probable, the waves do not necessarily originate from a velocity difference between different phases of a fluid. Nevertheless, the root cause is generally the under sizing of steam traps, resulting in the accumulation of condensate, which results in flooded conditions in equipment. For example, flooded shock water hammer is especially prevalent in condensing heat exchangers. Due to their confined space, accumulation of condensate is more expected to cause water hammer [15].

The more classical water hammer phenomena such as hydraulic flow and differential shock water hammer, that are caused by abrupt change in flow, have been researched abundantly. However, thermal shock water hammer or CIWH still requires major academical progress, and is still being investigated experimentally and numerically [14]. This chapter aims to illustrate what happens to steam pipelines when water hammer phenomena occur, with emphasis on CIWH.

### **3.1.1 Condensation-induced water hammer**

Thermal shock water hammer, or CIWH, is rather different from the other aforementioned phenomena. In contrast to the flow and differential shock, where water hammer effects are more related to the formation of liquid slugs, CIWH is not necessarily related to slug flow. This section intends to gather knowledge on the occurrence and repercussions of CIWH effects. There are a couple of specific circumstance where the risk of CIWH is expected to increase dramatically. However, a limited amount of

research on these topics can be found in the literature.

Although the occurrence of CIWH in steam transport pipelines has not been researched yet, a great deal of research on CIWH in smaller pipes is conducted in the field of Nuclear Power Plant (NPP) engineering. NPP engineers are reporting that CIWH events mostly occur within their gas removal units, steam generator headers, and heat-transfer tubes [14]. Opposed to steam pipeline applications, most of the experimental setups in the NPP field use subcooled counter-flowing liquid water. Therefore, the formation of large slugs that are maintained over a longer distances are unlikely to develop. In most NPP researches, CIWH phenomena are tested by gradually raising the subcooled liquid level.

Volkov et al. [14] reviewed several experimental setups that investigate the occurrence and severance of CIWH events in pipes. The experiments were all performed for NPP purposes. In detail, these experiments are different from steam pipeline applications. However, in both cases, the system deals with the accumulation of condensate (i.e., raising liquid levels), which is a realistic situation and a potential harmful scenario to steam pipelines. Especially considering the main goal of this research, the consequences of accumulating condensate can potentially disclose whether the HDD technique can be applied for steam pipelines or not.

Volkov et al. [14] investigated and summarized the results of CIWH measuring experiments performed at the RMK-2 test bench in Hungary, ROSA facility in Japan, Leipunski Institute of Physics and Power Engineering (IPPE) in Russia, Hamburg University of Technology in Germany, Xi'an Jiaotong University in China [14]. They created their own experimental setup and performed experiments at the new Elektrogorsk Research and Engineering Center (EREC) facility. Pressure peaks differentiate significantly between the various researches, varying from 0.8 MPa to 32 MPa. Along all experiments that were able to quantify CIWH effects, the events occurred as the liquid levels approached the top surface of the pipe.

A relation between the CIWH pressure peak and vapour pressure was observed at the ROSA facility in Japan [16]. The largest pressure peaks were measured at a vapour pressure of 1 MPa, and the intensity of the CIWH events appeared to decline at 4 MPa. Increasing the pressure above 7 MPa resulted in almost no or insignificant CIWH events. The largest peak pressure was measured at 32 MPa.

The experiments at IPPE [17], [18] showed that water hammer events constantly occur in a saturated vapour filled pipe, with subcooled liquid flowing through at strat-

ified flow. However, the pressure peaks were relatively low in this study, the largest pressure was measured at 0.8 MPa.

At the Hamburg University of Technology [19], the occurrence probability of CIWH was researched with varying liquid water temperatures and Froude numbers, determined from the liquid flow rate. They found that at a Froude number of 0.6 the highest CIWH occurrence probability was determined. Pressure peaks varied from 5 to 13.2 MPa.

From their own experimental setup, Volkov et al. [14] measured a maximum pressure caused by a CIWH event at 1.75 MPa. In their research, they observed that the pressure peak of a CIWH event has a relatively broad range over different studies, and is rather arbitrary of nature. They also noticed that the height of the CIWH pressure peaks varied with different vapour pressures, liquid water temperatures, and flow rates.

The main difference between the NPP experiments and a steam transport pipeline, is that in the latter application the liquid water is not subcooled and its level and flow are uncontrolled. So unless the liquid water level and flow parameters in steam transport pipelines can accurately be described over time, the results from the reviewed studies that include the variations in liquid water level and flow are not that beneficial in predicting CIWH events. The vapour pressure, however, is one of the few things that can be controlled. Thus, if the relation between vapour pressure and CIWH pressure peaks is consistent for steam transport applications, then this could be a significant analysis.

In case multiple slugs, that occupy the entire diameter of a pipeline, flow within a particular part of a pipeline, then a large gaseous volume, enclosed by the liquid slugs exists. If condensation of the enclosed gaseous volume starts, the slugs will accelerate towards each other due to the rapid change in volume, and ultimately lead to the water hammer effect. Although no research has been conducted for this specific circumstance, it is presumably the most disastrous type of water hammer that can occur in steam pipelines, as it involves the rapid condensing of a relatively large gaseous volume into liquid.

## 3.2 Flow regimes

In section 2.1.1 the fundamental states of matter, solid, gas, liquid, and plasma were briefly introduced. This section aims to investigate the coexistence and interaction of the fluid phases (liquid and gas) in steam pipelines by emphasizing the types of flow that can occur and how they can be predicted.

### 3.2.1 Two-phase flow regimes

The coexistence and simultaneously flowing of the liquid and gas phase in a confined space, is called two-phase flow, or multiphase flow. It is defined as the interactive flow between two or more specific phases. The distinct phases have unique thermodynamic and mechanical properties, and can therefore be worthwhile to analyse. Many two-phase flow applications exist, with various media, and for a diverse extent of industries. However, the most common medium in two-phase flow is water due to the fact that it is relatively cheap. The performed research on two-phase flow for steam transport pipelines is limited. However, other fields, and more fundamental researches, have conducted a great deal of research on the matter. Multiphase flow knows a wide variety of forms, making it challenging to deal with. Especially for engineering purposes, where spatial distributions and fluid velocities are generally important. Additionally, the local flow, especially in two-phase, has significant effects on pressure drops and heat transfer coefficients [20]

Vast amounts of research is dedicated to recognize different flow patterns for two-phase flows, and to identify their distinct characteristics. These flow patterns, or flow regimes, are categorized by the direction of flow relative to gravitational acceleration. In most textbook examples, this means just vertical or horizontal pipes and flow. More advanced researches sometimes investigate inclinations in two-phase flow pipelines. Steam transport pipelines, in most of their applications, are close to horizontal. In HDD applications, however, pipeline inclinations between 10 and 15° are common to reach specific depths. At the desired depth, the path of the HDD is mainly straight. Therefore, in the majority of the HDD, the flow regimes that are expected to be similar to the horizontal flow regimes. Figure 3.1 displays these typical horizontal flow patterns for two-phase flow. Note that the direction of flow is indicated by the arrow in the bottom right of the illustration. The two-phase flow regimes, depicted in Figure 3.1, are described from left to right, top to bottom, by the following bullet points.

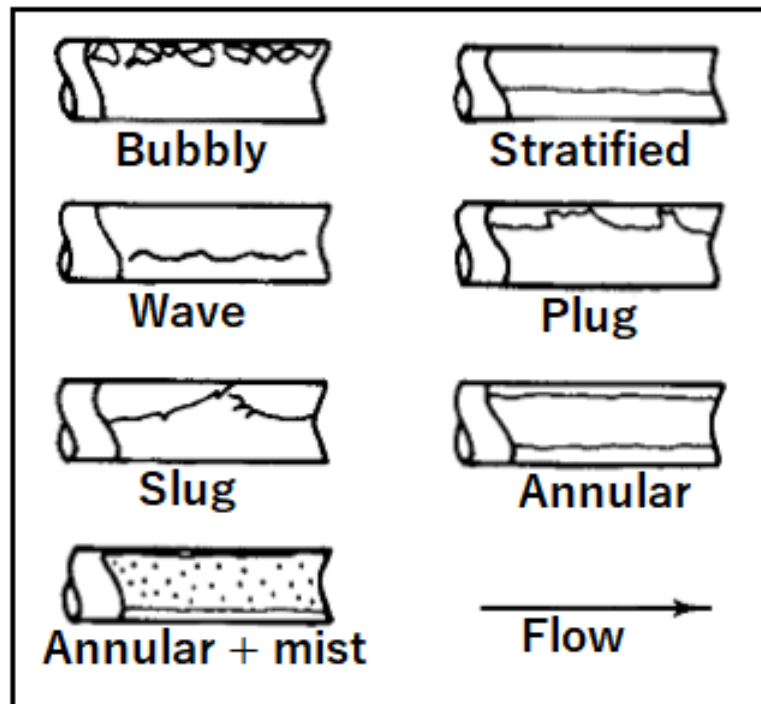


Figure 3.1: Two-phase flow patterns [20]

- **Bubbly flow**

At bubbly flow, nearly the entire flow of the pipe is liquid. Some gas bubbles co-exist within the top half of the pipe because of their buoyancy.

- **Stratified flow**

Stratified flow generally exists at lower flow velocities, where the liquid and gas are separated completely. The interface between liquid & gas phase are undisturbed, and can therefore be called fully stratified.

- **Wavy flow**

Wave, or wavy flow is essentially stratified flow, but with slight distortion at its interface, resulting in small waves. The waves in this regime more or less have the same height and do not show any disproportionate exceptions.

- **Intermittent flow**

Intermittent flow, which can be dissected into plug and slug flow, begins when the velocity of the gas is increased further with respect to wavy flow. The waves become sufficiently large that they reach the top of the pipe occasionally. Plug flow is when the majority of the flow is liquid, but contains elongated bubbles at the top of

the pipe, meaning the liquid flow at the bottom of the tube is continuous. Slug flow occurs at higher gas velocities. Liquid “slugs” are formed that cover the entire inner surface of the pipe. These slugs could also be described as waves with considerably large amplitudes.

- **Annular flow**

Annular flow commences at even higher gas flow rates, this creates an annular liquid layer around the perimeter of the pipe. However, due to gravitational forces, more liquid remains on the bottom than at the top of the pipe. The flow has a gaseous core in the middle of the pipe. This core may contain some liquid bubbles. At higher gas fractions, the top layer of liquid will evaporate first. As that happens, the flow regime then transitions to stratified-wavy flow.

- **Annular with mist flow**

Lastly, the mist phase is when the gas flow rate is sufficiently high that the shear force of the gaseous core breaks the liquid film apart. As a result, the liquid bubbles co-exist within the gaseous core as mist [20].

### 3.2.2 Flow pattern maps

A common way to predict the flow regime of a fluid in a channel is with a Flow Pattern Map (FPM). FPMs are practical tools that can work with various flow parameters as data to predict the flow regime of a fluid. According to Schmid et al. [21], two phase FPMs have the potential to accurately describe the occurring flow regimes in two-phase fluid flow in conduits. Although, one must take into account that FPMs will always contain uncertainties due to the gradual transition between said flow regimes [22].

In two-phase fluid flow engineering, three kinds of FPMs are prevalent. Adiabatic, evaporation, and condensation. Before condensation and evaporation FPMs were created, several adaptations of the adiabatic FPMs had to be developed first. These were also researched by the writer and are added to Appendix B if the reader is interested. For this research, however, FPMs for condensing applications are most relevant.

Adiabatic FPMs assume a flow without heat transfer. However, heat exchange can be a prevalent mechanism or even the intended purpose of a two-phase system. For example, in evaporators or condensers. Many FPMs exist for these heat

exchanging techniques for various kinds of fluids. The most common water hammer phenomena, which were discussed in the previous section, are a result of changes in flow regime. Specifically, in the intermittent flow regime, the most devastating types of water hammer can occur. Therefore, it is extremely valuable to create insight in what influences the transition of flow regimes, and the transition to intermittent flow specifically. However, FPMs that are designed explicitly for steam pipelines do not yet exist. But, a potential way to determine the flow regime in steam transport pipelines is to relate it to the existing applications of FPMs.

In section 2.2 it was established that steam transport pipelines continuously undergo condensation due to inevitable heat losses. Considering only three types of FPM exist within two-phase flow research, adiabatic, evaporation and condensation, the choice for a condensation FPM is self-evident. Although steam transport pipelines deal with varying heat transfer rates due to the warm-up and running phases, this should not matter for the FPM that one uses, since the condensation mechanism is prevalent in both cases.

There are two factors worth noticing when analysing flow patterns for condensation in horizontal tubes. Usually, the inlet circumstances in heat transferring tubes consist of cooling the superheated vapour which is entering the tube. Depending on the wall temperature, the process starts with a dry or wet wall. If the wall temperature is below the local saturation temperature, with corresponding local pressure, the steam starts to condense and a liquid film starts to form. This means that even in stratified flow patterns, the top half of the pipe will be covered with a liquid film due to condensation. This blurs the distinction between annular and stratified flow. Although the condensation starts rapidly, the process starts without any entrainment of liquid as the pipe is initially empty and filled with a gas. This results in three dominant condensation flow patterns in horizontal tubes [23].

- Annular flow (shear-controlled regime)
- Stratified-wavy flow (waves on liquid interface, liquid film at the top perimeter)
- Stratified flow (no waves, liquid film at the top perimeter)

To predict the transition from annular to stratified-wavy flow, Soliman proposed a method in 1982. This was later used by Dobson and Chato in 1998 to distinguish stratified and unstratified flows in their heat transfer model. However, this method showed some jumps in transition lines when passing through some Reynolds number conditions [23], and therefore, was concluded to be inaccurate in these areas.

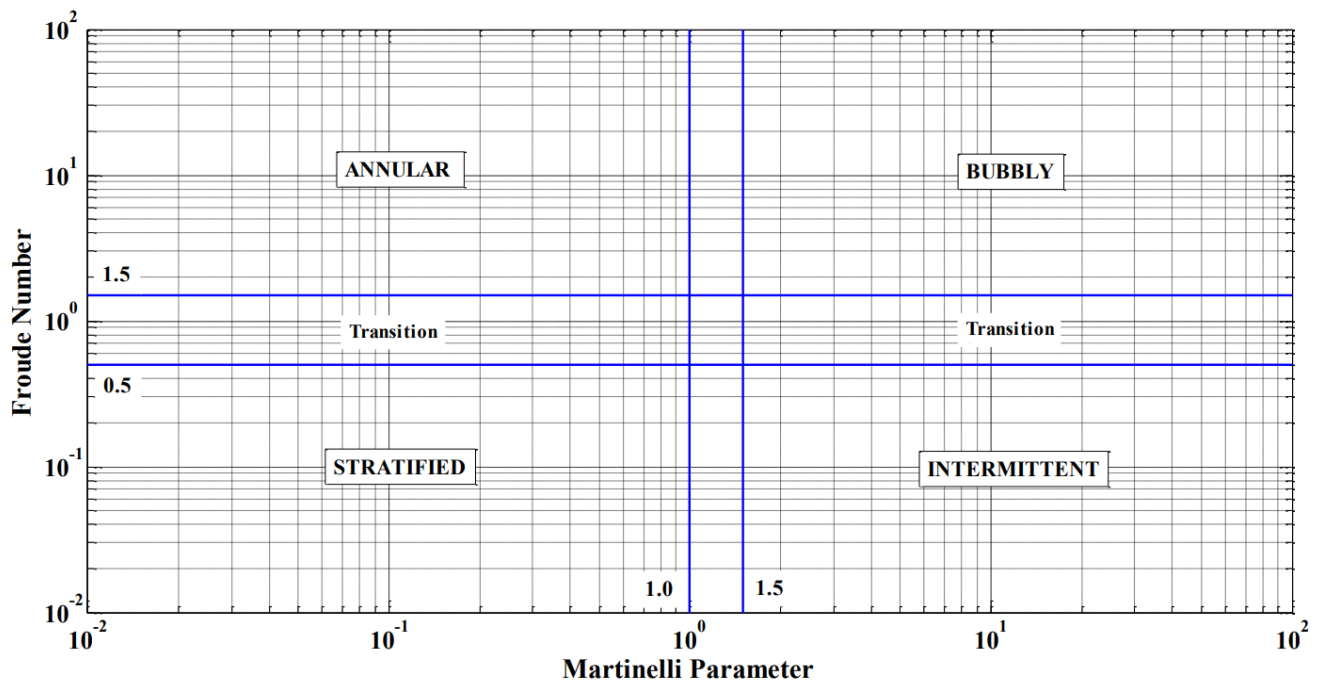


**Figure 3.2:** Two phase FPM for condensation in horizontal tubes by Breber et al. [24]

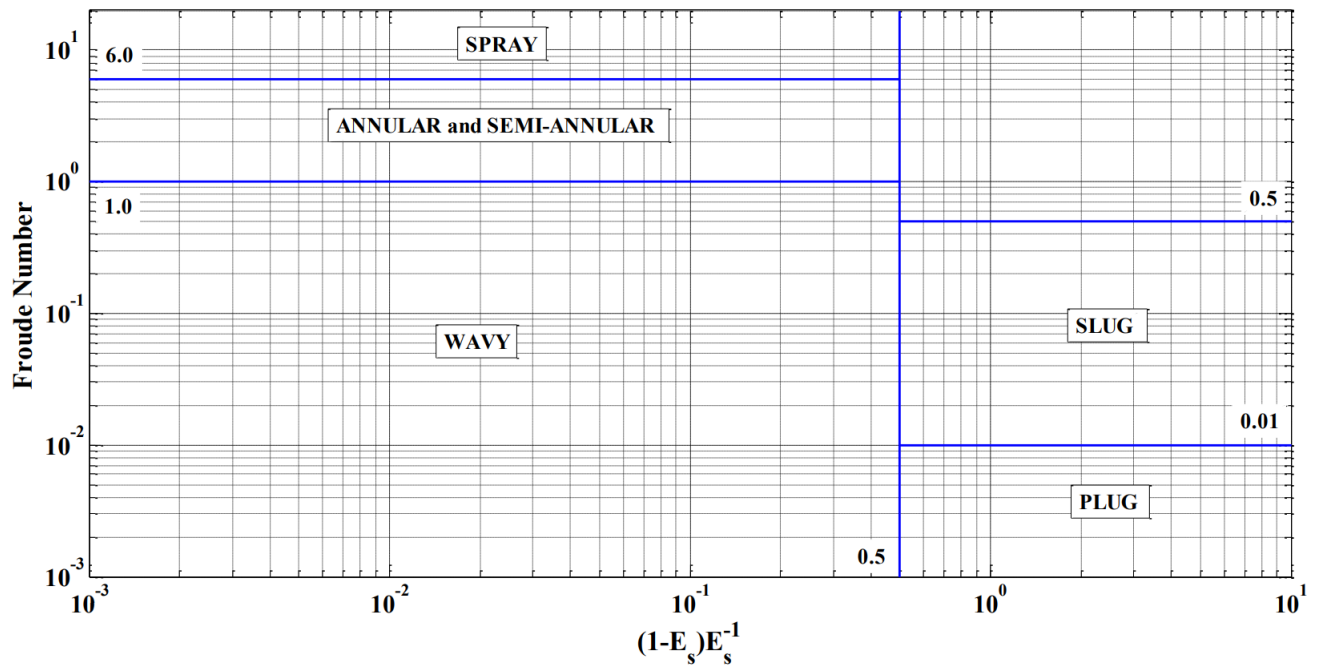


**Figure 3.3:** Two phase FPM for condensation in horizontal tubes by Tandon et al. [25]

Subsequent FPMs, developed by Breber et al. [24] and Tandon et al. [25] were

designed specifically for condensation of pure fluids in horizontal tubes, have proven to be significantly easier to work with due to their straight transition lines. This makes computer simulations of flow patterns substantially easier. Both FPMs are displayed in Figure 3.2 and 3.3, respectively.

The two FPMs in Figures 3.2 and 3.3 are the most updated two-phase FPMs on condensing pure fluids, and use the gas Froude number ( $Fr_G$ ), Martinelli parameter ( $X$ ) and void fraction ( $\epsilon$ ) on their axes [23]. To improve understanding of these parameters, their definitions and expressions are analyzed.

The Froude number represents the ratio between inertial and gravitational effects. In this case, it represents the effects of inertial and gravitational energy, described by Equation 3.1. The density of the liquid phase  $\rho_L$  in  $\text{kgm}^{-3}$ , inner diameter of the pipe  $D_i$  in m, and the gravitational acceleration  $g$  in  $\text{ms}^{-2}$  are considered constant. Variables  $\rho_c$  and  $u_c$  represent the density and velocity of the gas core of the flow in  $\text{kgm}^{-3}$  and  $\text{ms}^{-1}$ , respectively. However, Cioncolini and Thome [26] found that setting the gas core density  $\rho_c$  equal to the vapour density  $\rho_G$  showed sufficiently similar results compared to when a detailed expression for  $\rho_c$  is used. Therefore, the statement in Equation 3.2 can be used. Similarly, the velocity of the gaseous core  $u_c$  showed to be decently approximated dividing the superficial vapour velocity  $G_G$  in  $\text{kgm}^{-2}\text{s}^{-1}$ , by the vapour density  $\rho_G$ , leading to the statement in Equation 3.3 [26]. Substituting the statements of Equations 3.2 and 3.3 into Equation 3.1, results in Equation 3.4, which is considerably easier to use for modelling since it uses the superficial vapour velocity, and the liquid and gaseous densities.

$$Fr_G = \frac{\rho_c u_c^2}{(\rho_L - \rho_c)gD_i} = \frac{\text{inertial energy}}{\text{gravitational energy}} \quad (3.1)$$

$$\rho_c \approx \rho_G \quad (3.2)$$

$$u_c \approx \frac{G_G}{\rho_G} \quad (3.3)$$

$$Fr_G = \frac{G_G}{[\rho_G(\rho_L - \rho_G)D_i g]^{1/2}} \quad (3.4)$$

The Martinelli parameter  $X$  is a dimensionless number that describes the liquid fraction of a flowing fluid, commonly used within two-phase applications. According to Breber et al. [24], in condensing circumstances,  $X$  can be calculated with the

expression given in Equation 3.5. The expression does so by relating the pressure drop ( $dP$ ) in kPa over the axial distance of a fluid in a channel ( $x$ ) in m between the distinct liquid and gaseous phases, denoted as  $(dP/dx)_L$  and  $(dP/dx)_G$ , respectively.

$$X = \left[ \frac{(dP/dx)_L}{(dP/dx)_G} \right]^{1/2} \quad (3.5)$$

Similar to the Martinelli parameter, the void fraction ( $\epsilon$ ) is an expression of the liquid fraction in a two-phase flowing fluid. In fluid flow engineering, three different void fraction definitions are used. The local void fraction, cross-sectional void fraction, and the volumetric void fraction. Essentially, the local void fraction is described to be the same as the vapour quality ( $\zeta$ ), as described earlier in Equation 2.1. The cross-sectional void fraction is the area of gas that covers the cross-section of the tube, described in Equation 3.6, where  $A_G$  and  $A_L$  represent the areas that the distinct vapour and liquid phases cover in  $m^2$ , respectively.

$$\epsilon_{c-s} = \frac{A_G}{A_G + A_L} \quad (3.6)$$

The volumetric void fraction, instead of using the surface area, is described by the volumes of the respective phases. The expression is related to Equation 3.6, and therefore, looks similar to it. However, it is now described by  $V_G$  and  $V_L$  in  $m^3$ , by Equation 3.7.

$$\epsilon_v = \frac{V_G}{V_G + V_L} \quad (3.7)$$

Although the expressions for  $\epsilon_{c-s}$  and  $\epsilon_v$  appear straightforward in its use, it requires detailed information about the two-phase flow. To accurately determine the areas  $A_G$  and  $A_L$ , or volumes  $V_G$  and  $V_L$  for condensing flows, can be challenging. For that reason, estimation methods for the void fraction are used. The FPM in Figure 3.3 uses Smith's void fraction  $\epsilon_s$ , estimated with Smith's estimation method [27]. The estimation of void fractions will be discussed in more detail in section 3.4

### 3.3 Heat transfer in steam pipelines

From section 2.2 it was established that condensation of steam continuously occurs within steam transport pipelines. The start-up process of steam transport pipelines even knows distinct stages that are expected to vary in heat transfer. Therefore, the literature on two-phase heat transfer is reviewed, specifically for condensing applications.

#### 3.3.1 Shah's study on two-phase heat transfer

The phase change between liquid and gaseous water is either an exothermic or endothermic process, depending on its respective direction. Heat is exerted during condensation of water, so heat is transferred to another medium. The rate at which this heat is transferred remains a complex problem, that is generally solved by approximation in fluid engineering. This section primarily investigates the ongoing work of Mizra M. Shah [28] and intends to relate the use of his correlations to the presented thesis' case.

Mizra M. Shah [28] has continuously researched and developed heat transfer coefficient correlations for fluids condensing in pipelines. He intends to develop a correlation that is able to determine the heat transfer coefficient for all channel types, sizes, and inclinations. In his work, he presents two new theoretical correlations for the heat transfer coefficients in condenser pipes. Over the years, Shah [28] has constructed a wide-ranging database of other studies and uses this database to compare his work to. The database includes data from 33 fluids, hydraulic diameters ranging from 0.1 to 49 mm, various shapes and orientations, reduced pressures of 0.0008 to 0.946 and mass fluxes of 1.1 to 1400  $\text{kgm}^{-2}\text{s}^{-1}$ . The data are from 136 data sets and 67 sources.

Noticeably, Shah [28] has validated his correlation with data considering pipe diameters of up to 49 mm, while this thesis considers steam transport pipelines with diameters from 300 to 500 mm. Although the correlation has not been validated with for these diameters yet, Shah [28] states that the correlation can be used for all conventional channels, meaning all channels with a diameter larger than 0.3 mm. To understand this, it helps to look at the classification of channels that is used in Shah's work [28].

Shah [28] briefly mentions the classification of channels and refers to the work of Cheng and Mewes [29], which proposes criteria based on the effects of surface

tension and gravity on heat transfer. To analyse this, the Bond number is used as in Equation 3.8.

$$Bo = \frac{g(\rho_L - \rho_G)D^2}{\sigma} \quad (3.8)$$

The Bond number is a dimensionless number that relates the effect of gravitational forces per unit length, determined by gravitational pull ( $g$ ), density of the vapour and liquid phases ( $\rho_L$  and  $\rho_G$ ) and pipe diameter ( $D$ ), to the effects of surface tension  $\sigma$ , both in  $\text{Nm}^{-1}$ .

### 3.3.2 Effect of channel size

According to Cheng and Mewes [29], the classification of channels is correspondent to the following criteria:

$$\begin{aligned} \text{Microchannels} &: Bo < 0.5 \\ \text{Minichannels} &: 0.5 < Bo < 3.0 \\ \text{Macrochannels} &: Bo > 3.0 \end{aligned}$$

The classifications based on the Bond number imply the following:

1. Microchannels: negligible gravity effects
2. Minichannels: effects of gravity and surface tension present
3. Macrochannels: negligible surface tension effects

The surface tension of water is approximately  $0.072 \text{ Nm}^{-1}$  at room temperature. For this to correspond with a Bond number of 3.0, the diameter has to be relatively small, meaning that for any diameter beyond these criteria, the surface tension has no effect on the heat transfer coefficient. Shah [28] mentions that beyond the effects of surface tension and gravity, the diameter does not appear to be relevant to the deviations in his correlations. However, to justify this, further investigation is required.

### 3.3.3 Two-phase heat transfer coefficient

Since the presented model is a heat transfer model, heat transfer coefficients are the foundation of this model. In section 3.3, heat transfer coefficient correlations for condenser pipes by Shah [28] were introduced. The two-phase heat transfer coefficient  $\alpha_{TP}$ , in  $\text{Wm}^{-2}\text{K}^{-1}$ , is calculated for three separate regimes in which the heat transfer behaves differently, the governing equations for regime I, II and III are

given by equations 3.9, 3.10 and 3.11, respectively. This means that in regime I, the two-phase heat transfer coefficient is equal to a particular expression for this regime,  $\alpha_I$ . For regime II, the Nusselt heat transfer coefficient  $\alpha_{Nu}$  is added to amend for any surface tension effects. In regime III, the two phase heat transfer coefficient is solely determined by the Nusselt heat transfer coefficient  $\alpha_{Nu}$ . Naturally, all heat transfer coefficients are in  $Wm^{-2}K^{-1}$ .

$$\alpha_{TP} = \alpha_I \quad (3.9)$$

$$\alpha_{TP} = \alpha_I + \alpha_{Nu} \quad (3.10)$$

$$\alpha_{TP} = \alpha_{Nu} \quad (3.11)$$

In which regime the heat transfer occurs is determined by the relation between the effects of surface tension and inertia, which is also known as the dimensionless Weber number  $We$ . If the Weber number is calculated to be equal to the number of transitioning, an extra criterion for the dimensionless vapour velocity  $J_G$  is added. Equations 3.12 and 3.13 display the expressions for the Weber number and dimensionless vapour velocity, respectively.

$$We = \frac{G^2 D}{\rho_G \sigma} \quad (3.12)$$

$$J_G = \frac{\zeta G}{(gD\rho_G(\rho_L - \rho_G))^{1/2}} \quad (3.13)$$

The conditions for the regimes I and III are given by equations 3.14 and 3.15, respectively. All other values for  $J_G$  and  $We$  fall within regime II.

**Regime I:**  $We > 100$  and

$$J_G \geq 0.98(Z + 0.263)^{-0.62} \quad (3.14)$$

**Regime III:**  $We > 20$  and

$$J_G \geq 0.95(1.254 + 2.27 * Z^{1.249})^{-1} \quad (3.15)$$

After the regime is determined, the variables of the governing equations 3.9, 3.10 and 3.11 are to be substituted with equations 3.16, 3.17.

$$\alpha_I = \alpha_{LO} \left( 1 + \frac{3.8}{Z^{0.98}} \right) \left( \frac{\mu_L}{14\mu_G} \right) \quad (3.16)$$

$$\alpha_{Nu} = 1.32 Re_{LO}^2 - 1/3 \left[ \frac{\rho_L (\rho_L - \rho_G) g k_L^3}{\mu_L^2} \right]^{1/3} \quad (3.17)$$

Note that the two phase heat transfer coefficient for exclusively liquid flow  $\alpha_{LO}$  and Shah's [28] correlating parameter  $Z$  are required as well, which are calculated according to Equations 3.18 and 3.19.

$$\alpha_{LO} = 0.023 Re_{LO}^{0.8} Pr_L^{0.4} k_L / D \quad (3.18)$$

$$Z = (1/\zeta - 1)^{0.8} p_r^{0.4} \quad (3.19)$$

### 3.4 Void fraction estimation & vapour quality

The void fraction of two-phase flows is an important parameter in many engineering applications such as cooling, air conditioning, chemical processes, nuclear power system and of course, pipeline systems. Although the definition of void fraction was briefly introduced in section 3.2.2, this section attempts to investigate how void fractions can be estimated. For decades, predictive methods for vapour and gas void fractions in two-phase flow channel have been researched. Pietrzak and Płaczek [30] recently published a review article on the various kinds of predictive methods and in which circumstances to use them. Concurrently, there are three distinct main methods to predict void fractions in two-phase flows.

1. Homogeneous model
2. Phase slip model
3. drift-flux model

These three methods are based on different assumptions regarding the two-phase flow. The homogeneous model, for example, assumes that the two-phase fluid flows as a homogeneous mixture where both liquid and vapour flow with the same velocity. The homogeneous model estimates the homogeneous void fraction  $\epsilon_s$  with the expression displayed in Equation 3.20, using the vapour density  $\rho_G$  and liquid density  $\rho_L$  in  $\text{kgm}^{-3}$ , and the vapour quality  $\zeta$ , which was defined earlier by Equation 2.1.

$$\epsilon_h = \left[ 1 + \left( \frac{\rho_G}{\rho_L} \right) \left( \frac{1 - \zeta}{\zeta} \right) \right]^{-1} \quad (3.20)$$

The phase slip model introduces a phase slip coefficient that indicates a velocity inequality between liquid and vapour phases. However, over the years, more advanced expressions of the phase slip model have been developed. In its most generic form, the phase slip model is described as the expression in Equation 3.21. Notice that the expression is partially similar to homogeneous void fraction  $\epsilon_h$ , but that the dynamic viscosities ( $\mu_L$  and  $\mu_G$ ) are added here to account for the slip between the distinct phases.  $T$ ,  $b$ ,  $c$  and  $d$  are constants that are determined empirically.

$$\epsilon_{ps} = \left[ 1 + T * \left( \frac{\mu_L}{\mu_G} \right)^b \left( \frac{\rho_G}{\rho_c} \right)^c \left( \frac{1 - \zeta}{\zeta} \right)^d \right]^{-1} \quad (3.21)$$

Lastly, drift-flux model estimates void fractions based on the drift velocity  $u_{gm}$  and distribution parameter  $C$ . The drift velocity describes the relative difference between gas or vapour, and mixture velocities.

$$\epsilon_{df} = \frac{u_G}{Cu_m + u_{df}} \quad (3.22)$$

According to Pietrzak and Płaczek [30], for conventional channels, which means larger diameter channels where inertia overcomes the surface tension effects of two-phase flow, the phase slip and drift-flux models are most convenient to estimate the void fraction with. They explicitly refer to Smith's [27] and Steiner's [31] methods as phase slip and drift-flux model, and report mean absolute deviations of 11.9 and 12.6 percent from experiments in conventional channels, respectively.

### 3.4.1 Smith's void fraction estimation method

J.R. Thome, who was previously mentioned in section 3.2.2 for his work on FPMs together with A. Cioncolini [23], has published a data book for engineers on flow phenomena and heat and mass transfer [20]. In chapter 17 of Thome's book [20], he writes on the empirical use of void fraction equations. Thome [20] analyzes the practical use of various void fraction estimation methods, among which, Smith's phase slip approach, which Thome and Cioncolini [23] later use in their work on FPMs. Besides separated flow, Smith [27] assumes equal momentum fluxes in the two phases. With these assumptions, he expressed the velocity ratio ( $S$ ) as in Equation

3.23. The extreme values for  $e$ , which represents the fraction of liquid which resides within the vapour, are 1 and 0, which correspond to the homogeneous and fully separated flow assumptions, respectively. Setting  $e = 1$  would result in a velocity ratio of 1. Choosing  $e = 0$  results in the expression given by Equation 3.24.

$$S = e + (1 - e) \left[ \frac{\frac{\rho_L}{\rho_G} + e \frac{1-\zeta}{\zeta}}{1 + e \frac{1-\zeta}{\zeta}} \right]^{1/2} \quad (3.23)$$

$$S = \left[ \frac{\rho_L}{\rho_G} \right]^{1/2} \quad (3.24)$$

From the literature, which was discussed in section 4.5.2, it is found that the void fraction of a homogeneous mixture is defined as in Equation 3.20. Smith [27] extended on this expression with the velocity ratio, which resulted in Equation 3.25. Empirically, Smith [27] found that a value of  $e = 0.4$  showed the best agreement with data of void fraction experiments, and declared that his method guarantees an approximate maximum deviation of 10% from experimental results for two-phase flows, regardless of pressure, mass, velocity, flow regime and enthalpy change. Substituting  $e = 0.4$  into Equation 3.23 and subsequently, substituting  $S$  into Equation 3.25, results in a simplified form, as presented in Equation 3.26.

$$\epsilon_s = \left[ 1 + \left( \frac{\rho_G}{\rho_c} \right) \left( \frac{1-\zeta}{\zeta} \right) S \right]^{-1} \quad (3.25)$$

$$\epsilon_s = \left[ 1 + 0.79 \left( \frac{1-\zeta}{\zeta} \right)^{0.78} \left( \frac{\rho_G}{\rho_L} \right)^{0.58} \right]^{-1} \quad (3.26)$$

Since Smith's [27] void fraction estimation method, defined by Equation 3.26, depends mainly on the vapour quality  $\zeta$ , the relation between  $\epsilon_s$  and  $\zeta$  is plotted at different pressures in Figure 3.4. Noticeably, the void fractions are expected to be significantly lower at higher pressures.

### 3.4.2 Vapour quality

The vapour quality of a two-phase fluid  $\zeta$ , defined earlier by Equation 2.1, requires the enthalpy of the concerning fluid  $h_f$  in  $\text{kJkg}^{-1}$ . Although a two-phase flowing fluid can be perceived as a homogeneous mixture or a fully separated flow, the total

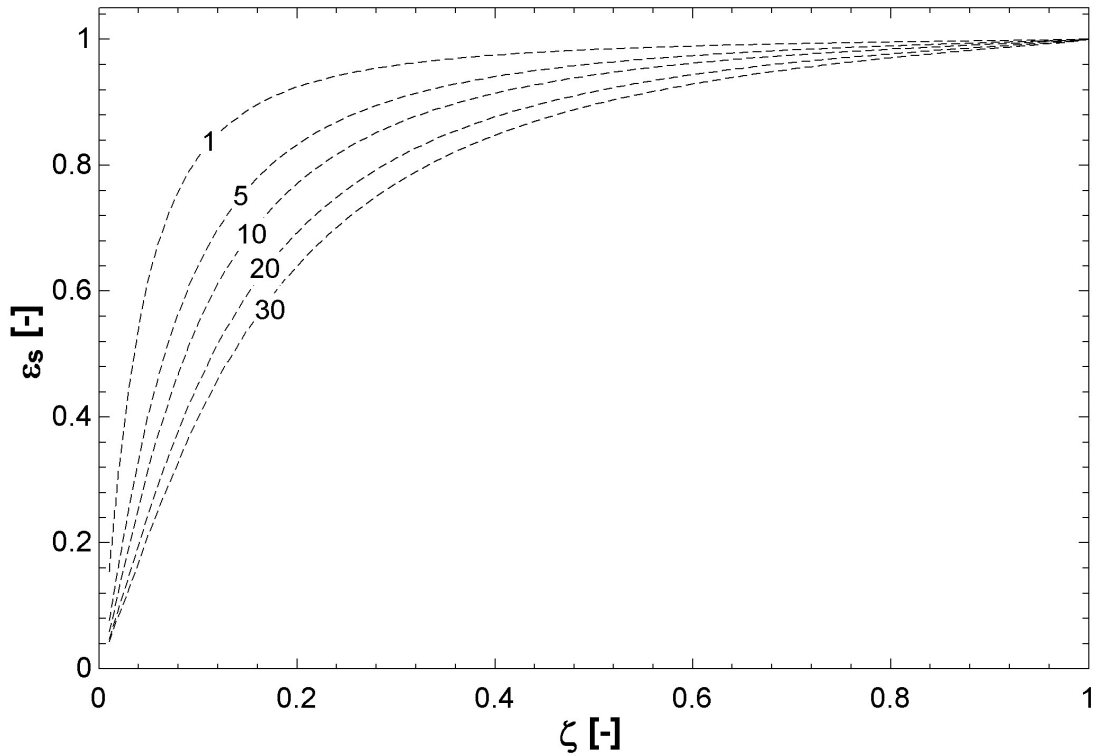


**Figure 3.4:** Smith's [27] void fraction  $\epsilon_s$  against  $\zeta$  at different pressures

enthalpy of the fluid  $h_f$  is defined by the expression of the mixture enthalpy, as in Equation 3.27.

$$h_f = \frac{m_G h_G + m_L h_L}{m_G + m_L} \quad (3.27)$$

In any type of flow, one could speculate what the distinct vapour and liquid enthalpy values  $h_G$  and  $h_L$  are. However, as one scrutinizes over this, it is evident that this would be a challenging problem to solve. Especially in the case of steam transport pipelines, where the masses of  $m_G$  and  $m_L$ , as far as research goes, are uncontrollable. Therefore, it would make sense to assume a more general expression of the total enthalpy of the fluid  $h_f$ , by dividing the total energy contents within the fluid  $Q_f$  by the total mass of the fluid  $m_f$ , as in Equation 3.28.

$$h_f = \frac{Q_f}{m_f} \quad (3.28)$$

## 3.5 Concluding remarks

Exploring the literature on large distance steam transport pipelines, it became promptly apparent that the research on this topic is limited. Most of the experiments that investigate flow properties of two-phase, pure fluid, condensing flow, showed little resemblance and used tubes in the range  $D < 0.1\text{m}$ . For that reason, more fundamental literature on two-phase fluid flow, such as its flow regimes, heat transfer and void fractions is reviewed. The idea of first time use of condensing fluids in pipelines is rarely mentioned in the literature and existing software of two-phase fluids virtually exclusively consider steady-state conditions, which composes a compelling research gap that this thesis wants to address using the literature reviewed in this chapter.

Besides indicating the research gap, the reviewed literature has also contributed to a couple of insights on water hammer phenomena that are potentially valuable to the field of steam transport pipeline engineering:

- CIWH has proven to occur consistently in experiments at liquid levels reaching the top surface of the channel
- The most disastrous cases of CIWH happen at system pressures between 1 and 4 MPa and are guaranteed to destroy steam transport pipelines with the commonly used dimensions
- The occurrence of water hammer effects are directly related to the liquid fraction within a pipeline
- According to the FPM by Tandon et al. [25], CS can occur from a void fraction of about 77% and lower

The bullet points above provide a solid framework in answering the first sub-research question: “How to demonstrate if CS or CIWH occurs?”, stated in section 1.2. Two-phase FPMs, as an accepted procedure in determining flow patterns of two-phase flows, can potentially provide an answer to whether CS occurs in the application of steam transport pipelines. However, to answer the second sub-research question: “How to mitigate condensate generation?”, fundamental research on the formation and behaviour of liquid condensate in steam transport pipelines is required.

Combining the existing research fields of condensing heat transfer, two-phase fluid flow properties and FPMs, the writer has decided to create a heat transfer

model that calculates liquid fractions and provides the parameters to use the FPM by Tandon et al. [25]. Additionally, the writer wants to introduce the first time use of steam transport pipelines to address the apparent gap in the literature.

# Methodology

## 4.1 General approach

As is mentioned in the concluding remarks of section 3.5, the first time use of steam pipelines is rarely addressed in the literature. The writer of this thesis wants to address this aspect for steam transport pipelines. In this chapter, a systematic approach is presented to model the first time use of steam transport pipelines using a heat transfer model. The model is built on the ascertained knowledge from the literature, and the background of the field of pipeline engineering.

### 4.1.1 Mathematical hierarchy of the model

To clarify how the heat transfer model is constructed, what its in- and outputs are and what the hierarchy of steps is, a schematic representation of the model is created to guide the reader in the thought process of the writer. The schematic representation is displayed as Figure 4.1.

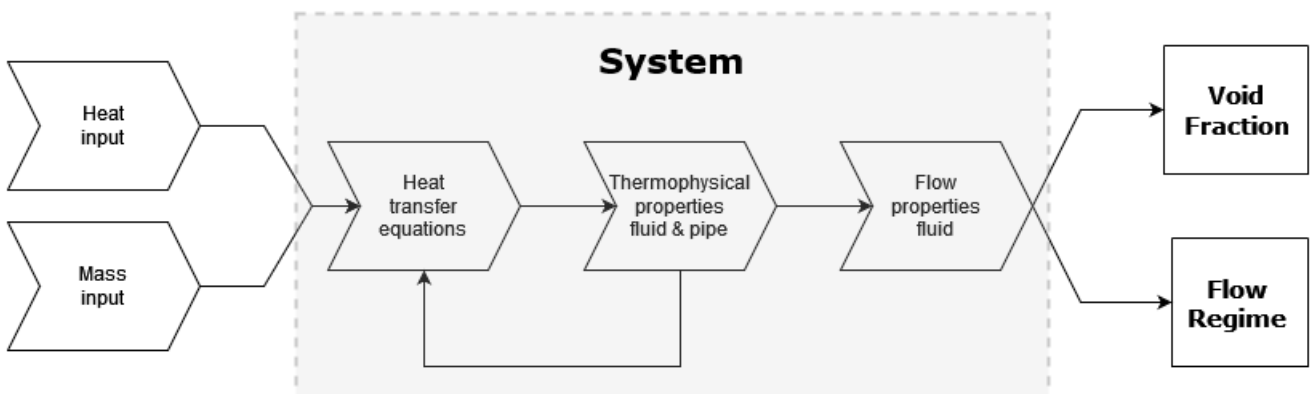


**Figure 4.1:** Schematic representation of the model

In Figure 4.1, the system can be considered as a steam transport pipeline. Heat

and mass are added to the system in the form of a fluid. The fluid exchanges heat with the system and the system exchanges heat with its surroundings, governed by heat transfer equations that will be specified later in this chapter. As heat values change, for both the fluid and pipe, their thermophysical properties change as well. For example, temperature  $T$  or density  $\rho$  increase or decrease. In turn, this influences the heat transfer rates determined by the heat transfer equations, indicated by the feedback loop. The thermophysical properties of the fluid also affect flow properties, which will be explained later. By continuously evaluating these thermophysical and flow properties, the model determines the void fraction of the two-phase fluid and its flow regime throughout the simulation process. That way, condensate levels and the flow regime are monitored over the duration of the simulation.

### 4.1.2 First time use of pipelines

Throughout this thesis, the first time use of steam transport pipelines has been referred to multiple times at this point. In sections 2.2.3 and 2.2.4, the consequences, in terms of liquid condensate, of the start-up process of steam transport pipelines, and how to calculate the condensate load, were brought to attention.

The start-up process of steam transport pipelines is a three-stage process that consists of:

1. Filling the pipeline by feeding with saturated steam at atmospheric pressure.
2. Building up pressure while feeding with saturated steam.
3. Increasing the feed to overheated steam and wait for insulation to reach steam temperature ( $T_s = T_p = T_{ins}$ ).

It has been stated that the research gap of filling pipelines is apparent. Stages 2 and 3 of the start-up process show more resemblance with the existing literature and overall knowledge within pipeline engineering. Therefore, stage 1 of start-up composes the largest threshold to investigating the entire start-up process. Stage 1 of start-up will, from here on, be referred to as "first-stage start-up". The writer of this thesis will address only the first-stage start-up of steam transport pipelines in this chapter.

## 4.2 Framework of the model

Before any equations are introduced, the framework of the model is established by addressing its constraints and assumptions. The writer does so by explaining each constraint and assumption. An additional section is created in the end to provide extensive reasoning for the assumptions that are made.

### 4.2.1 Constraints

The following constraints are discussed in this section:

- Physical shape, dimensions and material
- Constraints with regard to the HDD application

The constructed model represents a typical steam transport pipeline that connects waste incineration plants and other heat-using industries, most commonly executed at diameters varying from 300 to 500 mm, insulated with at least 100 mm of mineral wool insulation. The steel pipes are generally made of carbon steel and the exact dimensions and wall thickness is usually according to standardization by the Deutsches Institut für Normung (DIN). Since the most common diameters vary between 300 and 500 mm, three standardized pipe sizes are examined in this research, which are the DN300, DN400 and DN500 carbon steel pipes.

Keeping the main research question in regard, the model attempts to relate to the application of HDD for steam transport pipelines by abiding to the following set of rules:

- **No liquid condensate removal**

First and foremost, this means that no condensate can be removed from the modelled pipe. Underground dewatering systems are not applicable for the HDD technique yet, and one of the ambitions of this research is to disclose whether the application of HDD causes condensate related issues in the first place. Therefore, any liquid condensate that resides within the pipe, cannot be removed manually or by a steam trap.

- **Shape of the HDD**

Although the shape and underground path of HDD applications can vary significantly, a simplification of the shape is to be assumed in order to perform simulations in consistent circumstances. Figure 2.7, introduced earlier in section 2.3, resembles the most simplified shape of the HDD application, where a horizontal underground

path is considered. Note that this horizontal pipe length also resembles the lowest point in the HDD application, where any liquid condensate flowing through the HDD passage would accumulate. In Figure 2.7 this is indicated as the “accumulation zone”. Although this accumulation zone can also vary significantly based on the HDD application, again, for consistent simulation circumstances, the length of the accumulation zone indicated in Figure 2.7 is kept constant at 500 m.

- **Inclinations not included**

In addition to the previous bullet point, the indicated accumulation zone length in Figure 2.7 is also the modelled pipe length. This means that the inclinations of the HDD are not considered. Although the inclinations are expected to contribute to the build-up of liquid condensate and flow regime in the horizontal part, the effects of inclined flow are neglected in this model to avoid any overly complicated flow problems in this novel research. However, the effects should be accounted for in research after this thesis, which will also be recognized in the recommendations section of this thesis, section 7.2. Nevertheless, the accumulation zone length, indicated in Figure 2.7 is evidently the most crucial part to analyze. Note that this length, again, for consistent simulation circumstances, is kept at 500 m.

## 4.2.2 Assumptions

Throughout this chapter, a set of assumptions for the model is used. To maintain the readability of this text, the assumptions are listed, and the numbers are referred to throughout the text. In this section, the list of assumptions is provided, and the reasoning behind the assumptions is explained. The writer wants to clarify that, throughout this chapter, the water residing in a pipeline, in any state or number of phases, is referred to as “the fluid”.

*The following assumptions are made in this model:*

1. Any heat lost by the fluid is fully condensed into saturated liquid.
2. The fluid enters the pipe with saturated vapour quality at atmospheric pressure. Any arbitrary gas residing in the pipeline before start-up is replaced by the fluid, and they do not interact with each other.
3. The fluid maintains a cylindrical shape throughout first-stage start-up, as depicted in Figure 4.2.
4. Heat transfer between the fluid and the pipe only occurs over the fluid-pipe interface.

5. No pressure build-up for subsequent start-up stage, and no pressure variations within the pipeline are considered.
6. Frictional effects are ignored.
7. Temperatures of the pipe materials are uniform over its thickness and shift with respect to time due to heat transfer, meaning one temperature for the pipe's steel ( $T_p$ ) and one for the insulation ( $T_{ins}$ ), however, not constant.
8. Thermophysical properties of the fluid are considered to be uniform over its axial length  $x$ , and its distinct phases, correspondent to the illustrations in Figure 4.2.

*Extensive reasoning for respective assumptions is provided by the following list:*

1. This is a strong assumption that allows to estimate the amount of liquid that is created as a result of heat loss during condensation. Subsequently, this can be used to investigate consequences of the amount of condensate that is created. Whether this assumption is accurate, will have to be seen from the results of the presented model.
2. Assuming that the pipe is empty would imply there is a vacuum, which is not the case. During start-up of steam pipelines, the system is open and ambient air occupies the space in the pipeline. As steam enters the pipeline for the first time, the residing air is pushed out at the end of the system. No interaction means no mixing of the steam and air, which leads up to assumption #2.
3. In addition to assumption #1, the air initially residing in the pipeline is assumed to keep its shape. One could imagine a cylinder shaped steam volume pushing the air forward, without any extra resistance. This assumption helps to calculate the fluid-pipe interface area in a simple and consistent way by using the properties of the cylindrical shape.
4. The heat model needs a simplified expression for the heat that is transferred from fluid to pipe. Assuming that the fluid within the pipe has a cylindrical shape, it is convenient to calculate the area over which the heat is transferred without turning the model in an overly complex flow problem.
5. The start-up of steam pipelines can be dissected in stages, where pressure is raised between each stage. The first stage of start-up is at atmospheric pressure, which could already be concluded from assumptions #1 and #2. The presented model only includes first stage start-up, and therefore, does not include

pressure build-up of the fluid. Pressure drop as a result of frictional forces is a significant phenomenon. However, this is especially prevalent in long distance travelling, high velocity flowing fluids. Since the presented model aims to describe a relatively short distance of a HDD, and the start-up process deals with comparatively low mass flows, the pressure drop over the distance of a HDD is assumed to be negligible.

6. In assumption 5 the pressure drop due to frictional forces was already mentioned. The same goes for the fluid velocity, due to relatively low fluid velocities, frictional effects are not nearly as prevalent compared to higher velocities. On top of that, since steam transport pipelines are dealing with relatively large diameter pipes, the fluid-pipe interface area is significantly lower in relation to the fluid volume compared to smaller diameter pipelines. Therefore, the friction between fluid and the inside diameter of the pipe is assumed to be zero. This also means that heat transfer in the axial direction of the steel pipe and insulation is not considered.
7. Detailed temperature gradients over the thickness of the steel and insulation will not affect the overall heat transfer from fluid towards the atmosphere. Therefore, this is an easy simplification of the model that does not interfere with its outcomes.
8. This is an addition to assumption #3, assuming the pressure does not drop, automatically means that temperature stays constant for fluids that are in between saturation conditions. Therefore, the heat energy that resides within the fluid is what determines the remainder of its thermophysical properties. Although determining local energy levels of a fluid would be interesting to investigate, this is neglected for now.

### 4.3 First-stage start-up

Previously stated in section 4.1.2, the presented model only considers the first stage of start-up by feeding a pipeline with saturated steam  $T_{\text{sat}}$  and atmospheric pressure  $P_{\text{atm}}$  at the inlet. The simulation begins when saturated steam starts entering the pipe at the inlet, and ends when the entire modelled pipeline length is filled by the fluid. This process is expected to look similar to the schematically represented sequence of figures in Figure 4.2.

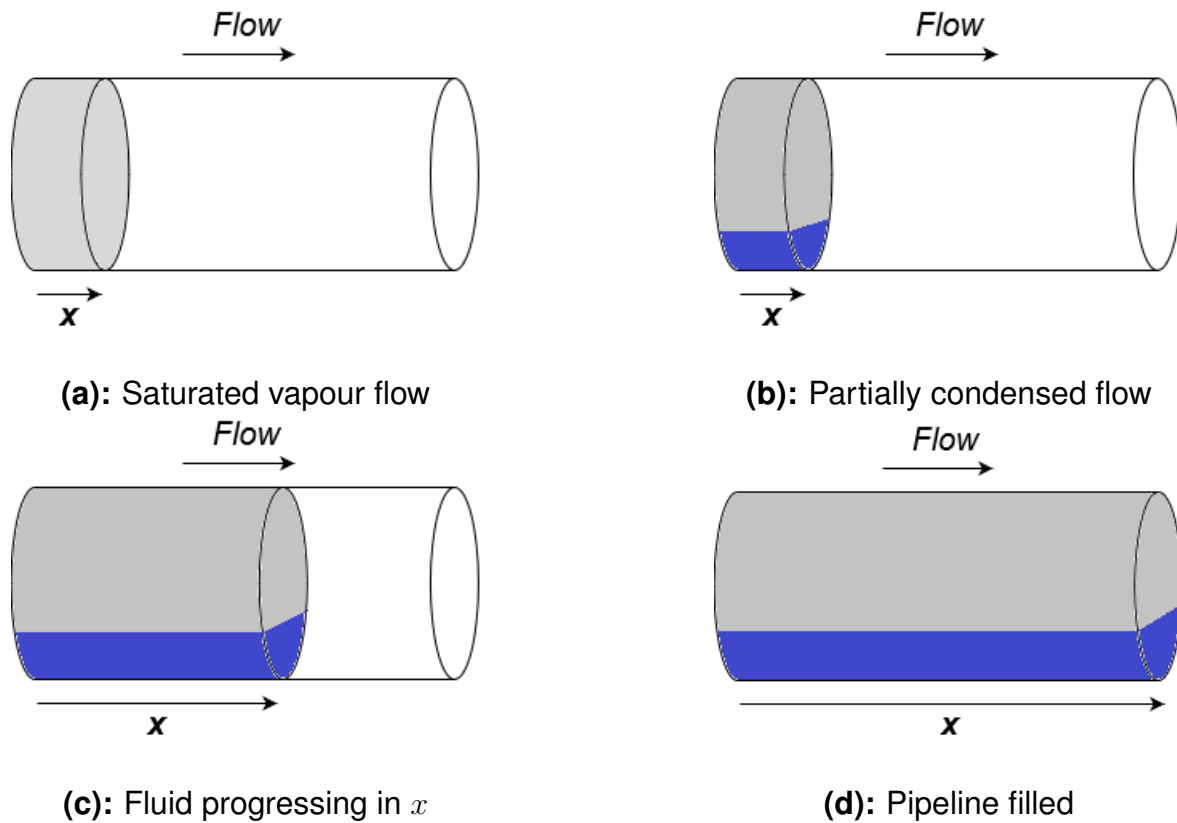


**Figure 4.2:** Filling process of first-stage start-up

In Figure 4.2a, saturated vapour is fed at the inlet of the pipeline, which starts filling the pipeline, and will be referred to as “the fluid” from here on. In Figure 4.2b, the fluid partly condenses, and a separated two-phase flow emerges. As more vapour is fed at the inlet of the pipeline, the two-phase fluid progresses through the pipe as in Figure 4.2c with an increasing horizontal coordinate  $x$ . Finally, after the pipe is entirely filled, as in 4.2d, the first stage of start-up has completed.

## 4.4 The heat transfer model

Now that the approach and the framework of the model are established, the equations that are used by the model to calculate its outcomes are introduced. The equations will be presented similarly with regard to the hierarchy displayed earlier in Figure 4.1. Starting off with the governing heat transfer equations of the heat transfer model.

### 4.4.1 Heat transfer equations

The typical cross-sectional heat transfer diagram of a steam transport pipeline is displayed in Figure 4.3. Heat is transferred from the hot steam towards the steel pipe,

indicated by the dark red arrow with annotation  $Q_1$  in Figure 4.3. Subsequently, heat is transferred from the steel pipe to the insulation, indicated by the light red arrows, annotated with  $Q_2$  in Figure 4.3. Finally, the heat is transferred towards the pipe's surroundings, indicated with the orange arrows and annotated with  $Q_3$ . To continuously calculate the heat transfer from the fluid towards pipe materials, and eventually, the pipes surroundings, time dependent expressions must be established.

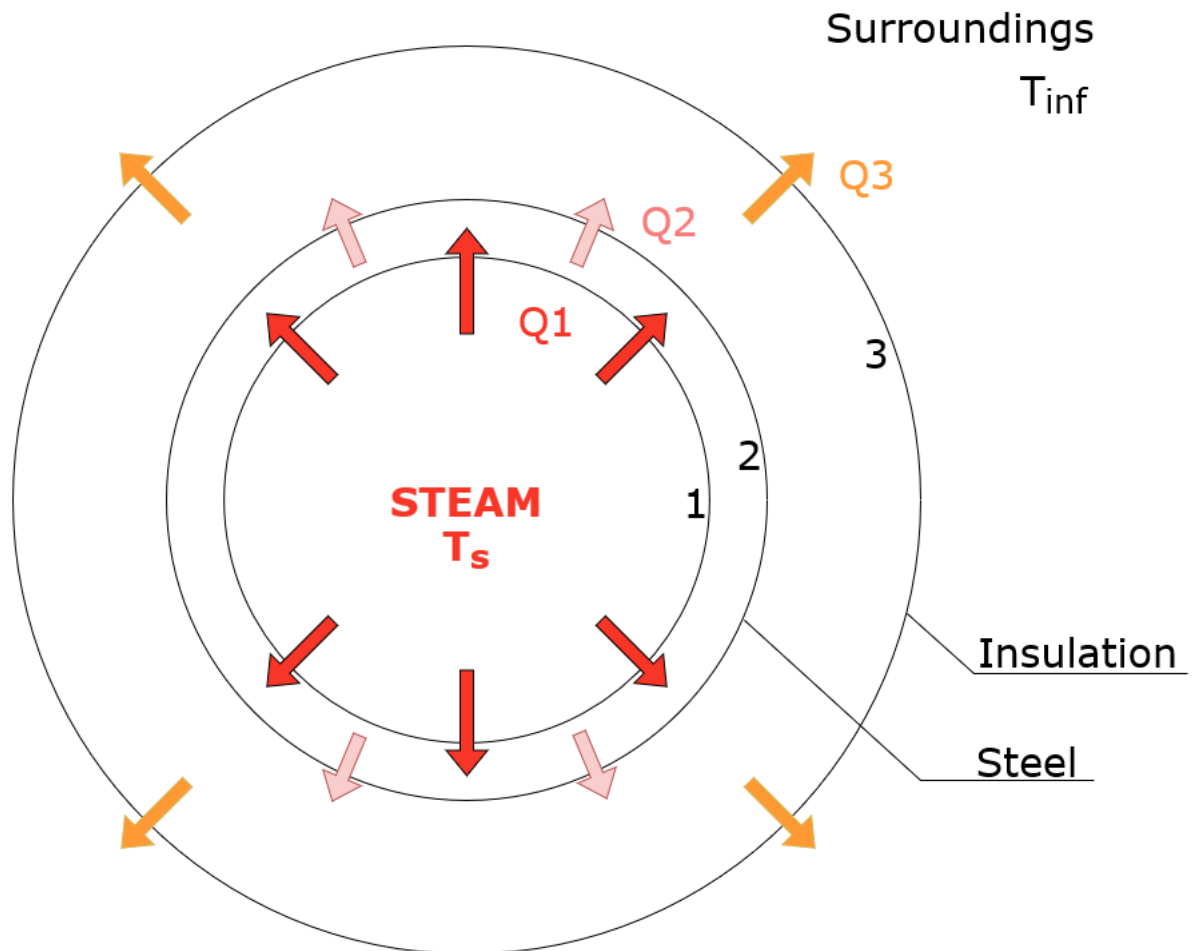


**Figure 4.3:** Cross-sectional heat transfer diagram of the steam pipeline

Equation 4.1 represents the heat transfer rate  $\frac{dQ_1}{dt}$  across the boundary indicated with index 1 in Figure 4.3. In other words, this is the heat transfer rate from the steam to the steel pipe in W. This heat transfer rate is determined by a two-phase heat transfer coefficient  $\alpha_{TP}$  in  $\text{Wm}^{-2}\text{K}^{-1}$ , a temperature increment between the steam  $T_s$  and the steel pipe  $T_p$  in K and the fluid-pipe interface area, determined by the inner diameter of the pipe  $D_i$  and the length of the fluid cylinder  $x$ , both in m. To clarify, the latter variable  $x$  corresponds with the earlier presented illustration in Figure 4.2.

$$\frac{dQ_1}{dt} = \alpha_{TP} * \pi D_i x * (T_s - T_p) \quad (4.1)$$

In Equation 4.2, the expression for the heat transfer rate  $\frac{dQ_2}{dt}$  from the steel pipe to the insulation layer is displayed, in W. In this case, the rate of heat transfer is determined by the conduction heat transfer coefficient of the insulation material  $k_{ins}$  in  $W/mK^{-1}$ , the axial length of the pipe and insulation  $L$  in m over which heat is transferred, and the temperature increment between the steel pipe and insulation,  $T_p$  and  $T_{ins}$  in K, respectively.

$$\frac{dQ_2}{dt} = \frac{2 * \pi * k_{ins} * L * (T_p - T_{ins})}{\ln\left(\frac{r_3}{r_2}\right)} \quad (4.2)$$

The third governing expression for heat transfer is added to Equation 4.3. This represents the heat transfer rate  $\frac{dQ_3}{dt}$  from the outer surface of the pipe towards the pipe's surroundings. Usually, the outer surface of the insulation is covered by a thin film of aluminium. This is negligible in terms of heat losses, and is therefore not included in the equation. In Equation 4.3, the heat transfer coefficient  $\alpha$  encompasses the heat transfer coefficient towards the surroundings of the pipe in  $Wm^{-2}K^{-1}$ . Naturally, this depends on what the outer surface of the pipe is in contact with. In the current simulations, an overall heat transfer coefficient for convection and radiation is used. The outer diameter of the pipe  $D_o$  and the axial length  $L$  determine the surface area over which heat is transferred in  $m^2$ , and finally, the expression is multiplied by the temperature increment between the outer surface temperature  $T_o$  and surrounding temperature  $T_\infty$  in K.

$$\frac{dQ_3}{dt} = \alpha * \pi D_o L * (T_o - T_\infty) \quad (4.3)$$

Note that the variables  $\alpha_{TP}$ ,  $x$ ,  $L$ ,  $T_p$ ,  $T_{ins}$  and  $T_o$  depend on time. How they depend on time will be explained in the following sections, and their mathematical expressions will be provided.

#### 4.4.2 Fluid-pipe heat transfer interface area

Before Equations 4.1, 4.2 and 4.3 can be integrated, expressions for the travelled distance of the fluid  $x$  and the length variable  $L$  have to be determined. The travelled

distance of the fluid,  $x$ , is described as the position of the front of the cylinder with respect to the inlet of the modelled pipe, while assuming the shape of the fluid with assumption 3.

The change of  $x$  with time is described by Equation 4.4. The bracket term in the equation represents the change in volume of the fluid in  $\text{m}^3\text{s}^{-1}$  based on the conservation of mass and assumption 1.

The mass flow  $\dot{m}$  divided by the initial density  $\rho_{\text{Gi}}$  is assumed to be a constant volume flow at the inlet of the pipe. This volume changes as the fluid starts to condense according to a condensing rate of  $\dot{Q}_1$  over  $\Delta h$  in  $\text{kg}\text{s}^{-1}$ . Dividing by the density of fully condensed liquid  $\rho_{\text{L}}$ , the term then complies with units of  $\text{m}^3\text{s}^{-1}$ . Due to mass conservation, the term is multiplied with a density ratio  $\rho_{\text{L}}/\rho_{\text{Gi}}$  to take into account the vapour mass that has condensed into liquid. Multiplying the entire expressions by  $1/A$ , where  $A$  is the circular surface area of the fluid head, describes the change in distance of the fluid  $\frac{dx}{dt}$  in  $\text{ms}^{-1}$ .

However, since the fluid loses heat, and its mass is conserved, the enthalpy of the fluid  $h_{\text{f}}$  in  $\text{kJkg}^{-1}$  decreases. Since the pressure is assumed to be constant, the consequence of declining enthalpy is a reduced vapour quality  $\zeta$ . Consecutively, this results in an increased density of the vapour  $\rho_{\text{G}}$ , and thus, reducing its volume. Equation 4.4 does not include this behaviour, therefore, after integration of Equation 4.4, the reduction in volume is amended for with correction distance  $dx$ , calculated by Equation 4.5, where  $V_{\text{G}}$  is the actual vapour volume and  $V_{\text{Gi}}$  the vapour volume at inlet properties. Applying the correction distance  $dx$  after integrating Equation 4.4 results in the expression for the travelled distance of the fluid  $x$ , displayed in Equation 4.6.

$$\frac{dx}{dt} = \frac{1}{A} * \left( \frac{\dot{m}}{\rho_{\text{Gi}}} - \frac{\dot{Q}_1}{\rho_{\text{L}} * \Delta h} * \frac{\rho_{\text{L}}}{\rho_{\text{Gi}}} \right) \quad (4.4)$$

$$dx = \frac{V_{\text{G}} - V_{\text{Gi}}}{A} \quad (4.5)$$

$$x = \int \frac{1}{A} * \left( \frac{\dot{m}}{\rho_{\text{Gi}}} - \frac{\dot{Q}_1}{\rho_{\text{L}} * \Delta h} * \frac{\rho_{\text{L}}}{\rho_{\text{Gi}}} \right) dt - dx \quad (4.6)$$

In Equations 4.2 and 4.3, the length variable  $L$  was used to define the heat transfer surface area from steel to insulation, and from the outer surface of the pipe to the

pipe's surroundings.

This length  $L$  in m represents the length of the pipe and insulation and cannot be equal to previously mentioned length  $x$  due to the fact that  $x = 0$  at the start of simulation. For example, if the pipe length would have a minimal value at the start of simulation, this would result in a minimal heat capacity of the pipe, and any heat transferred to the pipe would surge pipe temperature  $T_p$ . Therefore, the model calculates the length variable  $L$  as a multiple  $N$  of section lengths  $L_{sec}$ . This way, the heat capacity of the pipe, and the heat transfer surface area between steel and insulation, will increase accordingly while the fluid progresses through the pipe.

The multiple  $N$  is calculated by dividing the length of the fluid cylinder  $x$  by the section length  $L_{sec}$  and rounding to the nearest higher integer. In EES, rounding to the nearest higher integer can be done with the ceiling function (`ceil`). Equations 4.7 and 4.8 display how  $N$  and  $L$  are calculated, respectively.

$$N = \text{ceil}\left(\frac{x}{L_{sec}}\right) \quad (4.7)$$

$$L = N * L_{sec} \quad (4.8)$$

### 4.4.3 Heating up of the pipe materials

Now that all dimensions of the pipeline are defined, their heat capacities can be determined. Equations 4.9 and 4.10 provide the expressions for the heat capacities of the steel pipe and the insulation material in  $\text{JK}^{-1}$ , respectively. Note that  $L$  represents the length of both the steel pipe and its insulation in and increases with time, as described in the previous section. Constants  $\rho_s$  and  $\rho_{ins}$  are the densities,  $c_{p-s}$  and  $c_{p-ins}$  the specific heat capacities in  $\text{kgm}^{-3}$  and  $\text{Jkg}^{-1}\text{K}^{-1}$  for the steel pipe and the insulation, respectively.

$$C_{st} = \pi * (r_2^2 - r_1^2) * L * \rho_s * c_{p-s} \quad (4.9)$$

$$C_{ins} = \pi * (r_3^2 - r_2^2) * L * \rho_{ins} * c_{p-ins} \quad (4.10)$$

Then, all variables are defined to determine the change in temperature with time  $\frac{dT_p}{dt}$  and  $\frac{dT_{ins}}{dt}$  in  $\text{KS}^{-1}$  for the steel pipe and insulation with Equations 4.11 and 4.12,

respectively.

The change in temperature of the steel pipe,  $\frac{dT_p}{dt}$  is determined by the net heat that has been added to the steel. Figure 4.3 illustrates how heat is transferred to the steel pipe over boundary 1, and how heat leaves the steel over boundary 2. Using the earlier defined heat transfer rate expressions in Equations 4.1 and 4.2, which define the heat transfer rate in  $W$ , and dividing by the heat capacity in  $JK^{-1}$ , results in the temperature change with time in  $Ks^{-1}$ .

$$\frac{dT_p}{dt} = \frac{1}{C_s} * \left( \frac{dQ_1}{dt} - \frac{dQ_2}{dt} \right) \quad (4.11)$$

The same can be said for  $\frac{dT_{ins}}{dt}$ . However, the heat capacity and heat transfer rates must be replaced correspondingly, resulting in Equation 4.12, also in  $Ks^{-1}$ .

$$\frac{dT_{ins}}{dt} = \frac{1}{C_{ins}} * \left( \frac{dQ_2}{dt} - \frac{dQ_3}{dt} \right) \quad (4.12)$$

## 4.5 Thermophysical fluid properties

The previous section described how heat is transferred from the fluid to the pipe materials, eventually, to the pipe's surroundings. Referring to the overview in Figure 4.1, the heat transfer equations and the thermophysical properties of the pipe are now defined. The next step of the model is to determine the thermophysical properties of the fluid.

### 4.5.1 Heat contents & vapour quality

A lot of two-phase fluid properties are determined from the vapour quality, which was defined earlier in Equation 2.1. From the literature, it was found that void fractions can be estimated accurately by just knowing the vapour quality of a two-phase fluid. This alone shows that the vapour quality is a powerful property in two-phase flow problems.

From Equation 2.1 it is known that the vapour quality is determined with the enthalpies of the fluid in consideration  $h_f$  and the liquid part  $h_L$ , and the latent heat  $h_{fg}$ . Since the model considers first-stage start-up only, and therefore, the pressure is maintained constant throughout the process,  $h_L$  and  $h_{fg}$  are known constants from

steam tables, or in this case, the EES database. However, the enthalpy of the fluid  $h_f$  in  $\text{kJkg}^{-1}$ , must be calculated.

In section 3.4.2, it was established that  $h_f$  is actually the definition of the mixture enthalpy, which is defined by Equation 3.27. However, it was stated that the definition is difficult to apply in this case. Therefore, the more general expression in Equation 3.28 is used, which requires the total heat contents of the fluid  $Q_f$  in kJ and the total mass of the fluid  $m_f$  in kg.  $Q_f$  can be determined by taking the total amount of heat added to the fluid  $Q_{in}$  and subtracting the heat that is *taken* from the fluid  $Q_1$ , both in kJ, displayed by Equation 4.13.

$$Q_f = Q_{in} - Q_1 \quad (4.13)$$

The mass flow  $\dot{m}_f$  and the inlet quality of the steam are practically the only variables that are controllable in steam transport pipelines, which allows for control over  $Q_{in}$ . To determine  $Q_{in}$ , constant mass flow  $\dot{m}$  in  $\text{kg s}^{-1}$  with inlet enthalpy  $h_i$  in  $\text{kJkg}^{-1}$ . This leads to the expression for  $Q_f$  in Equation 4.14 in kJ. Various mass flows are evaluated in this research, however, the inlet enthalpy  $h_i$  is chosen to be constant at saturated vapour quality.

$$Q_{in} = \dot{m} * h_i \quad (4.14)$$

The heat that is *taken* from the fluid  $Q_1$ , explained earlier in Figure 4.3 as the heat that crosses the boundary from fluid to the steel pipe, is calculated through integration of the first governing heat transfer equation 4.1. Subtracting  $Q_1$  from  $Q_{in}$  then gives  $Q_f$  according to Equation 4.13. Referring back to Equation 3.28, the total mass of the fluid  $m_f$  is easily acquired from the mass flow  $\dot{m}$  during simulation, since one would track the simulation time. Then, the enthalpy of the fluid  $h_f$  is defined and allows for the calculation of the vapour quality  $\zeta$  according to 2.1.

Two variables depend on the vapour quality  $\zeta$ :

1. Two-phase heat transfer coefficient  $\alpha_{TP}$
2. Vapour density  $\rho_G$

The two-phase heat transfer coefficient  $\alpha$  was introduced earlier in Equation 4.1, and its underlying equations were provided in section 3.3. Although the vapour density  $\rho_G$  has not been defined yet, the vapour volume  $V_G$  was used before in Equation 4.5 to account for the change in volume of the fluid due to condensation. It may be self-evident that the vapour volume  $V_G$  in  $\text{m}^3$  depends on the vapour density  $\rho_G$  in  $\text{kgm}^{-3}$  and is determined by Equation 4.15.

$$V_G = \frac{m_G}{\rho_G} \quad (4.15)$$

Vapour density  $\rho_G$  is determined with a function in EES that looks up the value in steam tables using the pressure  $P = P_{\text{atm}}$  and the vapour quality  $\zeta$ . To explain how the mass of the vapour is determined, the writer wants to re-emphasize a couple of things that were introduced earlier in this thesis.

In section 2.2.4, a practical approach to calculate the total amount of condensed fluid as a result of the warm-up load was presented. This approach was included as one of the main assumptions of the model as assumption 1, stating that any heat lost by the fluid condenses to a saturated liquid state. Subsequently, this was applied in Equation 4.4. This means that the mass of the liquid  $m_L$  is defined through assumption 1. Creating a separate expression for the condensation rate  $\frac{dm_L}{dt}$  in  $\text{kgs}^{-1}$  results in Equation 4.16.

$$\frac{dm_L}{dt} = \frac{1}{h_{fg}} \frac{dQ_1}{dt} \quad (4.16)$$

Integrating the expression in Equation 4.16 results in the expression for the mass of the liquid  $m_L$  in kg, as in Equation 4.17:

$$m_L = \int \frac{1}{h_{fg}} \frac{dQ_1}{dt} dt \quad (4.17)$$

Since the model describes the first-stage start-up process, the mass of the fluid that enters the pipeline is conserved for the duration of the simulation. This equates the total mass of the fluid  $m_f$  to the sum of the masses of vapour and liquid phases,  $m_G$  and  $m_L$ , according to Equation 4.18.

$$m_f = m_G + m_L \quad (4.18)$$

Knowing the total mass of the fluid  $m_f$  from the mass flow  $\dot{m}$  in  $\text{kgs}^{-1}$  and simulation time  $t$  in seconds, one only needs to substitute the expression of  $m_L$  of Equation 4.17 into Equation 4.18 to determine  $m_g$ . Lastly, the vapour volume  $V_G$  can be calculated.

### 4.5.2 Void fraction

As a consequence of assumption 1, the simulated volumetric void fraction  $\epsilon_v$  is calculated with the new vapour volume  $V_G$  and the volume of the condensed liquid  $V_L$  according to its definition as in Equation 3.7.

In section 3.4.1, Smith's void fraction estimation method [27] was introduced alongside the work of J.R. Thome [20], where Smith's void fraction expression for  $\epsilon_s$  was denoted by Equation 3.26. This is convenient to calculate with the heat transfer model since it is exclusively determined by the vapour quality  $\zeta$ , because  $\rho_G$  is acquired from the EES database knowing pressure and vapour quality. It was indicated earlier that  $\epsilon_s$  is used in two-phase FPMs. However, since  $\epsilon_s$  is a validated method of calculating void fractions, it can also be used to confirm the validity of  $\epsilon_v$ , and therefore, that of assumption 1.

## 4.6 Determining flow patterns with FPMs

In section 3.2.2, the use of FPMs was introduced. From the investigated FPMs, the FPMs designed specifically for condensation of pure fluids in horizontal tubes, added as Figures 3.2 and 3.3, seemingly are most capable of determining flow regimes during start-up of steam pipelines.

Considering these two options, the latter is most convenient for the same reason that was mentioned in the end of the previous section. The reason being that the FPM by Tandon et al. [25] in Figure 3.3 uses Smith's void fraction estimation instead of the Martinelli parameter. Smith's void fraction estimation is performed with the vapour quality of the fluid, which is conveniently obtained by the heat transfer model.

The Martinelli parameter uses the relative pressure gradients between the vapour and liquid phases in the vertical direction, which would be in conflict with assumption 5, which is a crucial simplification of the system for assumption 1 since pressure fluctuations would influence the latent heat of the fluid. Besides that, other parameters that are fundamental to the presented model, such as the heat transfer coefficient  $\alpha_{TP}$  and position of the fluid  $x$ , require the vapour quality in their calculations anyway. Therefore, the use of an extra parameter, such as the Martinelli parameter, is redundant in this case. Besides that, the FPM by Tandon et al. [25] is a more recently updated version that also distinguishes specific flow patterns instead of using categorization names. For example, categorizing slug and plug flow as intermittent flow.

Using Tandon et al.'s [25] FPM as in Figure 3.3, to determine which flow regime the two-phase flow occurs, Smith's void fraction ( $\epsilon_s$ ) and the Froude number for the gas phase ( $Fr_G$ ) need to be calculated by the heat transfer model. The x-axis is determined by the smith relation, as in Equation 4.19. The y-axis by the Froude number as in Equation 3.4. Note that Equation 3.4 was previously studied in section 3.2.2. However, for readability purposes, the Equation is repeated here as Equation 4.20.

$$s = \frac{\epsilon_s - 1}{\epsilon_s} \quad (4.19)$$

$$Fr_G = \frac{G_G}{[\rho_G(\rho_L - \rho_G)D_i g]^{1/2}} \quad (4.20)$$

Smith's void fraction  $\epsilon_s$  is calculated with Equation 3.26 and was extensively discussed in section 4.5.2. In essence, to calculate  $\epsilon_s$ , only the vapour quality is required since the density of the vapour phase depends on vapour quality as well.

For the gas Froude number  $Fr_G$ , the mass flow per unit area of the gas  $G_G$  in  $\text{kgm}^{-2}\text{s}^{-1}$  is to be determined through Equation 4.21, with the vapour velocity  $u_G$  and vapour density  $\rho_G$ , in  $\text{ms}^{-1}$  and  $\text{kgm}^{-3}$ , respectively. Vapour density  $\rho_G$  is again determined from steam tables with the vapour quality. Vapour velocity  $u_G$  requires the mass flow of the vapour  $\dot{m}_G$  in  $\text{kgs}^{-1}$ , which can, since mass is conserved, be determined from Equation 4.23. The area of the vapour that covers the cross-section of the pipe  $A_G$  can be derived with the void fraction  $\epsilon_v$  by the definition presented in Equation 3.6. Substituting Equation 4.22 into Equation 4.21 defines the  $G_G$  in  $\text{kgm}^{-2}\text{s}^{-1}$ .

$$G_G = u_G * \rho_G \quad (4.21)$$

$$u_G = \frac{\dot{m}_G}{\rho_G A_G} \quad (4.22)$$

$$\dot{m}_G = \dot{m} - \dot{m}_L \quad (4.23)$$

Although discussed before in 3.2.2, the density of the liquid  $\rho_L$ , inner diameter of the pipe  $D_i$  and gravitational acceleration  $g$  are constant throughout simulation of the model. Ultimately, the gas Froude number  $Fr_G$  can be calculated and used, together with the Smith parameter  $s$ , to plot the data onto the FPM in Figure 3.3.

## 4.7 Concluding remarks

The model proposed in this chapter uses consists of a heat transfer model that uses the fundamental heat transfer equation to determine the average energy contents of a flowing fluid. A set of assumptions are made to simplify the circumstances and to relate to the situation of application of HDD for a steam transport pipeline and its start-up process. To summarize, the model will attempt to simulate the following most significant things:

- The void fraction  $\epsilon_v$  during first-stage start-up of a steam pipeline.
- Flow regime of the flowing fluid to check the risk for dangerous flow patterns.

Note that all simulations are carried out for three common pipe sizes, which are the DN300, DN400 and DN500 pipe types, at mass flows varying from 15 to 100  $\text{kgm}^{-2}\text{s}^{-1}$ . The model will be modelled within the EES environment.

# Results

## 5.1 Condensation induced water hammer

The conducted research on CIWH is rather limited, and the studied cases share minimal resemblance to the start-up mechanisms of steam transport pipelines. The performed experiments, which are mainly conducted in the field of NPP engineering, report that CIWH effects were observed when liquid water levels neared the top surface of the pipe. According to the literature in this field, most extreme cases were observed at a system pressure of 1 MPa and the pressure peaks were measured at 32 MPa. The height of the pressure peaks seemed to reduce at system pressures higher than 4 MPa, and practically stopped occurring after 7 MPa. Additionally, the highest probability of CIWH events was observed at a Froude number of 0.6. These are the most significant results of studies in the existing literature. The results of these studies consist, for the most part, of the observation of consistent critical parameter combinations.

## 5.2 Heat transfer model & thermophysical properties

To answer the research question on how to demonstrate whether CS can occur during the start-up of steam transport pipelines, various thermophysical properties of the fluid such as  $x$ ,  $\alpha_{TP}$ ,  $\zeta$  and  $\epsilon$  are calculated in the process. In this section, graphs with the simulation data of these parameters are presented and analyzed. However, it is not until section 6 that these parameters are discussed.

### 5.2.1 Length of the fluid cylinder

Referring back to Figure 4.2, the length of the fluid cylinder  $x$  represents the distance that the fluid has travelled towards the end of the pipe. This also means that

the larger parameter  $x$  is, the longer the fluid cylinder shaft is, and therefore, its area is larger as well. The area of the shaft is the contact area between fluid and pipe, and is called the fluid-pipe interface area. Note that this area is also the area over which heat is transferred from the fluid to the pipe.

Plotting parameter  $x$  against time  $t$ , which is done for various mass flow rates  $G$  in the graph in Figure 5.1, indicates how fast the pipe length of 500  $x$  is filled. From Equation 4.6, it was established that the length of the fluid cylinder  $x$  is a function of the mass flow  $\dot{m}$  and heat transfer rate  $\dot{Q}_1$  that continuously calculates the volume of the fluid residing in the pipe. This volume constantly changes due to mass being added to the system, heat loss and condensation.

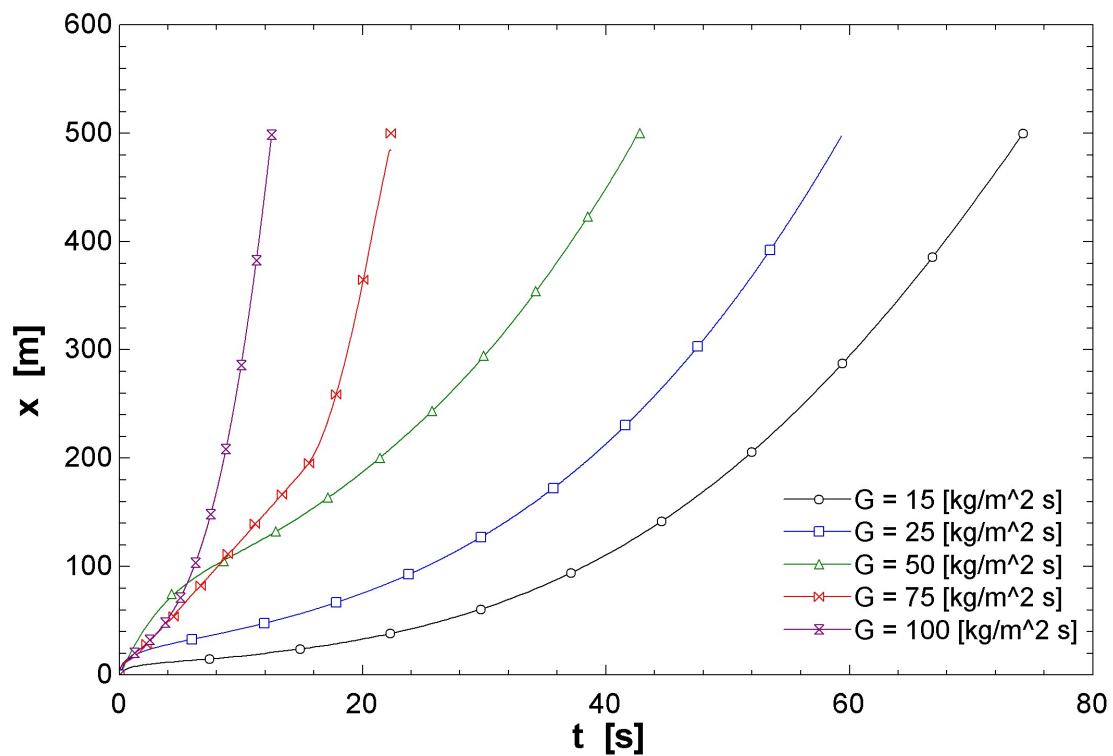


**Figure 5.1:** Fluid length  $x$  against time  $t$  for a DN300 pipe with  $L = 500\text{m}$

Figure 5.1 intends to display the effects of mass flow per unit area  $G$  in  $\text{kgm}^{-2}\text{s}^{-1}$  and heat transfer rate  $\dot{Q}_1$  in  $\text{W}$  on parameter  $x$  in  $\text{m}$ . The influence of these parameters was explained in section 4.4.1 with the aid of Equation 4.4. In short, the effects of  $\dot{Q}_1$  and  $G$  on  $x$  can be observed in the following way:

- **Descending or constant**  $x$ :  $\frac{dx}{dt} \leq 0$

In case a decreasing or constant  $x$  with an increase in  $t$  is observed, the effects of heat loss are dominant over the mass and energy of the fluid added to the system. In other words, the change in volume due to condensation is larger or equal to the volume added at inlet conditions. To clarify, the inlet conditions are saturated vapour  $\zeta = 1$  at atmospheric pressure  $P_{\text{atm}}$  and, of course, saturation temperature  $T_{\text{sat}}$ .

- **Ascending**  $x$ :  $\frac{dx}{dt} > 0$

If  $x$  increases with  $t$ , the mass and energy of the fluid added to the system are dominant over the effects of heat loss. In essence, the volume change of the fluid due to condensation is less significant than the volume increase due to mass being added at inlet conditions.

The simulations vary with  $G$  at 15, 25, 50, 75 and 100  $\text{kgm}^{-2}\text{s}^{-1}$  are plotted in Figure 5.1. As stated, the graph represents the first-stage filling process of 500m steam transport pipe. Therefore, the simulation ends after  $x$  reaches this pipe length. Noticeable from the graph in Figure 5.1, the lines at 15, 25, and 100  $\text{kgm}^{-2}\text{s}^{-1}$  show a similar curve. At 50  $\text{kgm}^{-2}\text{s}^{-1}$ , however, the onset of the curve appears to be steeper than its equivalent expressions with higher mass flow rates. After about 3 seconds, the fluid seems to decelerate and converge to a path similar to the other mass flow rates that showed analogous curves. At 75  $\text{kgm}^{-2}\text{s}^{-1}$  the curve displays a more abrupt acceleration compared to its counterparts. The sudden acceleration appears to occur at approximately 15 seconds of simulation time.

Zooming in to the first few seconds of the simulation, one can notice that all curves, to some degree, show a similar trend. Figure 5.2 displays the first 8 seconds of the graph in Figure 5.1 and for every distinct mass flow the fluid starts by being accelerated, followed by a deceleration of the fluid which then accelerates again. However, note that the lines for 50 and 75  $\text{kgm}^{-2}\text{s}^{-1}$  are not perfectly matching the data points. The line was drawn by applying a moving average of the data points.

Conclusively, from Figures 5.1 and 5.2, one can observe that the effects of volume change due to condensation are most evident during the first seconds of simulation, slowing the fluid down. The effect of condensation appears to diminish over time for any of the simulated mass flows per unit area  $G$ , as  $x$  increases exponentially. In other words, the simulation implies a decreasing heat transfer rate over time, which accelerates the fluid as the pipe gets filled.

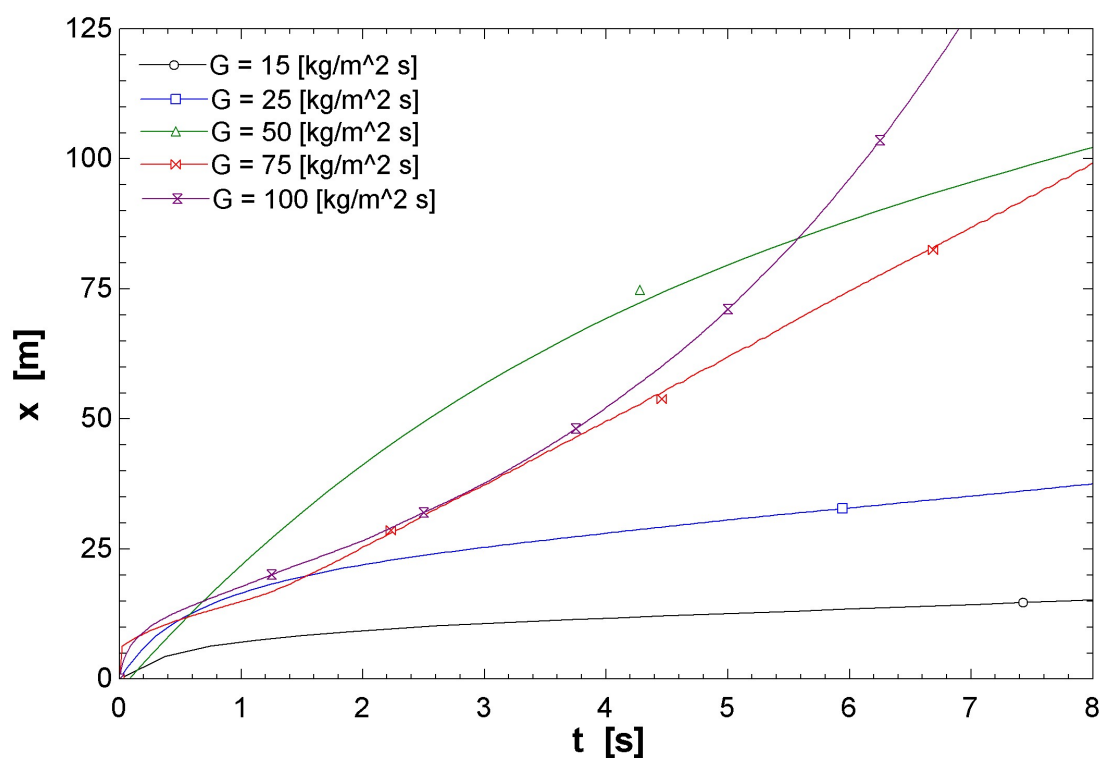


**Figure 5.2:** First 8 seconds of simulation time of the graph in Figure 5.1

### 5.2.2 Vapour quality

The vapour quality  $\zeta$ , which was defined in the beginning of this thesis by Equation 2.1, is the dimensionless value that describes the energetic state in terms of heat contents for the two-phase fluid within its saturation zone. If this definition has become unclear, the writer wants to refer the reader back to section 2.1.1. Figure 5.3 displays the vapour quality  $\zeta$  of the fluid at each point in time. The writer wants to reiterate that a specific point in time relates to a specific stage in the filling process of the pipeline. Revisiting Figure 4.2 might benefit the reader in understanding what these points in time represent.

By plotting the vapour quality  $\zeta$  against time  $t$ , the graph exhibits the average heat content that the fluid has at a specific moment in time during first-stage start-up. Note that the duration of simulation corresponds with the graph presented earlier in Figure 5.1. Therefore, the time values on the horizontal axis correspond to the same stage of filling of the pipeline. From the literature in section 3.4.1, it was established that a low value of  $\zeta$  relates to a low void fraction  $\epsilon_s$ . In other words, at a low vapour quality  $\zeta$ , the liquid fraction in the pipeline is higher. Additionally, it was concluded that higher liquid fractions increase the risk of intermittent flow. Conclu-

sively, the following two points on the graph in Figure 5.3 are most significant:

- **Minimum value of  $\zeta$**

The literature on the estimation of void fractions learned that low vapour qualities correspond to low void fractions. Specifically, this means that liquid fractions are high when the heat contents of the fluid are low. Therefore, the minimum value for  $\zeta$  indicates the moment in time at which the risk of intermittent flow is the highest during first-stage start-up.

- **End value of  $\zeta$**

Since the latest value in time indicates the end of simulation of first-stage start-up, the end value of  $\zeta$  indicates the vapour quality at which the system transitions to the next stage of start-up. This is significant information if any future work on subsequent stages of start-up is carried out.

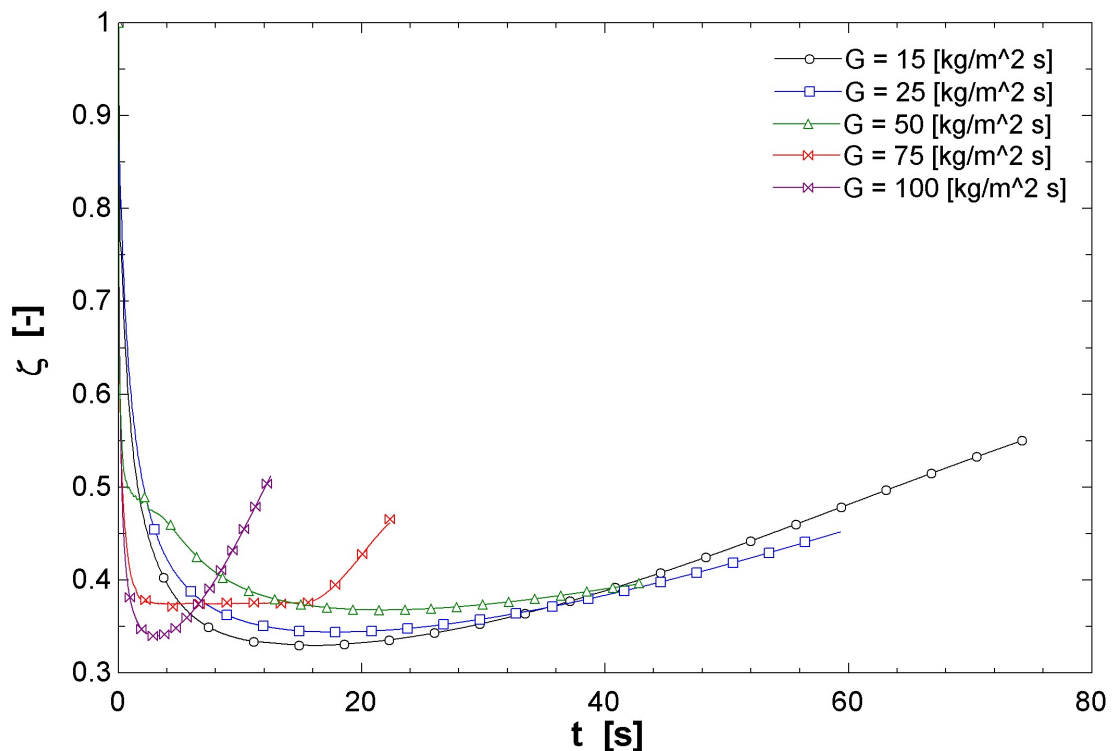


**Figure 5.3:** Vapour quality  $\zeta$  against time  $t$  at various mass flow rates  $G$

The simulations at mass flow rates 15, 25, 50, 75 and 100  $\text{kgm}^{-2}\text{s}^{-1}$  are displayed in Figure 5.3. At all mass flow rates, the vapour quality drops rapidly to a lowest point, from which it then starts to increase again, resulting in a final simulation value which is higher than the low-point value. Analyzing these low-point and

final values, mass flow rates of 15 and 100  $\text{kgm}^{-2}\text{s}^{-1}$  appear to have the most extreme values at these points, while at other mass flow rates the vapour quality does not drop as low and the increase afterwards is not as significant. The extreme values are obtained from the data of the integral tables computed by the model, from which the code can be found in Appendix D. The extreme values for diameters 300, 400 and 500m are displayed in tables 5.1, 5.2 and 5.3, respectively. Noticeably, for diameters of 400 and 500m, the same mass flows of 15 and 100  $\text{kgm}^{-2}\text{s}^{-1}$  show the most extreme values. Interestingly, the minimal values of  $\zeta$  at 15 and 100  $\text{kgm}^{-2}\text{s}^{-1}$  shifted up by roughly 14%. For the end value of  $\zeta$ , however, a small decrease of 3% was observed at 15  $\text{kgm}^{-2}\text{s}^{-1}$ , and a significant increase of 34% at 100  $\text{kgm}^{-2}\text{s}^{-1}$ .

DN300	15 $\text{kgm}^{-2}\text{s}^{-1}$	25 $\text{kgm}^{-2}\text{s}^{-1}$	50 $\text{kgm}^{-2}\text{s}^{-1}$	75 $\text{kgm}^{-2}\text{s}^{-1}$	100 $\text{kgm}^{-2}\text{s}^{-1}$
Lowest value of $\zeta$	0.3294	0.3438	0.3675	0.3711	0.3395
End value of $\zeta$	0.5502	0.452	0.3964	0.4658	0.5119

**Table 5.1:** Minimal and final simulation values of vapour quality  $\zeta$  at various mass flow rates  $G$  for a DN300 pipe

DN400	15 $\text{kgm}^{-2}\text{s}^{-1}$	25 $\text{kgm}^{-2}\text{s}^{-1}$	50 $\text{kgm}^{-2}\text{s}^{-1}$	75 $\text{kgm}^{-2}\text{s}^{-1}$	100 $\text{kgm}^{-2}\text{s}^{-1}$
Lowest value of $\zeta$	0.3539	0.3612	0.3706	0.4338	0.3601
End value of $\zeta$	0.5194	0.4645	0.3985	0.4352	0.5039

**Table 5.2:** Minimal and final simulation values of vapour quality  $\zeta$  at various mass flow rates  $G$  for a DN400 pipe

DN500	15 $\text{kgm}^{-2}\text{s}^{-1}$	25 $\text{kgm}^{-2}\text{s}^{-1}$	50 $\text{kgm}^{-2}\text{s}^{-1}$	75 $\text{kgm}^{-2}\text{s}^{-1}$	100 $\text{kgm}^{-2}\text{s}^{-1}$
Lowest value of $\zeta$	0.3795	0.3883	0.3973	0.4662	0.3858
End value of $\zeta$	0.5323	0.4659	0.4094	0.4721	0.6877

**Table 5.3:** Minimal and final simulation values of vapour quality  $\zeta$  at various mass flow rates  $G$  for a DN500 pipe

In summary, observed from the simulations plotted in Figure 5.3, the minimal values for the vapour quality  $\zeta$ , and the highest end values were observed at mass flows of 15 and 100  $\text{kgm}^{-2}\text{s}^{-1}$ . In terms of the minimal value for  $\zeta$ , this is a disadvantageous property since it indicates the highest risk of slug formation. Considering

the end values of  $\zeta$ , this could potentially be a beneficial property for the subsequent stage of start-up. The vapour quality values maintained a more average value at mass flows of 25, 50 and 75  $\text{kgm}^{-2}\text{s}^{-1}$ . Most notably, compared to the DN300 pipe, the vapour quality  $\zeta$  sees an overall increase with DN400 and DN500 pipes, meaning the risk of intermittent flow reduces with larger diameter pipes.

### 5.2.3 Void fraction

The definition of void fraction was first introduced in section 3.2.2 by Equation 3.7. For clarity, the definition is reiterated. The volumetric void fraction  $\epsilon_v$  is the ratio of a gaseous volume  $V_G$  over the entire volume of a two-phase fluid. Specifically, this means the percentage of the gaseous volume  $V_G$  of a two-phase fluid that resides in a pipeline.

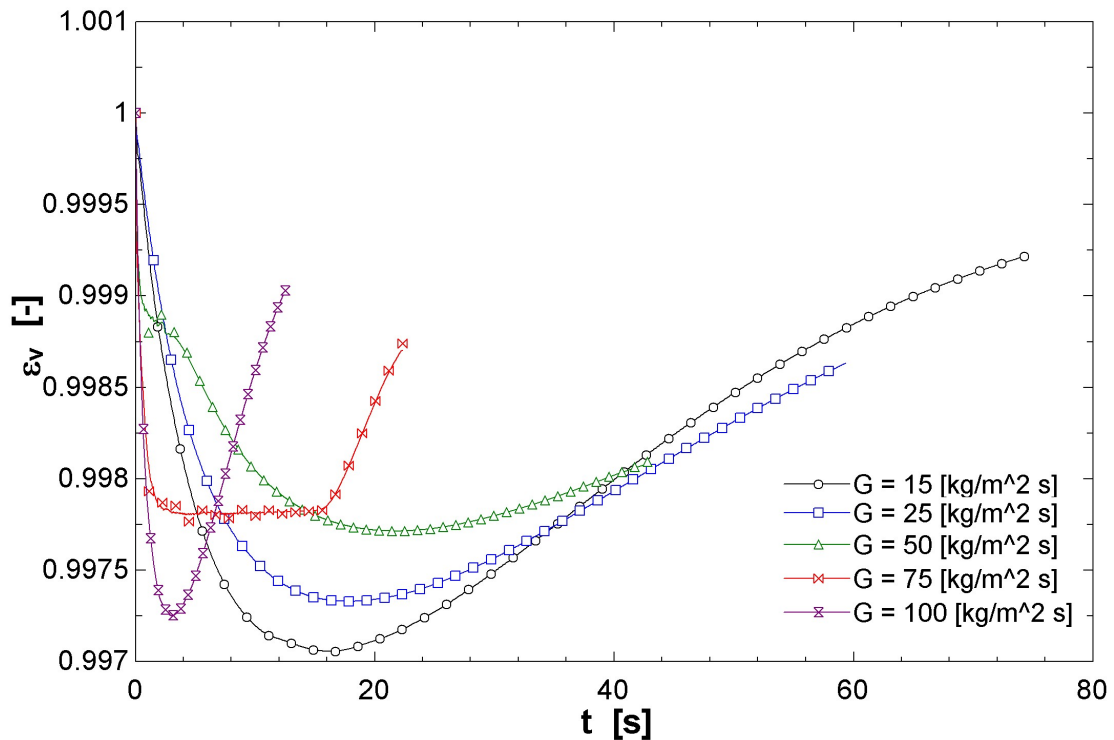


**Figure 5.4:** Volumetric void fraction  $\epsilon_v$  against time  $t$  at various mass flow rates  $G$

The relation between the vapour quality  $\zeta$  and Smith's void fraction estimation method was already demonstrated in section 3.4, Figure 3.4, which seems to resemble as a logarithmic relation. However, the volumetric void fraction  $\epsilon_v$  is calculated with a different approach and must be validated. To investigate and verify the relation between vapour quality  $\zeta$  and the volumetric void fraction  $\epsilon_v$  with the presented

approach, Figures 5.4 and 5.5 are analyzed. In Figures 5.4 and 5.5, the volumetric void fraction  $\epsilon_v$  and Smith's void fraction  $\epsilon_s$  are plotted against time, respectively.

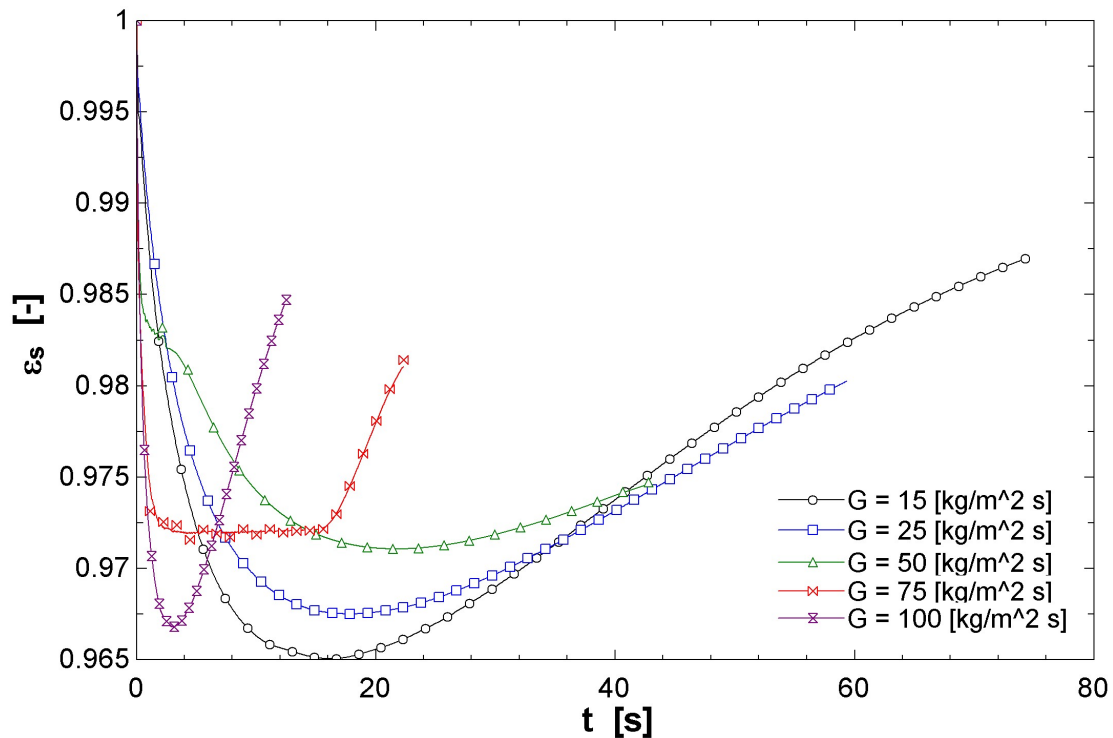


**Figure 5.5:** Smith's [27] void fraction  $\epsilon_s$  against time  $t$  at various mass flow rates  $G$

Analyzing Figures 5.4 and 5.5, their similarity instantaneously stands out. The lowest void fractions for  $\epsilon_v$  and  $\epsilon_s$  occur at the exact time values where  $\zeta$  has its lowest values in Figure 5.3. This means that the behaviour of the equations of  $\epsilon_s$  and  $\epsilon_v$ , with respect to the vapour quality  $\zeta$  and mass flow  $G$  in  $\text{kgm}^{-2}\text{s}^{-1}$ , comply with each other. However, compared to  $\epsilon_v$  in Figure 5.4,  $\epsilon_s$  in Figure 5.5 displays a noticeable shift in value. Tables 5.4 and 5.5 prove that the values of Smith's void fraction  $\epsilon_s$  is about 3% lower than the volumetric void fraction  $\epsilon_v$ . This improved slightly for larger diameter pipes where the values were 2.8% and 2.5% lower for DN400 and DN500 pipes, respectively.

To conclude the observations from Figures 5.4 and 5.5, the behaviour of the void fractions  $\epsilon_v$  and  $\epsilon_s$  with respect to time is exactly the same and complies with the vapour qualities from Figure 5.3. This verifies the summarizing statements of section 3.4.2, which were:

DN300	15	25	50	75	100
	$\text{kgm}^{-2}\text{s}^{-1}$	$\text{kgm}^{-2}\text{s}^{-1}$	$\text{kgm}^{-2}\text{s}^{-1}$	$\text{kgm}^{-2}\text{s}^{-1}$	$\text{kgm}^{-2}\text{s}^{-1}$
Lowest value of $\epsilon_v$	0.9971	0.9973	0.9977	0.9978	0.9973
End value of $\epsilon_v$	0.9992	0.9986	0.9981	0.9987	0.9990

**Table 5.4:** Minimal and final simulation values of volumetric void fraction  $\epsilon_v$  at various mass flow rates  $G$  for a DN300 pipe

DN300	15	25	50	75	100
	$\text{kgm}^{-2}\text{s}^{-1}$	$\text{kgm}^{-2}\text{s}^{-1}$	$\text{kgm}^{-2}\text{s}^{-1}$	$\text{kgm}^{-2}\text{s}^{-1}$	$\text{kgm}^{-2}\text{s}^{-1}$
Lowest value of $\epsilon_s$	0.9651	0.9675	0.9711	0.9715	0.9668
End value of $\epsilon_s$	0.9870	0.9803	0.9747	0.9814	0.9847

**Table 5.5:** Minimal and final simulation values of Smith's [27] void fraction  $\epsilon_s$  at various mass flow rates  $G$  for a DN300 pipe

- **Most extreme minima for  $G = 15$  and  $G = 100\text{kgm}^{-2}\text{s}^{-1}$**

The lowest vapour quality  $\zeta$ , and void fractions  $\epsilon_v$  and  $\epsilon_s$  were observed at mass flows of 15 and 100  $\text{kgm}^{-2}\text{s}^{-1}$  at a DN300 pipe. For DN400 and DN500 pipes, an increase of these values is observed. This means that the highest risk of intermittent flow during first-stage start-up exists for a DN300 pipe at mass flows of 15 and 100  $\text{kgm}^{-2}\text{s}^{-1}$ .

- **Highest end values for  $G = 15$  and  $G = 100\text{kgm}^{-2}\text{s}^{-1}$**

The end values for void fractions  $\epsilon_v$  and  $\epsilon_s$  were in compliance with the vapour qualities in Figure 5.3. This implies that for mass flows of 15 and 100  $\text{kgm}^{-2}\text{s}^{-1}$  the end values are the highest, which are potentially advantageous circumstances for subsequent start-up stages.

To illustrate the discrepancy in the values of the void fractions  $\epsilon_v$  and  $\epsilon_s$ , Figure 5.6 is added, relating the void fractions  $\epsilon_v$  and  $\epsilon_s$  against vapour quality  $\zeta$ . The dotted line is the relation of Smith's void fraction estimation  $\epsilon_s$  against vapour quality  $\zeta$  at atmospheric pressure  $P_{\text{atm}}$ . The relation was explained earlier in section 3.4, Figure 3.4. The overlapping lines, that are indicated with symbols, represent the volumetric void fractions  $\epsilon_v$  at the various mass flow rates  $G$ . Noticeably, the void fraction is expected to drop more rapidly at lower vapour qualities, meaning that the liquid levels would rise more rapidly if vapour quality were to decrease further. However, it appears that the simulations do not fall below a vapour quality of 0.3294 for DN300 pipelines, and therefore, maintain a relatively high void fraction. Specifically, this means that throughout first-stage start-up of steam pipelines, the fractions of liquid

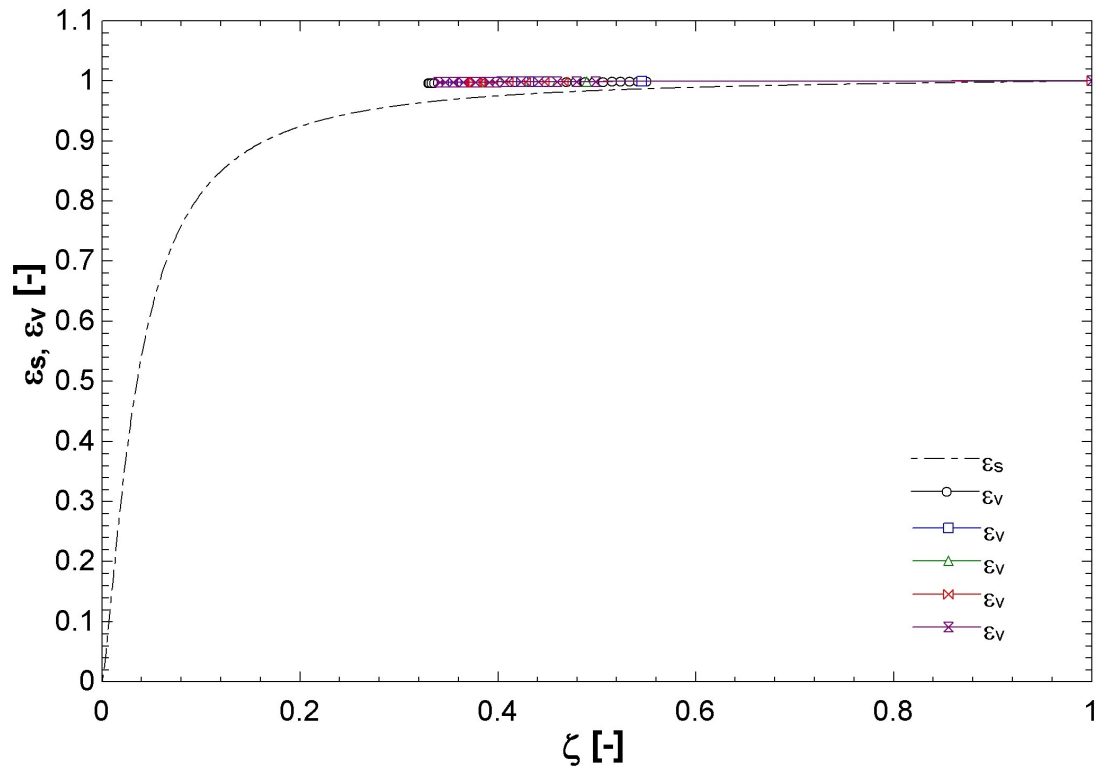


**Figure 5.6:** Simulated volumetric void fraction  $\epsilon_v$  and Smith's [27] method for  $\epsilon_s$  compared, plotted against time  $t$

condensate remain relatively low.

## 5.2.4 Two-phase heat transfer coefficient

Since the presented model is a heat transfer model, and the model is fundamentally built from heat transfer coefficients, Figure 5.7, which displays the heat transfer coefficients during simulation, is added to demonstrate what previous graphs in this section are working with. Although in this graph the simulation data is used to display the heat transfer coefficients, and therefore plotted against time, the two-phase heat transfer coefficient  $\alpha_{TP}$  is a produce exclusively of Shah's [28] work.

The simulation data in Figure 5.7 show a clear and significant contrast between high and low mass flow rates. All the plotted data sets show a significant drop in heat transfer coefficient in the first few seconds of simulation. However, at mass flow rates of 15, 25 and 50  $\text{kgm}^{-2}\text{s}^{-1}$  the heat transfer coefficient appears to drop much lower than at, for example, 100  $\text{kgm}^{-2}\text{s}^{-1}$ . More notably, the data set at 75  $\text{kgm}^{-2}\text{s}^{-1}$  shows substantial jumps in heat transfer coefficient throughout the simu-

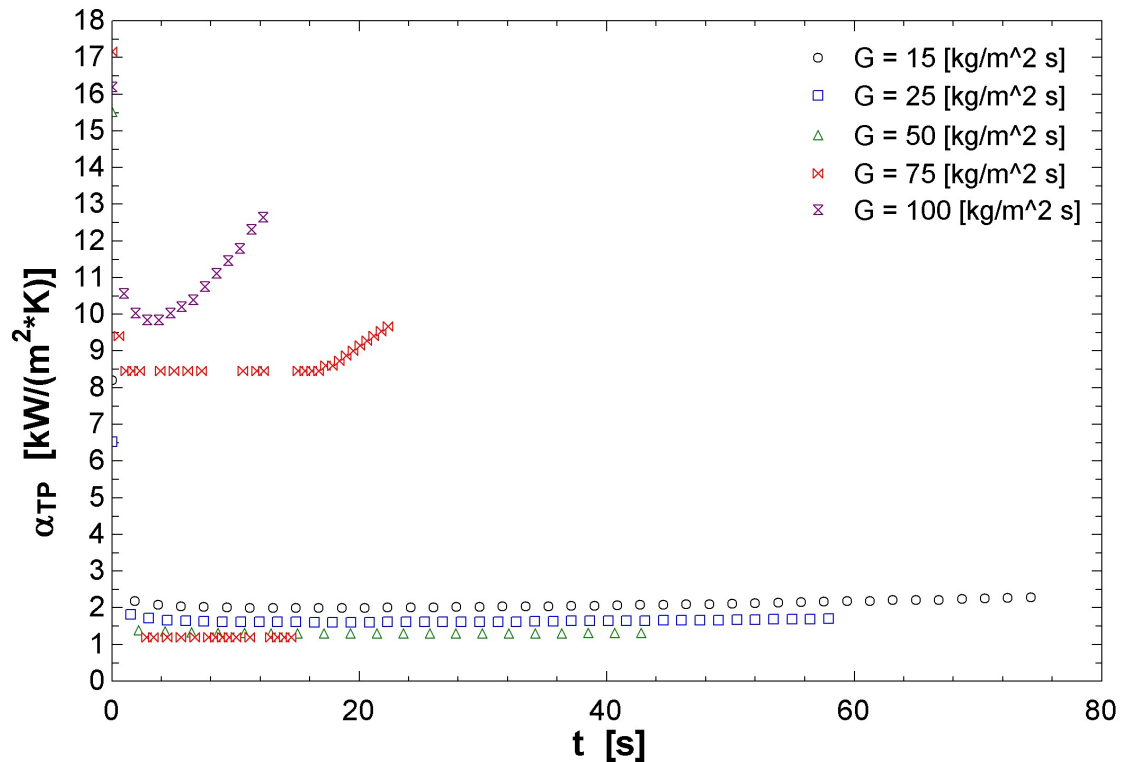


**Figure 5.7:** Simulated values for Shah's [28] two-phase heat transfer coefficient  $\alpha_{TP}$  against time  $t$  at various mass flow rates  $G$

lation. Although the data around values of 8 and 9  $\text{Wm}^{-2}\text{K}^{-1}$  seem to be in the right place, it may be clear that its behaviour is suspicious and ought to be discussed. At 50  $\text{kgm}^{-2}\text{s}^{-1}$ , the data points showed jumps in the heat transfer coefficient as well, and average movement of the points is displayed by the line. However, this is also discussed later in section 6.

As a consequence of the observations from Figure 5.7, the computation of the two-phase heat transfer coefficient  $\alpha_{TP}$  is analysed further in this section. Since the model uses a large data set with pre-calculated heat transfer coefficients as so-called lookup tables for each diameter, the values are looked up by mass flow and vapour quality. The particular mass flow and vapour quality combinations were investigated, and the heat transfer coefficients from the lookup tables indeed show substantial jumps over the course of relatively small vapour quality changes. These jumps seem to occur at lower mass flow rates. However, it seems to shift towards lower vapour qualities as the mass flow increases. For higher mass flow rates, the jumps in heat transfer coefficients practically disappear.

DN300	$\alpha_{TP}$
$\zeta$ [-]	$Wm^{-2}K^{-1}$
0.48	1.378
0.49	1.387
0.50	8.732
0.51	8.842

(a):  $G = 50 \text{ kgm}^{-2}\text{s}^{-1}$

DN300	$\alpha_{TP}$
$\zeta$ [-]	$Wm^{-2}K^{-1}$
0.36	1.195
0.37	1.201
0.38	8.462
0.39	8.601

(b):  $G = 75 \text{ kgm}^{-2}\text{s}^{-1}$

DN300	$\alpha_{TP}$
$\zeta$ [-]	$Wm^{-2}K^{-1}$
0.21	0.9969
0.22	1.001
0.23	7.690
0.24	7.896

(c):  $G = 100 \text{ kgm}^{-2}\text{s}^{-1}$

DN300	$\alpha_{TP}$
$\zeta$ [-]	$Wm^{-2}K^{-1}$
0.11	0.851
0.12	0.854
0.13	6.834
0.14	7.152

(d):  $G = 150 \text{ kgm}^{-2}\text{s}^{-1}$

**Table 5.6:** Tabulated values of the two-phase heat transfer coefficient  $\alpha_{TP}$  at specific combinations of vapour quality  $\zeta$  and mass flow  $G$  for a DN300 pipe

In Table 5.6 displays selective data from the heat transfer coefficient lookup tables, indicating the ranges of vapour qualities at which the heat transfer coefficient undergoes a sudden jump in value at respective mass flows. Note that in Table 5.6a the jump occurs when the vapour quality transitions from 0.49 to 0.5, and at higher mass flow rates 75, 100 and 150  $\text{kgm}^{-2}\text{s}^{-1}$ , Tables 5.6b, 5.6c and 5.6d indicates that this transition range shifts to 0.37 to 0.8, 0.22 to 0.23 and 0.12 to 0.13, respectively. From the lookup tables, for diameters DN300, DN400 and DN500, no significant jumps in heat transfer coefficients over the saturation range from  $\zeta = 0.01$  to  $\zeta = 1$  were present at mass flows of 254.6, 294.4 and 361.6  $\text{kgm}^{-2}\text{s}^{-1}$ , respectively.

After analyzing the two-phase heat transfer coefficient  $\alpha_{TP}$  more carefully, the following points were concluded:

- **Unexpected behaviour at  $G = 75 \text{ kgm}^{-2}\text{s}^{-1}$**

In Figure 5.7, where the heat transfer coefficient  $\alpha_{TP}$  is plotted against time for a DN300 pipe, unexpected behaviour is observed at a mass flow of  $G = 75 \text{ kgm}^{-2}\text{s}^{-1}$ . Sudden drops in the heat transfer coefficient  $\alpha_{TP}$  are observed, and could potentially cause deviations in the heat transfer calculations of the heat transfer model.

- **Noticeable shift in heat transfer coefficient**  $\alpha_{TP}$

The Tables in 5.6 indicate a clear shift in the two-phase heat transfer coefficient  $\alpha_{TP}$  at a corresponding vapour quality  $\zeta$ . The shift in  $\alpha_{TP}$  appears to move towards a lower vapour quality  $\zeta$  for higher mass flow rates  $G$  in  $\text{kgm}^{-2}\text{s}^{-1}$ . Thus far, there is no apparent reason for this shift in heat transfer coefficient  $\alpha_{TP}$ . However, this will be discussed further in chapter 6.

## 5.3 Flow properties of the fluid

The subsequent step in the hierarchy of the model was to determine the flow properties of the fluid with the calculated thermophysical properties of the fluid. This section is dedicated towards displaying the end results of the presented model by plotting the fluid flow properties on the FPM in order to track the flow regime of the fluid during first-stage start-up.

### 5.3.1 Flow Pattern Map

As stated in the research questions, one of the aims of this research is to find a way to compute the flow regime during start-up of steam transport pipelines. In section 4.6, it was established that the Froude number  $Fr_G$  and Smith parameter  $s$ , are required to do this. The Froude number represents the relation between the effects of inertia and gravity of the flow, where a higher Froude number indicates dominant inertial effects. For a more detailed reiteration of the Froude number, the writer refers back to section 3.2.2, Equation 3.4. The Smith parameter  $s$  is an empirically determined parameter that is defined with Smith's void fraction  $\epsilon_s$ , the definition of the Smith parameter was given by Equation 4.19.

The FPM by Tandon et al. [25] is used to track the flow regime during the performed simulations. Figure 5.8 displays plotted values for the Froude number  $Fr_G$  and the Smith parameter  $s$  at mass flows  $G$  of 15, 25, 50, 75 and 100  $\text{kgm}^{-2}\text{s}^{-1}$  for a DN300 pipe. Only the DN300 pipe is analyzed here, since in sections 3.4.2 and 5.2.3, it was established that this type of pipeline has the most risk of intermittent flow to occur.

Plotting the data of these parameters at various mass flows, resulted in the graph presented as Figure 5.8. It is evident that at mass flows of 50 and 75  $\text{kgm}^{-2}\text{s}^{-1}$  the graph display deviating behaviour, while mass flows of 15, 25 and 100  $\text{kgm}^{-2}\text{s}^{-1}$

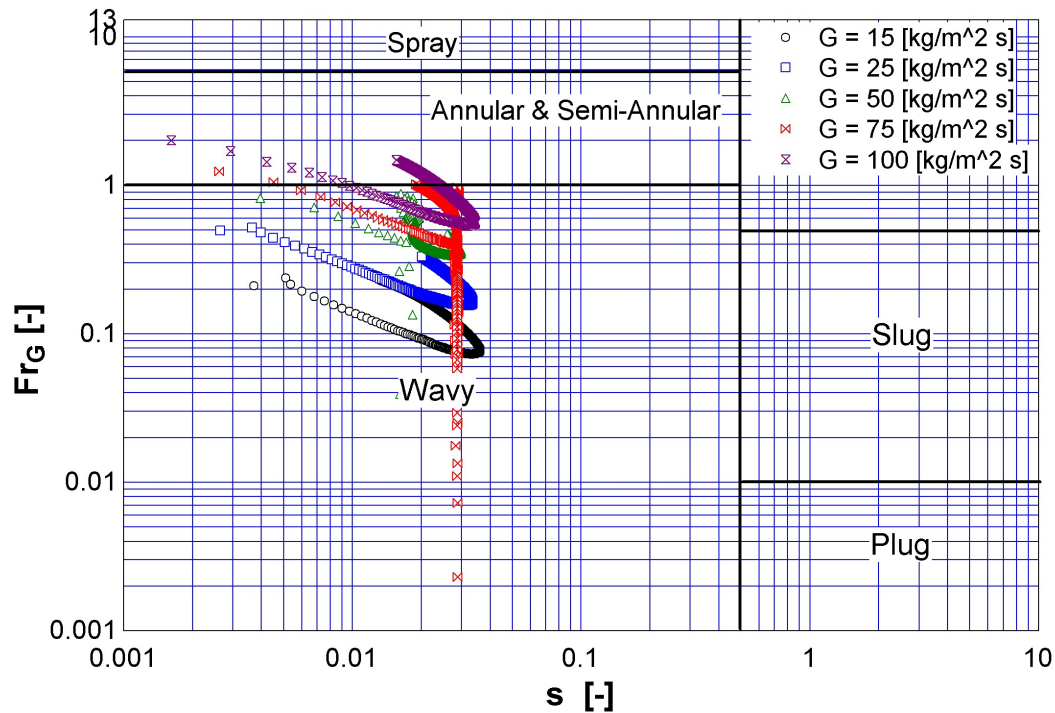


**Figure 5.8:** Simulated values for the Froude number  $Fr_G$  and Smith parameter  $s$  plotted on the FPM of Tandon et al. [25]

again show analogous trends and signify a smoother progression of the axes' parameters. However, noticeably, the various data sets clearly show to range largely within the stratified-wavy area of the FPM. The larger mass flows, 75 and 100  $\text{kgm}^{-2}\text{s}^{-1}$  seem to dip into the Annular and Semi-Annular flow range due to higher Froude numbers. However, throughout simulation, the smith parameter maintains a significant distance to the more dangerous intermittent flow regimes, slug and plug flow. The observations from Figure 5.8 are summarized by the following bullet points:

- **Deviating  $Fr_G$  at  $G = 50$  and  $G = 75\text{kgm}^{-2}\text{s}^{-1}$**

For mass flows  $G = 50$  and  $G = 75\text{kgm}^{-2}\text{s}^{-1}$ , the graphs in Figure 5.8 display a deviating shape compared to the other mass flows. Specifically for  $G = 75\text{kgm}^{-2}\text{s}^{-1}$ , the Froude number  $Fr_G$  displays suspicious data. Presumably, this is a consequence of the shifts in heat transfer coefficient  $\alpha_{TP}$ , which were also prevalent for  $G = 75\text{kgm}^{-2}\text{s}^{-1}$ .

- **Wavy & Annular flow**

The simulation data, plotted on the FPM in Figure 5.8, display to be relatively far away from the intermittent flow regimes. This means that slug or plug formation is

unlikely to happen during first-stage start-up of steam transport pipelines.

## 5.4 Concluding remarks

The presented model successfully calculated the required parameters to plot the simulation data onto a two-phase FPM to track the flow regime during the first-stage start-up of a simplified implementation of a steam transport pipeline. Along the way, various thermophysical properties of the fluid are determined and reveal some of the most important characteristics and time-specific situations of the first-stage start-up process. The most significant results of this chapter are summarized by the following bullet points:

- Over the course of first-stage start-up, the fluid is accelerated due to a diminishing condensation rate.
- Minimal values for  $\zeta$  and  $\epsilon_v$  were observed at mass flow rates of  $G = 15$  and  $G = 100 \text{ kgm}^{-2}\text{s}^{-1}$ , indicating an increased risk of slug formation. However, the void fraction  $\epsilon_v$  was maintained sufficiently high throughout the simulation such that slug formation is unlikely to happen during first-stage start-up.
- The largest values for  $\zeta$  and  $\epsilon_v$  at the end of simulation time were also observed at mass flow rates of  $G = 15$  and  $G = 100 \text{ kgm}^{-2}\text{s}^{-1}$ , indicating lower liquid fractions within the pipeline.
- The volumetric void fraction  $\epsilon_v$  showed an absolute deviation of 3%, 2.8% and 2.5% in comparison to Smith's estimation method for pipe types DN300, DN400 and DN500, respectively.
- The vapour quality  $\zeta$  does not appear to drop below a value of roughly 0.33 during simulations, for any mass flow  $G$  or pipe diameter  $D$ . This means that, during first-stage start-up, the fluid maintains sufficient heat to not descent lower than  $\zeta \approx 0.33$ .
- Shah's [28] heat transfer coefficient values  $\alpha_{\text{TP}}$  in  $\text{Wm}^{-2}\text{K}^{-1}$  displayed unexpected shifts at certain combinations of mass flow  $G$  and vapour quality  $\zeta$ . These shifts are emphasized in Table 5.6.
- Plotting flow properties such as the Froude number  $Fr_G$  and Smith parameter  $s$  onto a two-phase FPM indicated no risks of intermittent flow during simulation. This implies that no formation of slug and plug flow is expected during first-stage start-up of steam transport pipelines.

The provided set of bullet points encompasses the most significant observations. However, for some results it may not be evident as to why they emerge. In the following chapter, the results will be discussed in order to clarify whether the results are expected or not, and to shed light on the potential roots of the observations.

# Discussion

## 6.1 Discussing results

### Condensation Induced Water Hammer

Although the literature on CIWH has minimal resemblance with the studied problems of steam transport pipelines, the performed studies do contain significant findings that can be used in preventing CIWH events. As mentioned in section 5.1, the studies reviewed by Volkov et al. [14], showed consistently that CIWH events occurred when liquid water levels reached the top surface of the pipe. Although this may seem obvious to some, this does prove that disproportionate condensate levels can cause problems. The influence of system pressure and flow parameters such as the Froude number were studied and were found to have influence on the CIWH events. These are one of the few parameters that can be controlled during the start-up of steam transport pipelines. Since the highest pressure peaks were observed at a system pressure of 1 MPa, and steam transport pipelines often operate around pressures up to 3 MPa, the build-up to 1 MPa is a crucial stage in the start-up process. Regarding the Froude parameter, in section 5.1 it was stated that the highest probability of occurrence for CIWH events was observed at a Froude number of 0.6, which represents sub-critical flow of the fluid. This means that most CIWH were observed at lower liquid flow rates.

### Two-phase heat transfer coefficient

Since the heat transfer coefficients are fundamental to the presented heat model, this is discussed first. Although the behaviour seems unusual, there appears to be no real reason why it would be wrong. In the EES code, a function, provided by EES itself, is used to calculate the heat transfer coefficients. However, the EES function is backed up by the equations in section 3.3 provided by Shah [28]. Since

the method uses three distinct regime regions of heat transfer, one could expect that a sudden surge or decline of the heat transfer coefficient is caused by a change in heat transfer regime. However, according to Shah's [28] work, for any  $We > 100$  the heat transfer occurs in regime 1. Since the diameters of steam transport pipelines are relatively large, and mass flows of at least  $15 \text{ kgm}^{-2}\text{s}^{-1}$  are used, the Weber number stays significantly higher than 100 throughout the simulations. Therefore, the sudden jumps in heat transfer coefficient cannot be justified by a change in heat transfer regime. Another sensible argument could be that Shah's work [28] has not been validated at diameters larger than 49 mm. Yet still, when heat transfer coefficients for a 45 mm diameter pipe were computed, similar jumps in heat transfer coefficient were observed. Thus, the meaning of these sudden jumps in heat transfer coefficient remains unknown.

### Vapour quality

Since Shah's work [28] has been validated for a mean deviation of 17%, one could dispute any argument whether the correlations provide incorrect values. However, the presented study proves that the correlations can create some suspicious situations. For example, in Figure 5.7, deviating behaviour of the heat transfer coefficient was observed for a 0.3 m diameter pipe, at a mass flow of  $75 \text{ kgm}^{-2}\text{s}^{-1}$ , where the vapour quality ( $\zeta$ ) lingers around its minimum value of approximately 0.37 for a couple of seconds. From Table 5.6b it was seen that this is the exact point where the heat transfer coefficients jumps between  $1.201$  and  $8.462 \text{ Wm}^{-2}\text{K}^{-1}$  at vapour qualities 0.37 and 0.38, respectively. This also showed in other graphs of the simulation. With regard to the consequences of this, it appears that the simulations that experienced these fluctuations in heat transfer coefficient had higher values for  $\zeta$ ,  $\epsilon_v$  and  $\epsilon_s$  than expected, meaning that heat is transferred at a slower rate than expected. On top of that, it is difficult to imagine a real-life scenario where the heat transfer coefficient undergoes such abrupt changes. Nevertheless, for the presented study, this only affected the simulations at  $75 \text{ kgm}^{-2}\text{s}^{-1}$  and, to a lesser extent, at  $50 \text{ kgm}^{-2}\text{s}^{-1}$ .

From Tables 5.1 to 5.5, in section 5.2, it was observed that the simulation values for the vapour quality, and void fractions saw an increase with diameter, and stayed about the same for an increasing mass flow. Although it was found from Figure 5.7 that the heat transfer coefficient increases with mass flow, apparently this does not result in disproportional condensation rates during first stage start-up. Since the mass flow rate is proportional to the energy that is added at the inlet of the system, this seemingly prevents the vapour quality from dropping below 0.3294, 0.3539 and 0.3795 for pipe types DN300, DN400 and DN500, respectively.

The increase in vapour quality with regard to pipe diameter is potentially justified by the volume to surface area ratio of a cylinder, which increases for larger diameters. This means that, for larger diameter pipes, the heat transfer surface area is smaller in relation to the energy that is being added at the inlet of the pipe. Knowing the relation between vapour quality and void fraction, similar behaviour for the void fraction with respect to diameter and mass flow is according to expectations.

### Void fraction

In previous section, section 5.2, Figure 5.6 was presented and the discrepancy between the simulated void fraction ( $\epsilon_v$ ) and predicted void fractions by Smith's estimation method ( $\epsilon_s$ ) [27] was specified. Although the discrepancy seems to be increasing, no vapour qualities below a value of 0.3294 were observed during simulations. Therefore, no comparison between the model and Smith's method [27] could be made for lower vapour qualities. However, the simulated void fraction showed a maximum deviation of 3% from Smith's method at this lowest vapour quality, which confirms a reasonable agreement of the values for the performed simulations.

### Flow Pattern Map

Figure 5.8 demonstrated that during first-stage start-up, only wavy and annular flow occur. Evidently, the Froude number increases proportionally with mass flow rate, since the inertia over gravity effects of the flow increase. However, from the gas Froude equation as in Equation 4.20, it is evident that an increasing diameter, and a decreasing vapour quality, have opposite effects. Nevertheless, the void fraction is most decisive in whether intermittent flow occurs, since intermittent flow, such as slug and plug flow, occur at smith parameters of 0.5 or higher, which correlates to a void fraction of  $\epsilon_s < 2/3$ . From the analysis of the void fraction, it was established that the void fraction is hardly influenced by mass flow, but an increasing void fraction was observed for larger pipe diameters. Although the margin with respect to transitioning to intermittent flow patterns is relatively large during first-stage start-up, a lower void fraction could result in significant consequences for subsequent stages of start-up. Therefore, a larger diameter pipe would have a more favourable position with regard to preventing intermittent flow in the subsequent stages of start-up.

## 6.2 Answering research questions

This section is committed towards answering the main research question that were stated in section 1.2. First, answers to the sub-research questions are given, and afterwards, an answer to the main research question is formulated.

### 1. *How to demonstrate whether CS or CIWH occurs?*

One of the first objectives of this research was to find a way to demonstrate how CS or CIWH occurs. From the literature it was found that the occurrence of CIWH is rather arbitrary in nature and can happen under various circumstances. The research on modelling CIWH events appears to be far from mature, however, somewhat consistent results were generated in various experiments in the field of NPP engineering. The consistency was noticed in the occurrence of CIWH events when liquid water levels neared the top surface of a two-phase vapour-liquid channel. The objective to demonstrate whether CIWH occurs could not be accomplished, however, the relation between CIWH and the void fraction is indisputable, self-evident and the literature has learned what circumstances to circumvent.

This thesis has found a way to demonstrate whether CS occurs in a two-phase flow through studying literature. The FPM provided by the work of [23], which uses the Froude number and Smith's void fraction estimation method [27], was found to be a convenient way to demonstrate in what flow regime a two-phase flow occurs. Both parameters could be acquired using a heat transfer model that simulates the first stage of start-up for a steam transport pipeline.

### 2. *At first time use of steam transport pipelines, what are the variables that can be adjusted to mitigate condensate generation?*

The condensate that is generated during start-up of steam transport pipelines is caused by heat losses. Any heat that is lost, condenses from vapour to liquid phase. During the first stages of start-up, most of the heat of the steam is lost to the pipe's material as it needs to heat up. Other than reducing the heat capacity of the pipe's material, no parameters were found that could influence the amount of condensate that is generated throughout first stage start-up. However, it was found that for an increasing diameter of the pipe, vapour quality and void fractions maintained higher values, meaning that the total volume of condensate in relation to the total volume of the two-phase fluid within the pipe is lower.

3. *What are the repercussions of CIWH and CS if one of them occurs in steam pipelines?*

The initial goal of this research question was to model CIWH events in a steam pipeline. However, the field of modelling CIWH events appeared to be more immature than expected, and any experiences had to be collected from NPP literature. It appears that for pressures equivalent to operating pressures of steam transport pipelines, the highest pressure peaks were observed up till 32 MPa, which is far higher than any steam pipeline with standardized wall thickness can handle. Therefore, in these extreme cases, a steam transport pipeline would yield in an explosive manner.

*How do water hammer phenomena, or other condensate related issues, influence the choice and application of a HDD boring for steam-condensate system pipelines?*

To prevent dangerous flow pattern such as slug flow, or even CIWH events in steam transport pipelines, void fractions must be maintained high. In the case of HDD, condensate will inevitably accumulate at its lowest point and void fractions will decrease with time. Whether, if and when, water hammer phenomena will occur for the application of HDD without drainage, remains to be investigated. However, void fractions during first-stage start-up were found to increase with pipe diameter and could prove to be significant for subsequent stages of start-up as well. No relation between the mass flow and void fraction was found during first-stage start-up. Since assumption 1 was validated with a maximum deviation of 3%, relatively simple methods such as increasing the horizontal accumulation zone volume of the HDD and lowering the heat capacity of the pipe's material are expected to be effective in maintaining high void fractions.

## 6.3 Limitations

This section aims to indicate the limitations of the presented model. Specifically, what the model cannot be used for, and some of the related areas that require more research to strengthen the outcomes of the presented model.

- **First-stage start-up**

As previously stated, the presented model aims to model first-stage start-up of a horizontal pipeline. This means that no pressure build-up is included in the model. Still, this is an important component of the total start-up process, since increasing the pressure will reduce the void fraction significantly. For example, according to

Smith's prediction method, a vapour quality of 0.35 corresponds to a void fraction of approximately 0.9 and 0.7 for 0.1 and 3 MPa, respectively. This means that if similar vapour qualities occur for later stages with higher pressures, the risk of slug flow increases significantly. How subsequent stages of start-up can be modelled with a similar approach of the presented model will be explained in section 7.2.

- **Pipe structure simplified**

In section 4.1, supported by Figure 2.7, it was explained that the presented model exclusively considers the accumulation zone of a simplified HDD application. Although this is the most critical point in terms of dangerous flow patterns, in reality, the inclinations are of influence for the filling process of the accumulation zone as well. Specifically, the downwards flow inclination will influence the inlet flow characteristics, such as the velocity, vapour quality and heat transfer rate for the accumulation zone. On top of that, the pipe material at the inclination zones will absorb heat just as the accumulation zone, resulting in extra liquid condensate and eventually decreasing the void fraction in the accumulation zone.

- **Insufficient understanding of two-phase heat transfer coefficient**

Shah's correlations [28] for two-phase heat transfer coefficients were extensively discussed in chapter 6, where some of its outcomes were labelled as unrealistic. It may be self-evident that the jumps in heat transfer coefficients require further investigation. The diameters used for steam transport pipelines could not be validated by Shah [28] since no experiments for two-phase heat transfer coefficients exist within concurrent literature. Although similar unrealistic events were observed at validated diameters, the presented work is unable to draw any well-founded conclusions, and therefore Shah's [28] heat transfer correlations remain an unreliability and is therefore, a limitation of the presented work.

# Conclusions and recommendations

## 7.1 Conclusions

The goal of this thesis was to investigate condensate related issues that could occur with respect to the application of HDD with long distance steam transport pipelines. The research has developed towards a fundamental and intuitive approach of modelling the influential variables in condensation of steam, and specifically, the first time use of steam transport pipelines. The presented model describes the void fraction and flow regime throughout the first-stage of the startup process, on which is to be expanded with future research on subsequent stages of startup.

This thesis has contributed to the academic world by providing:

1. A validated heat transfer model for a flowing fluid that is able to calculate the amount of condensate generated during first-stage startup of steam transport pipelines by setting the startup conditions and choosing pipe dimensions. The simulated void fractions are compared to the theory of a void fraction estimation method and has shown to be in agreement.
2. An onset to the research field on the first time use of long distance steam transport pipelines in acknowledgement of the growing demand for steam transport as a consequence of the urgency for CO<sub>2</sub> emission reduction.

In summary, the most significant findings of this research are:

1. Most extreme pressure peaks of CIWH events happen between 1 and 4 MPa system pressure and can amount up to 32 MPa.
2. During the first stage of startup, no risk of slug formation was observed by the model.

3. Increasing the pipe diameter of steam transport pipelines results in better heat retention of the fluid inside the pipe, at least during the first-stage of start-up. Overall, this results in lower fractions of liquid condensate within pipelines and, and therefore, less risk of water hammer phenomena.
4. The highest liquid fractions in the modelled pipeline were observed at mass flow rates of 15 and 100 kg/m<sup>2</sup>s<sup>-1</sup> during first-stage start-up.
5. The lowest liquid fractions at the end of first-stage startup were also observed at 15 and 100 kg/m<sup>2</sup>s<sup>-1</sup>.

## 7.2 Recommendations

As stated in section 7.1, this research has delivered an onset to the field of the startup of steam transport pipelines, and covered a first-stage of the startup process. However, to comprehend the entire startup process of steam transport pipelines, further investigation of the process is required. Throughout this research, awareness of the various aspects of the entire startup process is acquired. Based on his acquired knowledge, the writer would like to share his recommendations on how to proceed the presented research.

- **Review of two-phase condensation heat transfer**

Due to lack of research with larger diameter channels, the two-phase heat transfer coefficients by Shah [28] could not have been validated by his study. Although the relations are used for higher diameters in this study, validations of Shah's correlations would strengthen the results of this thesis. The two-phase heat transfer coefficients for condensing flows needs a more detailed study to understand its behaviour, experiments with larger diameter channels are desired.

- **Subsequent startup stages**

The presented work covers the first stage of start-up for steam transport pipelines. In the future, the entire start-up process must be analysed to make more significant engineering decisions. Ideally, subsequent stages of start-up are modelled as well. The writer suggests that his is to be followed up by a semi-steady state model that progresses from the end state of the transient model. The manner in which pressure is built up in this stage is to be investigated.

- **Inclinations of the HDD**

The effects of inclinations on flow in case of an actual HDD are not considered and are to be investigated and ultimately modelled in subsequent work. The writer suggest that extra assumptions are made to simplify the effects. For example, once the accumulation zone of the HDD application is filled, inclination upwards begins, liquid is unlikely to travel all the way up the inclination, and therefore, at the end of the transient model, the liquid velocity could be assumed to reduce to zero. The effects of inclinations on flow regime has not been researched and needs further investigation.

# Bibliography

- [1] S. Shukla, Skea, "Ipcc, 2022: Climate change 2022: Mitigation of climate change. contribution of working group iii to the sixth assessment report of the intergovernmental panel on climate change," Cambridge University Press, New York, 2022 [Online]. [Online]. Available: <https://www.ipcc.ch/report/ar6/wg2/>
- [2] Eurostat, "Waste statistics explained," Jan 2023. [Online]. Available: [https://ec.europa.eu/eurostat/statistics-explained/index.php?title=Waste\\_statistics#Total\\_waste\\_generation](https://ec.europa.eu/eurostat/statistics-explained/index.php?title=Waste_statistics#Total_waste_generation)
- [3] SpiraxSarco, "The steam and condensate loop: An engineer's best practice guide for saving energy," SpiraxSarco Limited, 2008.
- [4] M. Boles, M. Kanoglu, and Y. Cengel, in *Thermodynamics: An engineering approach*. published by McGraw-Hill Education, 2020.
- [5] A. I. Morozov, Ed., *Introduction to plasma dynamics*. CRC Press, 2013, pp. 4–5.
- [6] TexasGateway, "Phase change and latent heat," July 22, 2022. [Online]. Available: <https://www.texasgateway.org/resource/113-phase-change-and-latent-heat>
- [7] M. Mhadhbi, *Phase Change Materials and Their Applications*. Rijeka: IntechOpen, 2018. [Online]. Available: <https://doi.org/10.5772/intechopen.71894>
- [8] Rotterdam-Engineering, "Company owned documents from company database," Unpublished, 2022.
- [9] TLV. Calculator: Condensaatbelasting van leidingen bij opstarten. [Online]. Available: <https://www.tlv.com/global/NL/calculator/condensate-load-piping-start-up.html>
- [10] T. controls. How to calculate condensate load in steam pipe. [Online]. Available: <https://techmatic.com.sg/2021/02/11/how-to-calculate-condensate-load-in-steam-pipe/>

- [11] X. Yan, S. T. Ariaratnam, S. Dong, and C. Zeng, "Horizontal directional drilling: State-of-the-art review of theory and applications," *Tunnelling and Underground Space Technology*, vol. 72, pp. 162–173, 2018. [Online]. Available: <https://www.sciencedirect.com/science/article/pii/S0886779817309665>
- [12] Nederlandse vereniging voor Sleufloze Technieken en Toepassingen (NSTT), "Sleufloze aanleg," Jun. 15, 2022 [Online]. [Online]. Available: <https://www.nstt.nl/kenniscentrum/technieken/aanleg>
- [13] *Richtlijn Boortechneken en open ontgraving voor kabels en leidingen*, Versienummer Juni 2019-v1.0, Rijkswaterstaat, Ministerie van Infrastructuur en Waterstaat, The Netherlands, 2019.
- [14] G. Volkov, I. Elkin, A. Kapustin, V. Melikhov, O. Melikhov, S. Nikonov, and O. Trubkin, "Experimental and calculated studies of condensation-induced water hammer," *Thermal Engineering*, vol. 68, pp. 142–151, 02 2021.
- [15] K. Paffel, "Steam and condensate system waterhammer — part 2/3: The different types of waterhammer," Company website, 2018. [Online]. Available: <https://invenoeng.com/different-types-of-waterhammer>
- [16] H. Nakamura, T. Watanabe, T. Takeda, Y. Maruyama, and M. Suzuki, "Overview of recent efforts through rosa/istf experiments," *Nuclear Engineering and Technology*, vol. 41, 08 2009.
- [17] Y. F. Selivanov, A. D. Yefanov, and P. L. Kirillov, "Water hammer phenomena occurring in nuclear power installations at filling horizontal pipe containing saturated steam with liquid," in *Proc. 7th Int. Meeting on Nuclear Thermal-Hydraulics (NURETH-7)*, 1995, pp. Vol.4, p. 2916.
- [18] Y. F. Selivanov, A. D. Yefanov, and A. D. Martynov, "Study of the modes of occurrence and magnitude of condensation hydraulic impacts in the equipment elements of reactor plants with vver," in *Proc. Int. Conf., Obninsk, Russia, May 26-29, 1998*, 1998, pp. Vol. 1, p. 180.
- [19] C. Urban and M. Schlueter, "Investigations on the stochastic nature of condensation induced water hammer," *International Journal of Multiphase Flow*, vol. 67, 12 2014.
- [20] J. R. Thome, *Wolverine Engineering Databook III*. (web book updated yearly), 2006, web-based reference book available for free at the website, 16 chapters so far., url = <http://www.wlv.com/products/databook/db3/DataBookIII.pdf>.

- [21] D. Schmid, B. Verlaat, P. Petagna, R. Revellin, and J. Schiffmann, "Flow pattern observations and flow pattern map for adiabatic two-phase flow of carbon dioxide in vertical upward and downward direction," *Experimental Thermal and Fluid Science*, vol. 131, p. 110526, 2022. [Online]. Available: <https://www.sciencedirect.com/science/article/pii/S0894177721001692>
- [22] F. Holland and R. Bragg, "7 - gas-liquid two-phase flow," in *Fluid Flow for Chemical Engineers (Second Edition)*, second edition ed., F. Holland and R. Bragg, Eds. Oxford: Butterworth-Heinemann, 1995, pp. 219–267. [Online]. Available: <https://www.sciencedirect.com/science/article/pii/B9780340610589500098>
- [23] J. R. Thome and A. Cioncolini, "Two-phase flow pattern maps for macrochannels," *Encyclopedia of Two-Phase Heat Transfer and Flow I*, p. 5–45, 2015.
- [24] G. Breber, J. W. Palen, and J. Taborek, "Prediction of Horizontal Tubeside Condensation of Pure Components Using Flow Regime Criteria," *Journal of Heat Transfer*, vol. 102, no. 3, pp. 471–476, 08 1980. [Online]. Available: <https://doi.org/10.1115/1.3244325>
- [25] T. N. Tandon, H. K. Varma, and C. P. Gupta, "A New Flow Regimes Map for Condensation Inside Horizontal Tubes," *Journal of Heat Transfer*, vol. 104, no. 4, pp. 763–768, 11 1982. [Online]. Available: <https://doi.org/10.1115/1.3245197>
- [26] A. Cioncolini and J. R. Thome, "Liquid film circumferential asymmetry prediction in horizontal annular two-phase flow," *International Journal of Multiphase Flow*, vol. 51, pp. 44–54, 2013. [Online]. Available: <https://www.sciencedirect.com/science/article/pii/S0301932212001760>
- [27] S. L. Smith, "Void fractions in two-phase flow: A correlation based upon an equal velocity head model," *Proceedings of the Institution of Mechanical Engineers*, vol. 184, no. 1, pp. 647–664, 1969. [Online]. Available: <https://doi.org/10.1243/PIME.PROC.1969.184.051.02>
- [28] M. M. Shah, "Comprehensive correlations for heat transfer during condensation in conventional and mini/micro channels in all orientations," *International Journal of Refrigeration*, vol. 67, pp. 22–41, 2016. [Online]. Available: <https://www.sciencedirect.com/science/article/pii/S0140700716300342>
- [29] L. Cheng and D. Mewes, "Review of two-phase flow and flow boiling of mixtures in small and mini channels," *International Journal of Multiphase*

- Flow*, vol. 32, no. 2, pp. 183–207, 2006. [Online]. Available: <https://www.sciencedirect.com/science/article/pii/S0301932205001369>
- [30] M. Pietrzak and M. Płaczek, “Void fraction predictive methods in two-phase flow across a small diameter channel,” *International Journal of Multiphase Flow*, vol. 121, p. 103115, 2019. [Online]. Available: <https://www.sciencedirect.com/science/article/pii/S0301932219304665>
- [31] D. Steiner, “Heat transfer to boiling saturated liquids,” *VDI-Warmeatlas (VDI Heat Atlas)*, 1993.
- [32] T. Mishra. Microtunneling vs. horizontal directional drilling: Understanding the differences between these key trenchless methods. [Online]. Available: <https://www.trenchlesspedia.com/whats-the-difference-between-microtunneling-and-hdd/2/3641>
- [33] M. A. BOLES, M. KANOGLU, and Y. A. CENGEL, *Thermodynamics: An engineering approach*. McGraw-Hill Education, 2020.
- [34] Y. Taitel and A. E. Dukler, “A model for predicting flow regime transitions in horizontal and near horizontal gas-liquid flow,” *AIChE Journal*, vol. 22, no. 1, pp. 47–55, 1976. [Online]. Available: <https://aiche.onlinelibrary.wiley.com/doi/abs/10.1002/aic.690220105>
- [35] S. Henclik, “Application of the shock response spectrum method to severity assessment of water hammer loads,” *Mechanical Systems and Signal Processing*, vol. 157, p. 107649, 2021. [Online]. Available: <https://www.sciencedirect.com/science/article/pii/S0888327021000443>
- [36] S. Miwa, M. Mori, and T. Hibiki, “Two-phase flow induced vibration in piping systems,” *Progress in Nuclear Energy*, vol. 78, pp. 270–284, 2015. [Online]. Available: <https://www.sciencedirect.com/science/article/pii/S0149197014002674>
- [37] M. Lesser, “Thirty years of liquid impact research: a tutorial review,” *Wear*, vol. 186-187, pp. 28–34, 1995, 8th International Conference on Erosion by Liquid and Solid Impact. [Online]. Available: <https://www.sciencedirect.com/science/article/pii/0043164895071903>
- [38] *The Barlow Equation for Tubular Burst: A Muddled History*, ser. SPE/IADC Drilling Conference and Exhibition, vol. Day 3 Thu, March 08, 2018, 03 2018, d031S013R001. [Online]. Available: <https://doi.org/10.2118/189681-MS>

- 
- [39] S. Korzilius, T. Abdelouaheb, Z. Bozkus, M. Anthonissen, and W. Schilders, "Modeling liquid slugs accelerating in inclined conduits," *Journal of Pressure Vessel Technology*, vol. 139, 08 2017.
- [40] T. Abdelouaheb, Q. Hou, and Z. Bozkus, "An improved one-dimensional model for liquid slugs traveling in pipelines," *Journal of Pressure Vessel Technology*, vol. 138, 02 2015.



# Alternative drilling techniques

An alternative technique, similar to the HDD, is the directly driven method. For this technique, the drilling head is immediately attached to the pipeline. This way, the pipeline is installed directly after the first bore. However, to perform this with a single bore, the drilling head encounters far more resistance compared to the HDD method. To start the drilling the head needs to be pressed into the ground to provide sufficient force to drill through the surface with a relatively large diameter. Since the pipeline is installed at first bore, the technique requires almost no equipment at the exit side of the bore. However, since a heavy pressing installation is required at onset location, it takes up more space at the entry side compared to HDD [13].

Another common technique is microtunneling. The concept of microtunneling is to press pipeline segments into the ground from a pressing-pit. The first segment is equipped with a cutting head, and is generally pressed horizontally to the exit-pit. Microtunneling is generally performed in two distinct ways, either with an open or closed front. The open front microtunneling method can either be directionally driven like HDD, or not. However, if the cutting head is not directionally driven, it may deviate from its path since it is likely to follow the path with the least resistance. As the name suggests, the first segment has an open front which allows soil and water to enter the pipe. This can be removed by hand, or with an auger. Since water can enter the pipe, the method is not suitable for drilling below groundwater level. Therefore this method has a limited drilling depth, depending on the location. Opposite to the open front technique, closed front microtunneling uses a closed drilling head that is equipped with a liquid shield. This helps the drilling head to maintain its stability while the excess liquid is being pumped away together with the drilling waste. A notable advantage of the closed front microtunneling, is that the technique is suited for drilling below ground water level. Microtunneling is widely applied since its result is a reliable, and sturdy pipeline installation. Which allows for limited maintenance compared to other techniques. The downsides are that it is a rather

expensive technique which is relatively damaging to its environment due to the excavation pits [13] [32].



**Figure A.1:** Example of microtunneling and its excavation [33]

Sometimes pipeline tunnels are installed to accommodate multiple pipelines with distinct purposes. These tunnels are usually installed with closed front microtunneling techniques and are extremely expensive. For such an effort to be profitable, many different users need to be involved in order to make optimum use of the tunnel. Therefore, such a project is reliant on many different parties with similar goals. The main benefit of such a tunnel is the spacious underground environment. Figure A.2 shows an application of an underground tunnel. Often

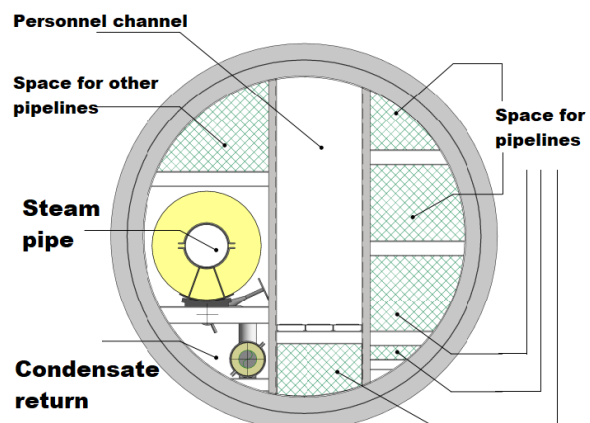


**Figure A.2:** Example of a pipe tunnel [8]

Often

times, space is reserved to allow for mechanics to be able to reach the pipelines, for example for maintenance.

In contrast to the aforementioned techniques, a pipe bridge is an above ground level method to pass obstructions. The pipe bridge is a steel construction that supports pipes that are elevated to pass the obstruction. This technique is an effective solution for relatively short crossings. However, whether pipe bridges are suitable, relies heavily on the distance that it needs to pass, and how the structure can be supported along the way. For obvious reasons, this can get problematic for larger distances. However, for shorter distances (e.g., small roads), there is no apparent reason why a pipe bridge is an invalid solution. Opposed to the underground techniques, a pipe bridge allows to design the pipelines in a slight angle. Guiding any excess condensate to a low-point, where condensate can be safely discarded from the steam main, as described earlier in Figure 2.4. However, excessively large length pipe bridges might demand condensate removal on the bridge itself, which could be problematic since a 100 meter distance between drain points is recommended [3]. On top of that, longer distance pipe bridges require more complex structures as it has to deal with larger expansion distances due to the pipe heating up. An example of a steam pipeline crossing a railway supported by a pipe bridge is added as Figure A.3.



**Figure A.3:** Steam & condensate pipelines crossing a railway with a pipe bridge [8]

# Adiabatic two-phase Flow Pattern Maps

The earliest FPM is a simplified one that assumes no heat transfer between the two distinct phases. Logically, this is the adiabatic FPM. One of the oldest, yet still commonly used, is Baker's adiabatic FPM for horizontal tubes, created in 1954 [23]. Figure B.1 represents this adiabatic FPM. On the vertical and horizontal axes,  $G_G$  and  $G_L$  are the gas and liquid mass fluxes in  $kg/m^2s^{-1}$ , respectively. The dimensionless parameters  $\psi$  and  $\lambda$  represent the physical property ratios of the two-phase flow. In this case, water and air, which are determined by Equations B.1 and B.2, respectively. Initially, Baker's FPM was designed for water and air as working fluids [23]. The physical property ratios  $\psi$  and  $\lambda$  correct the use of alternative two-phase conditions by relating the actual physical properties dynamic viscosity  $\mu$  in  $Nsm^{-2}$ , surface tension  $\sigma$  in  $Nm^{-1}$  and density  $\rho$  in  $kgm^3$ , to those of air and water.

$$\lambda = \left( \frac{\rho_G \rho_L}{\rho_a \rho_w} \right)^{1/2} \quad (B.1)$$

$$\psi = \left( \frac{\sigma_w}{\sigma} \right) \left[ \left( \frac{\mu_L}{\mu_w} \right) \left( \frac{\rho_w}{\rho_L} \right)^2 \right]^{1/3} \quad (B.2)$$

The expressions for the transition lines of Baker's FPM in Figure B.1 can be used to compute the flow pattern of two-phase flow, using the mass flows  $G_G$  and  $G_L$  in  $kg/m^2s^{-1}$  and the relative physical property ratios  $\psi$  and  $\lambda$ .

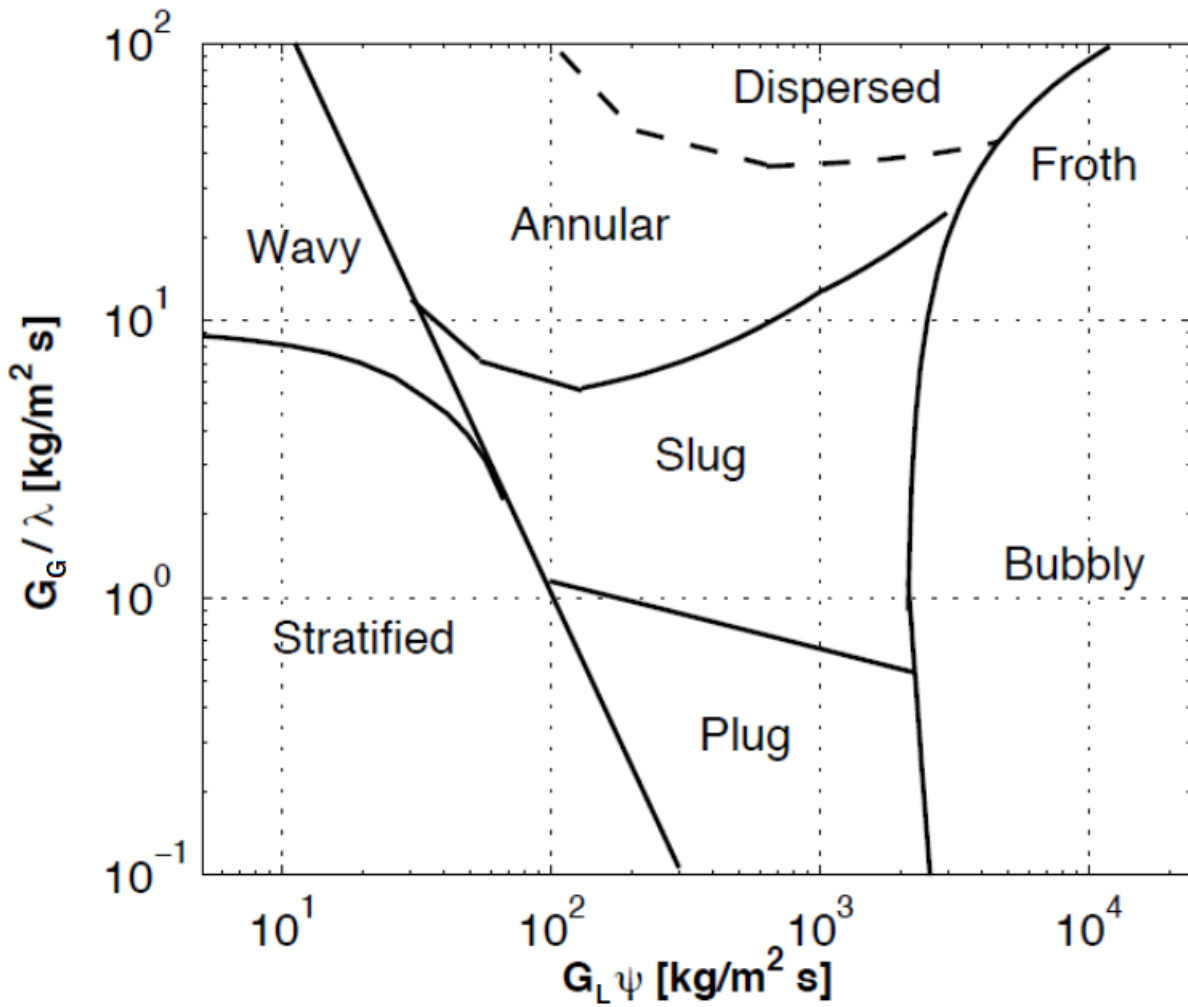


**Figure B.1:** Adiabatic two-phase flow pattern map [23]

Instead of Baker's FPM, Taitel and Dukler constructed possibly the most extensively used two-phase FPM for adiabatic horizontal tubes. This map introduces the Martinelli parameter ( $X$ ), the gas Froude number ( $Fr_G$ ) and non-dimensional parameters  $T$  and  $K$ . Originally, the map consists of three separate graphs, like in Figure B.2. However, a more commonly used FPM is the updated version by Cioncolini and Thome, which is depicted in B.3. The expressions for the used parameters  $Fr_G$ ,  $X$ ,  $T$ ,  $K$ ,  $Re_k$  in these graphs are given as Equations B.3, 3.5, B.5, B.6, B.7, respectively. The pressure gradient  $dp/dz$  is determined with Equation B.8, where  $f_k$  is the flow friction factor for phase  $k$ , which depends on the Reynolds number. The expressions for the flow friction factors at laminar and turbulent flow are added as Equations B.9 and B.10, respectively. Once the Martinelli parameter ( $X$ ) and Froude number are determined, and knowing the expressions of the flow pattern transition lines from the updated Taitel & Dukler [34] FPM in Figure B.3, the flow pattern of the adiabatic two-phase flow can be computed. The updated version of the original

three FPMs of Taitel & Dukler [34] is basically a simplified method that only requires one graph instead of three. However, the FPM is extended with a more detailed description of annular flow. Introducing symmetric, and asymmetric annular flow. The upgrade was performed by Cioncolini and Thome in 2013 [23].

$$Fr_G = \frac{G_G}{[\rho_G(\rho_L - \rho_G)Dg]^{1/2}} \quad (\text{B.3})$$

$$X = \left[ \frac{(dp/dz)_L}{(dp/dz)_G} \right]^{1/2} \quad (\text{B.4})$$

$$T = \left[ \frac{|(dp/dz)_L|}{g(\rho_L - \rho_G)} \right]^{1/2} \quad (\text{B.5})$$

$$K = Fr_G * Re^{0.5} \quad (\text{B.6})$$

$$Re_k = \frac{G_k * D}{\mu_k} \quad (\text{B.7})$$

$$(dp/dz)_k = -\frac{2f_k G_k^2}{\rho_k D} \quad (\text{B.8})$$

$$f_k(Re < 2000) = \frac{16}{Re_k} \quad (\text{B.9})$$

$$f_k(Re > 2000) = \frac{0.079}{Re_k^{1/4}} \quad (\text{B.10})$$

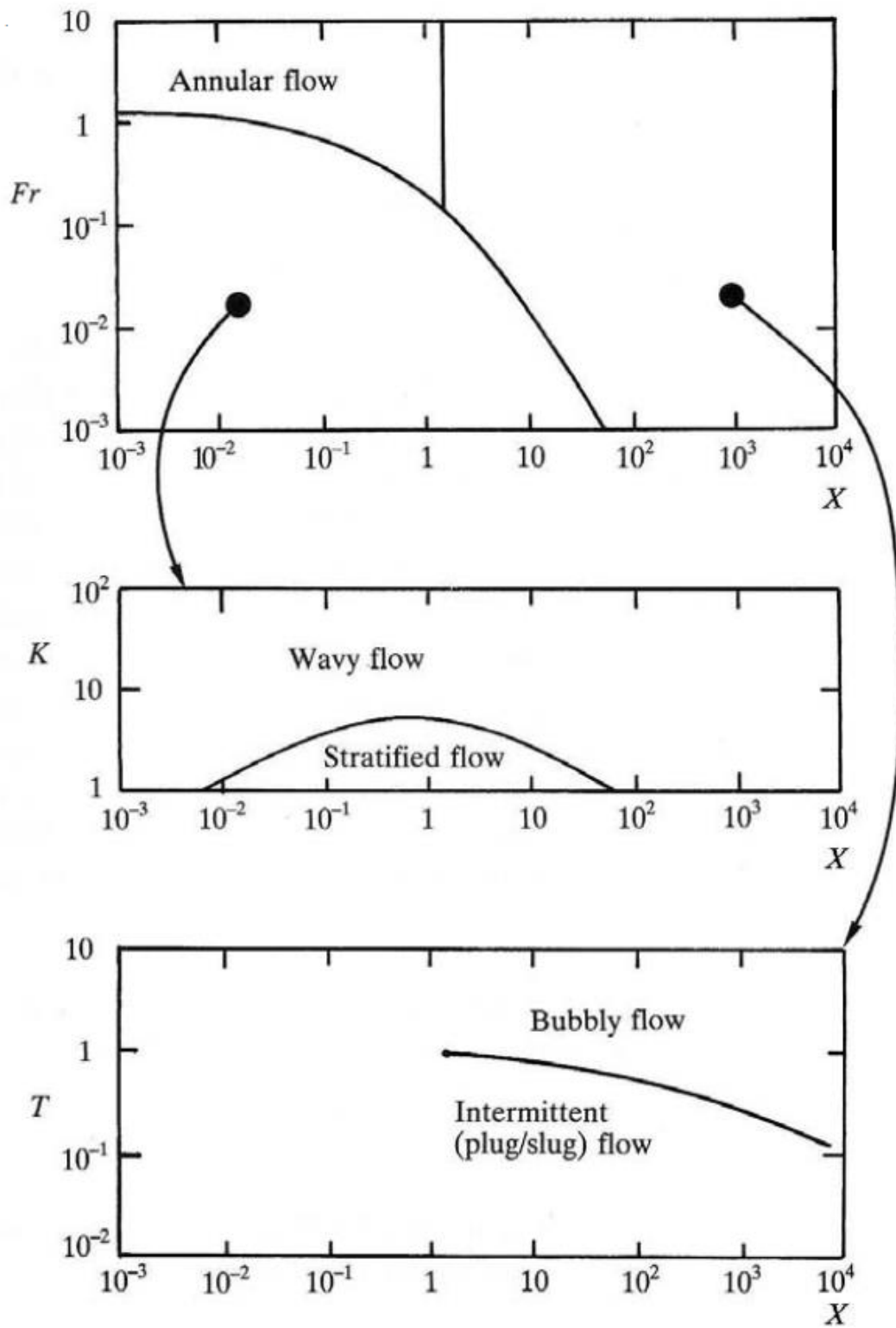


**Figure B.2:** Original three adiabatic Taitel & Dukler graphs [23]

## Taitel & Dukler: Updated

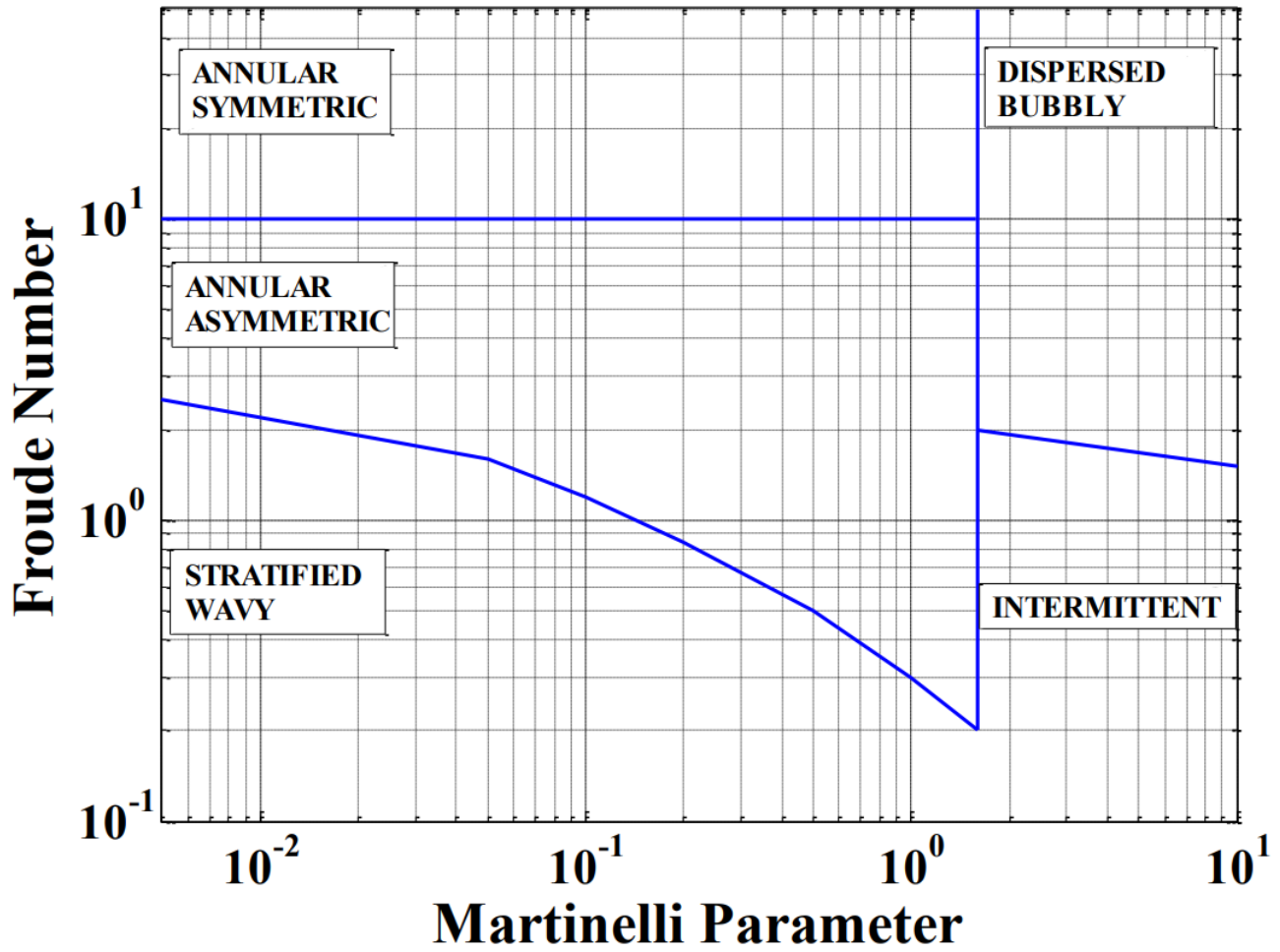


Figure B.3: Adiabatic Taitel & Dukler FPM, updated graph [23]

# Additional water hammer articles

## C.1 Flow & differential shock water hammer

Although the root causes of flow and differential shock water hammer are partially different, the resulting situation is more or less the same. Pressure variations, pipe stresses and vibrations occur due to the abrupt change in flow conditions of high incompressible liquids [35]. A typical situation for this type of water hammer is where a liquid slug approaches an elbow. SCS contain a great deal of elbow bends in order to deal with the expansion of the pipe material as it heats up. Although the effects of fluids on pipework is extensively researched, hardly any formal research has been performed on actual steam pipelines. Therefore, this section intends to review existing knowledge on fluid-pipe interactions, and relate this to steam pipelines.

According to Miwa et al. [36], when a two-phase fluid flows through an elbow, whilst in the slug flow regime, a pressure peak on the pipe occurs as it travels through the elbow. To evaluate the maximum possible force on the pipework, caused by the liquid slug on an elbow, a term for an impact force is developed. Miwa et al. modeled this as a slug colliding with a wall, as schematically illustrated in Figure C.1. Based on the Guided Acoustic Shock Theory [37], Miwa et al. have developed an expression for the exerted slug impact force on the pipe wall of an elbow. This expression is added as Equation C.2 and was validated by Miwa et al. for horizontal-upward and horizontal downward applications with experiments. Where the slug velocity is computed with Equation C.1, note that this expression assumes that the slug velocity in direction of the elbow starts at zero. Both Equations C.1 and C.2 consider a two-phase ( $2\phi$ ) slug that contains small gas bubbles, which affects the slugs density and speed of sound, resulting in a two-phase density ( $\rho_{2\phi}$ ) and speed of sound ( $c_{2\phi}$ ). These two-phase properties represent the averaged properties of the two single phases together. After the impact force is determined, the peak pressure as a result of the impact can be obtained by dividing by the surface

area [36].

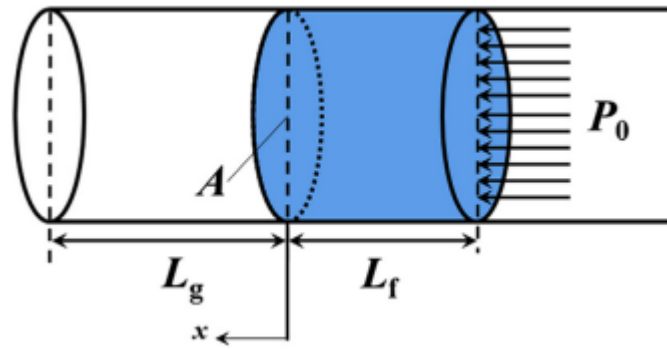


**Figure C.1:** Slug approaching a wall [36]

$$u_f = \sqrt{\frac{2P_0 L_g}{\rho_{TP} L_f}} \quad (C.1)$$

$$F_{IF} = \rho_{TP} c_{TP} A \sqrt{\frac{2 * P_0 L_g}{\rho_{TP} L_f}} \quad (C.2)$$

$$P_{peak} = \frac{F_{IF}}{A} \quad (C.3)$$

To determine whether a pipeline yields as a result of an internal pressure peak, Barlow's formula, like in Equation C.4, can be applied. This is a widely accepted formula in pipeline engineering, first used by Peter Barlow in 1836 [38].

$$P_t = \frac{2S_t * wt}{D_o} \quad (C.4)$$

## C.2 Slug propulsion & resistance, acceleration & deceleration

Since the force exerted by a slug on the pipework largely depends on the velocity of the slug, it is valuable to gain insight in what factors influence the velocity of a slug in two-phase conduits. Abdelouaheb et al. [39] modelled liquid slugs in inclined conduits. In preliminary work [40], they created a one-dimensional model that describes the most prevalent mechanism that influence the velocity of a liquid slug; pressure, gravity, friction, and holdup. Figure C.2 illustrates a liquid slug flowing through a horizontal conduit at velocity  $v$ . The planar front and tail, are at positions  $x_1$  and  $x_2$ , with corresponding pressures  $P_1$  and  $P_2$ , respectively. Holdup is defined as the mass of

liquid that is shed by the liquid slug.

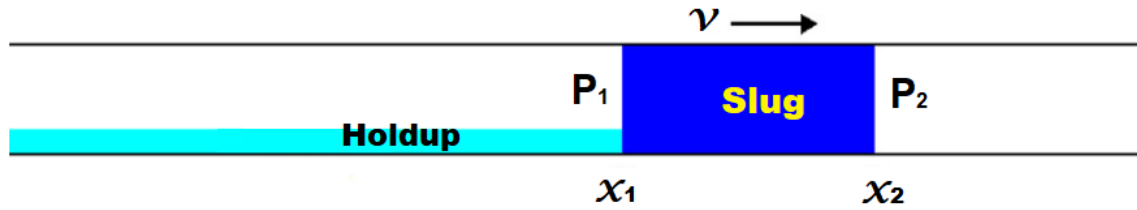


**Figure C.2:** Sketch of slug propagation [40]

The various mechanism that influence slug velocity can either work propulsive or resistive, i.e., accelerating or decelerating the liquid slug, respectively. Since the mechanics are rather intuitive, they are not discussed in further detail. Considering Figure C.2, where a slug covers the entire diameter of a conduit, pressure difference can either accelerate or decelerate the slug. The influence of pressure difference between front and tail of the slug can be described as Equation C.5. The effect of gravitational pull in inclined conduits is described as Equation C.6. Naturally, friction will always decelerate the slug as a result of friction factor  $f$ . Lastly, the holdup term in Equation C.8 is what determines whether the liquid slug gains or loses mass. Increasing or decreasing the mass of a slug determines whether the slug accelerates or decelerates, respectively.

$$a1 = (P_2 - P_1) \frac{A}{m} \quad (C.5)$$

$$a2 = g * \sin \theta \quad (C.6)$$

$$a3 = -\frac{f}{2 * D_i} u^2 \quad (C.7)$$

$$a4 = -\frac{u}{m} \frac{dm}{dt} \quad (C.8)$$

Combining the four mechanisms into one expression results in Equation C.9, which is a simplified form compared to the successive work of Abdelouaheb et al [39].

$$\frac{du}{dt} = \frac{P2 - P1}{\rho * L(t)} + g * \sin \theta - \frac{f}{2D} u^2 - \frac{u}{m} \frac{dm}{dt} \quad (C.9)$$

Being able to predict the acceleration and thus, velocity, is highly valuable to foresee high impact of slug in steam pipelines. For example, in case of a long distance straight steam pipeline, followed by an elbow, it is extremely important to be able to determine whether the slug accelerates or decelerates as it approaches the elbow. Therefore, it is worthwhile to further investigate how to define friction, pressure differences, and slug mass change in steam pipelines.

## Appendix D

**Code**

**This page is intentionally left blank.  
Appendix D continues on the next page.**

```

1:
2: "lookup('Cond_tube_(DIAMETER)_Tsat_Patm',i*100, round(pi/4*(DIAMETER)^2 * G))"
3: Function htp(zeta1)
4:   htp:=lookup('Cond_tube_0.3_Tsat_Patm',100,round(pi/4*(0.3)^2 * 100) )
5:   If (zeta1=1) Then Return
6:   i = 1
7:   Repeat
8:   i=i-0.01
9:   htp = lookup('Cond_tube_0.3_Tsat_Patm',i*100,round(pi/4*(0.3)^2 * 100) )
10:  Until((abs(zeta1-i)<5*10^(-3)))
11: End
12:
13: Duplicate i=1,100
14:   C[i] = (pi * ((Do/2)^2 - (Di/2)^2) * (L_sec*i) * rho_steel) * cp_steel
15:   L[i] = L_sec * i
16:   zeta[i] = 0.01*i
17:   rho_g_smith[i] = density(Water,P=P_atm,x=zeta[i])
18:   vf_smith[i] = 1/( 1+ 0.79* ((1-zeta[i]^0.78)/zeta[i] * (rho_g_smith[i]/rho_l)^0.58))
19: End
20:
21: "Mass flow: Check whether this corresponds with Function htp(zeta1)!!!"
22: G = 100
23: m_dot = round(G * A)
24: t_sim = 100 "Simulation time"
25: steps = 1000 "Amount of time steps, must match with steps in
   options>preferences>integration "
26:
27:
28: {Anti-zero conditions}
29: nozero_t = if(t,0,1,1,0)
30: zero_t = if(t,0,1,0,1)
31:
32: {Other helpful quantities/code}
33: t_u = if(x,L_max, if(x,L_max-2, 0 , m_f / m_dot , m_f / m_dot) , integralvalue(t-t_sim/steps,t_u) , integralvalue(t-t_sim
/steps,t_u) )
34: "note: t_u is used to indicate when the pipe is filled, i.e., this is the moment in time when fluid mass leaves the system"
35:
36:
37: zeta1 = integralvalue(t-t_sim/steps, zeta) "Uses zeta value of the previous time step to obtain h_TP"
38: h_TP = htp(zeta1) "Local heat transfer coefficient according to Shah(2016) relations"
39:
40:
41: {Known parameters}
42: Di = 0.3 [m] "Inner steel pipe diameter [m]"
43: wt = if(Di, 0.4, 5.6/1000, 6.3/1000, 6.3/1000) "Outer steel pipe diameter: DN300 from ISO [m]"
44: Do = Di + wt*2
45:
46: insul = 0.100 [m] "Thickness of insulation"
47: r1 = Di/2
48: r2 = Do/2
49: r3 = Do/2 + insul
50:
51:
52: L_sec = 10 [m]
53:
54: A = pi/4*Di^2
55: A_o = pi*(Do+2*insul)*L
56: T_inf = 20 [°C]
57:
58: {Material properties}
59: rho_steel = 7800 [kg/m^3] "Density of the steel pipe [kg/m^3]"

```

```

60: cp_steel = 0.530 [kJ/(kg*K)]           "Specific heat of the steel pipe [kJ/(kg*K)]"
61: k_steel = 0.045 [kW/(m*K)]           "Conductivity coefficient of the steel pipe [kW/(m*K)]"
62: N = ceil(x/L_sec)
63: C_steel = if(x,L_sec,C[1],C[1],N*C[1])
64: m_steel = C_steel / cp_steel
65:
66: {Pipe dimension calculations & maximum length}
67: L_max = 500 [m]
68: L = if(x,L_max, if(x,L_sec,L[1],L[1],N*L[1]) ,L_max,L_max)
69:
70: rho_ins = 70 [kg/m^3]
71: k_ins = 0.03 *10^(-3) [kW/(m*K)]
72: cp_ins = 1.030 [kJ/(kg*K)]
73: m_ins = pi * ((r3)^2 - (r2)^2) * L * rho_ins
74:
75: {Thermophysical properties of the 2p fluid}
76:
77: P_atm = 101.325 [kPa]
78: T_sat = temperature(Water,P=P_atm,x=1)
79: Ts = T_sat
80:
81: rho_gi = density(Water,P=P_atm,x=1)     "Initial density of the gas (steam) at inlet condition: zeta = 1"
82: rho_g = if(t,0,0,0,density(Water,P=P_atm,h=h_f)) "Density of the gas based on enthalpy value"
83: "rho_g = if(t,0,0,0,density(Water,P=P_atm,x=zeta))"
84: rho_l = density(Water,P=P_atm,x=0)     "Density of fully condensed liquid: zeta = 0"
85:
86: dH = enthalpy(Water,P=P_atm,x=1) - enthalpy(Water,P=P_atm,x=0)
87: h_fg = Enthalpy(Water,P=P_atm,x=1) - Enthalpy(Water,P=P_atm,x=0) "Specific
    enthalpy difference to fully condens from zeta=1 to zeta=0"
88: h_i = enthalpy(Water,P=P_atm,x=1)     "Enthalpy of the gas at the pipe inlet"
89: h_l = enthalpy(Water,P=P_atm,x=0)     "Enthalpy of fully condensed liquid (zeta = 0)"
90: h_f = Q_f / (nozero_t + m_f)         "Specific enthalpy of the fluid [kJ/kg]"
91:
92:
93:
94: {Differential equations}
95: dx = if(t,0,0,0,(V_g - V_gi) / (pi/4*Di^2))
96: dxdt = 1/A * (m_dot/rho_gi - 1/rho_l * 1.1/dH * h_TP * pi*Di*x * (Ts - Tp) * (rho_l/rho_gi)) "Change in
    velocity of the fluid. Note: the factor 1.1 indicates a 10% extra heat loss of "
97: x = if(x,L_max, dx + integral(dxdt,t,0,t_sim) , L_max, L_max)
98:
99:
100: "dTpdT = 1/(m_steel*cp_steel) * (dQ1dt)" "- dQ2dt)"
101: dTpdT = 1/(C_steel) * (dQ1dt - dQ2dt) "C_steel dependent on variable L instead of constant"
102: Tp = 20 + integral(dTpdT,t,0,t_sim) "Temperature of the pipe, assuming Tp = uniform"
103:
104: dQ1dt = if(t,0,0,0,h_TP *pi*Di*x * (Ts - Tp))
105: Q1 = 1.1*integral(dQ1dt,t,0,t_sim) "Heat transferred from the fluid to the pipe, factor 1.1 applied for
    extra 10% heat loss"
106:
107: dQ2dt = 2*pi*k_ins*L*(Tp-T2)/(ln(r3/r2))
108: Q2 = integral(dQ2dt,t,0,t_sim) "Heat transferred from the pipe to the insulation"
109:
110: dT2dt = 1/(m_ins*cp_ins) * (dQ2dt- dQ3dt )
111: T2 = 20 + integral(dT2dt,t,0,t_sim) "Temperature at the end of the outer insulation layer"
112:
113: dmlDt = 1/dH * dQ1dt "Condensation rate as a result of heat loss"
114: m_l = integral(dmlDt,t,0,t_sim)
115:
116: {Natural convection at pipe exterior}

```

```

117: Call fc_horizontal_cylinder('Air', T2, 10, P_atm, r3*2 : h_nc1, Nusselt, Ra)
118: h_nc = h_nc1 /1000
119:
120: dQ3dt = h_nc * A_o * (T2 - T_inf)
121: Q3 = integral(dQ3dt,t,0,t_sim) "Heat transferred from the insulation to the pipe's surroundings"
122:
123:
124: {Energy quantities per layer}
125: Q_in = m_dot*h_i*t "Energy added at the pipe inlet [kJ]"
126: dQindt = m_dot*h_i
127: dQfdt = dQindt - dQ1dt
128: dmfdt = G*(pi/4*Di^2)
129: Q_f = Q_in - Q1 "Energy that the fluid holds [kJ]"
130: Q_l = h_l * m_l "Energy that the liquid holds [kJ]"
131: Q_g = Q_f - Q_l "Energy that the gas holds [kJ]"
132:
133:
134: {Other fluid properties}
135: m_f = zero_t * m_dot * t "Mass of the fluid at time t [kg]"
136: m_g = m_f - m_l "Mass of the gas at time t [kg]"
137: m_dot_g = zero_t * (m_dot - dmldt)
138: u_gas = m_dot_g / (nozero_t + rho_g * epsilon_v * A) "Note: void fraction affects this velocity due to reduced area!!!"
139:
140: zeta = if(t,0,1,1,(h_f - h_l)/h_fg) "Vapor quality of the fluid"
141:
142: V_gi = if(t,0,0,0,m_g / rho_gi)
143: V_g = if(t,0,0,0,m_g / (nozero_t + 10^(-10) + rho_g))
144: V_l = if(t,0,0,0,m_l / rho_l)
145:
146: A_g = V_g / (nozero_t + x)
147: A_l = V_l / (nozero_t + x)
148:
149: epsilon_s = 1/( 1 + 0.79* ((1-zeta)/zeta)^0.78 * (rho_g/rho_l)^0.58)
150: epsilon_v = nozero_t + V_g / (nozero_t + V_g + V_l)
151: vf_a = nozero_t + A_g / (nozero_t + A_g + A_l)
152:
153: G_g = u_gas * rho_g
154: Fr_g = G_g / (nozero_t + rho_g*(rho_l - rho_g)*Di*9.81)^(1/2)
155: s = (1 - epsilon_s) / epsilon_s
156:
157: {Flow regime mapping}
158: FP$ = if$(s,0.5, if$(Fr_g,1, 'Wavy', 'Annu-wavy', if$(Fr_g,6, 'Annular', 'Annu-spray', 'Spray') ), if$(Fr_g,0.01, 'Wavy-plug',
'Wavy-plug-slug', if$(Fr_g, 0.5, 'Slug', 'Slug-int', if$(Fr_g, 1, 'Wavy-int', 'Wavy-annu-int', if$(Fr_g, 6, 'Annular-int', 'Annu-spray
-int', 'Spray-int') ) ) ), if$(Fr_g, 0.01, 'Plug', 'Plug-slug' , if$(Fr_g, 0.5, 'Slug', 'Slug-int', 'Intermittent' ) ) )
159:
160:
161: "less = if$(Fr_g,1, 'Wavy', 'Annu-wavy', if$(Fr_g,6, 'Annular', 'Annu-spray', 'Spray') )"
162:
163: "equal = if$(Fr_g,0.01, 'Wavy-plug', 'Wavy-plug-slug', if$(Fr_g, 0.5, 'Slug', 'Slug-int', if$(Fr_g, 1, 'Wavy-int', 'Wavy-annu-int',
if$(Fr_g, 6, 'Annular-int', 'Annu-spray-int', 'Spray-int') ) ) )"
164:
165: "greater = if$(Fr_g, 0.01, 'Plug', 'Plug-slug' , if$(Fr_g, 0.5, 'Slug', 'Slug-int', 'Intermittent' ) )"
166:
167:
168: $IntegralTable t,t_u,x,L,h_TP,Tp,T2,m_f,Q_in,Q1,Q_f,h_f,dmldt,m_l,V_l,m_dot_g,m_g,rho_g,V_g,zeta,epsilon_s,epsilon_v
,u_gas,G_g,Fr_g,s,FP$

```

## Appendix E

### Additional tables

DN400	15 kg/m <sup>2</sup> s <sup>-1</sup>	25 kg/m <sup>2</sup> s <sup>-1</sup>	50 kg/m <sup>2</sup> s <sup>-1</sup>	75 kg/m <sup>2</sup> s <sup>-1</sup>	100 kg/m <sup>2</sup> s <sup>-1</sup>
Lowest value of $\epsilon_v$	0.9975	0.9976	0.9978	0.9985	0.9976
End value of $\epsilon_v$	0.9991	0.9987	0.9981	0.9985	0.9990

**Table E.1:** Minimal and final simulation values of volumetric void fraction  $\epsilon_v$  at various mass flow rates  $G$  for a DN400 pipe

DN500	15 kg/m <sup>2</sup> s <sup>-1</sup>	25 kg/m <sup>2</sup> s <sup>-1</sup>	50 kg/m <sup>2</sup> s <sup>-1</sup>	75 kg/m <sup>2</sup> s <sup>-1</sup>	100 kg/m <sup>2</sup> s <sup>-1</sup>
Lowest value of $\epsilon_v$	0.9979	0.9980	0.9981	0.9987	0.9980
End value of $\epsilon_v$	0.9991	0.9987	0.9982	0.9988	0.9996

**Table E.2:** Minimal and final simulation values of volumetric void fraction  $\epsilon_v$  at various mass flow rates  $G$  for a DN500 pipe

DN400	15 kg/m <sup>2</sup> s <sup>-1</sup>	25 kg/m <sup>2</sup> s <sup>-1</sup>	50 kg/m <sup>2</sup> s <sup>-1</sup>	75 kg/m <sup>2</sup> s <sup>-1</sup>	100 kg/m <sup>2</sup> s <sup>-1</sup>
Lowest value of $\epsilon_s$	0.9691	0.9701	0.9715	0.9786	0.9700
End value of $\epsilon_s$	0.9852	0.9813	0.9750	0.9788	0.9842

**Table E.3:** Minimal and final simulation values of Smith's [27] void fraction  $\epsilon_s$  at various mass flow rates  $G$  for a DN400 pipe

DN500	15	25	50	75	100
	kg/m <sup>2</sup> s <sup>-1</sup>				
Lowest value of $\epsilon_s$	0.9726	0.9738	0.9748	0.9814	0.9734
End value of $\epsilon_s$	0.9860	0.9814	0.9762	0.9819	0.9927

**Table E.4:** Minimal and final simulation values of Smith's [27] void fraction  $\epsilon_s$  at various mass flow rates  $G$  for a DN500 pipe

DN400	125	150	175
	kg/m <sup>2</sup> s <sup>-1</sup>	kg/m <sup>2</sup> s <sup>-1</sup>	kg/m <sup>2</sup> s <sup>-1</sup>
Lowest value of $\zeta$	0.3608	0.3615	0.3618
End value of $\zeta$	0.4995	0.4938	0.4896

**Table E.5:** Minimal and final simulation values of vapour quality  $\zeta$  at various higher mass flow rates  $G$  for a DN400 pipe

DN500	125	150	175
	kg/m <sup>2</sup> s <sup>-1</sup>	kg/m <sup>2</sup> s <sup>-1</sup>	kg/m <sup>2</sup> s <sup>-1</sup>
Lowest value of $\zeta$	0.3854	0.3857	0.386
End value of $\zeta$	0.5180	0.5151	0.5504

**Table E.6:** Minimal and final simulation values of vapour quality  $\zeta$  at various higher mass flow rates  $G$  for a DN500 pipe

DN400	125	150	175
	kg/m <sup>2</sup> s <sup>-1</sup>	kg/m <sup>2</sup> s <sup>-1</sup>	kg/m <sup>2</sup> s <sup>-1</sup>
Lowest value of $\epsilon_v$	0.9976	0.9976	0.9976
End value of $\epsilon_v$	0.999	0.9989	0.9989

**Table E.7:** Minimal and final simulation values of volumetric void fraction  $\epsilon_v$  at various higher mass flow rates  $G$  for a DN400 pipe

DN500	125	150	175
	kg/m <sup>2</sup> s <sup>-1</sup>	kg/m <sup>2</sup> s <sup>-1</sup>	kg/m <sup>2</sup> s <sup>-1</sup>
Lowest value of $\epsilon_v$	0.9980	0.998	0.998
End value of $\epsilon_v$	0.9991	0.999	0.9992

**Table E.8:** Minimal and final simulation values of volumetric void fraction  $\epsilon_v$  at various higher mass flow rates  $G$  for a DN500 pipe

DN400	125	150	175
	kg/m <sup>2</sup> s <sup>-1</sup>	kg/m <sup>2</sup> s <sup>-1</sup>	kg/m <sup>2</sup> s <sup>-1</sup>
Lowest value of $\epsilon_s$	0.9701	0.9702	0.9702
End value of $\epsilon_s$	0.9839	0.9835	0.9832

**Table E.9:** Minimal and final simulation values of Smith's [27] void fraction  $\epsilon_s$  at various higher mass flow rates  $G$  for a DN400 pipe

DN500	125	150	175
	kg/m <sup>2</sup> s <sup>-1</sup>	kg/m <sup>2</sup> s <sup>-1</sup>	kg/m <sup>2</sup> s <sup>-1</sup>
Lowest value of $\epsilon_s$	0.9734	0.9734	0.9735
End value of $\epsilon_s$	0.9851	0.9849	0.987

**Table E.10:** Minimal and final simulation values of Smith's [27] void fraction  $\epsilon_s$  at various higher mass flow rates  $G$  for a DN500 pipe